THREE-DIMENSIONAL REDATUMING OF SEISMIC SHOT RECORDS

PROEFSCHRIFT

ter verkrijging van de graad van doctor
aan de Technische Universiteit Delft,
op gezag van de Rector Magnificus,
prof.drs. P.A. Schenck,
in het openbaar te verdedigen
ten overstaan van een commissie,
aangewezen door het College van Dekanen
op dinsdag 20 juni 1989 te 16.00 uur door

NICOLAUS ANTONIUS KINNEGING

geboren te Haarlem
natuurkundig ingenieur

Gebotekst Zoetermeer / 1989

Dit proefschrift is goedgekeurd door de promotor

prof.dr.ir. A.J. Berkhout

Voor mijn
onvergetelijke
vader

PREFACE

In the last years the seismic industry has gradually moved from two-dimensional acquisition and processing to three-dimensional techniques. However, because of the huge amount of data a proper 3–D processing is not yet feasible on modern computer systems. To find practical solutions for 3–D data processing in 1986 the TRITON research project was started at the Group of Seismics and Acoustics of the Delft University of Technology. In this industry sponsored project a scheme is developed, where a proper image is obtained of a small part of the subsurface, the target zone. One of the important steps in this scheme is the redatuming of the data, measured at the surface, to the upper boundary of the target zone. This part of the target oriented algorithm is described in this thesis.

CONTENTS

CHAPTER 5:   EXAMPLES OF SHOT RECORD REDATUMING

1

AN INTRODUCTION TO THE
SEISMIC METHOD

1.1 INTRODUCTION

In the last century our world has changed dramatically. Just over 100 years ago the first automobile was introduced, while the today's society is unthinkable without very advanced technologies. This change would have been impossible without the availability of energy, especially in the form of oil and gas.

In the 1970's we have become aware of the fact that the large known oil and gas fields could be exhausted within a certain time. It is therefore important to search constantly for new oil and gas reserves. Seismic exploration techniques have played and are still playing an irreplaceable role in this search. In the last decades the seismic technology is much refined, such that smaller details could be recovered from the seismic data. Especially the shift from 2-D exploration to 3-D exploration techniques was evident. With 3-D seismic techniques the total 3-D subsurface can be properly imaged. It is obvious that the seismic industry has benefited a lot from the advances in computer technology in recent years, but today the problem in seismic data processing is still to find efficient and accurate algorithms to handle the enormous data volumes involved in 3-D seismic processing.

Wave field extrapolation lies at the basis of advanced seismic processing. Here, from the measurements of the seismic wave field at the surface, the field at points in the subsurface is reconstructed. This thesis describes a method of wave field extrapolation, that can

efficiently reconstruct the wave field at a certain depth from surface measurements for a three-dimensional inhomogeneous subsurface. The scheme results in seismic data as if they were measured in the subsurface instead of measurements done at the surface of the earth.

1.2   THE SEISMIC EXPERIMENT

In this section a seismic experiment will be described and a few basic seismic principles will be reviewed. It is not in the scope of this thesis to give a detailed description the full range of seismic acquisition and processing techniques. The main purpose of this section is to give the non-expert reader a basic understanding of the seismic method. The goal of seismic exploration is to provide the geologists with information on the structure of the subsurface of the earth. With this information they may decide to choose an optimum location for drilling an exploration well in search for oil and gas reservoirs.

I will now outline the global steps of a seismic experiment as illustrated in figure 1.1. At the surface of the earth a seismic source transmits seismic waves into the subsurface. Depending on the local situation different types of sources can be used, e.g. dynamite, vibroseis or air guns. The seismic source wave field propagates downward into the earth. At each velocity and/or density contrast in the subsurface part of the seismic source wave field is reflected and will propagate upward to the surface. The vibrations of these waves are measured at many positions at the surface as a function of time. In fact seismic measurements can be seen as a sampled (in both the spatial and the temporal direction)
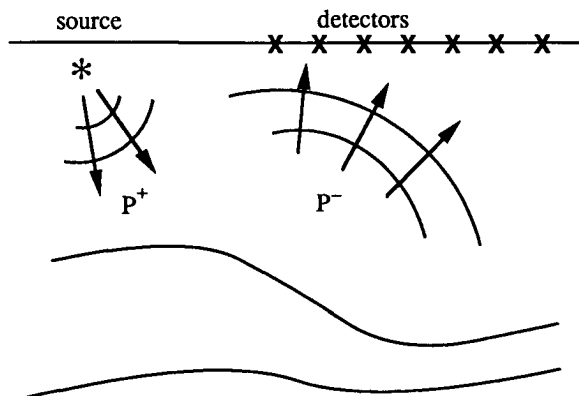
Figure 1.1:   In a seismic experiment the subsurface is illuminated by a downward propagating source wave field (P^+). This source wave field gets reflected at layer interfaces and the reflected waves (P^-) propagate upwards to the surface.

version of the upcoming wave field at the surface. All data associated with one source location is called a seismic shot record.

In a seismic survey the single seismic experiment, as described above, is repeated for many source locations, so that a seismic data set consists of many shot records.

In 2-D seismic exploration the sources and receivers are (as much as possible) positioned along a line at the surface, where it is assumed that the earth is largely two dimensional, which means invariant in one lateral direction (perpendicular to the line of measurement).

Actually the earth's subsurface is three-dimensional. Therefore in the last years the amount of 3-D seismic surveys increased enormously, when it became economic to perform such measurements. In a 3-D survey sources and receivers are positioned along an area at the surface of the earth. In this way a 3-D image of the subsurface below the acquisition area can be obtained.

Finally, let us consider the size of a typical 3-D seismic survey. A large 3-D survey may cover an area of about 30 x 40 km and consists of about 1 Terabyte (10^{12} byte) of information. It is expected that this size will even grow in the near future. The enormous amount of data of a 3-D survey is one of the most important problems in 3-D data processing.

1.3   SEISMIC PROCESSING

In the previous section a seismic experiment was outlined and in this section the aim of seismic processing is described. Also some aspects of conventional processing schemes versus the scheme, described in this thesis are discussed. For a thorough description of seismic processing techniques one is referred to text books, like those of Hatton et al. (1986) and Yilmaz (1987).

In the previous section it was mentioned that seismic data contain the measurements at the surface of the reflected wave fields as a function of time. The aim of seismic processing is to obtain from all available measurements an image of the subsurface as a function of depth. In order to obtain this image, inversion for two effects of wave propagation is necessary, namely spatial dispersion and refraction of the waves at velocity contrasts in the subsurface.

Most of the available seismic processing techniques are oriented around Common MidPoint (CMP) gathers. The data are reordered in such a way that the source and detector positions lie symmetric around certain midpoints. To these CMP data a hyperbolic correction is

applied (the Normal Move-out correction) and these corrected data are summed (stacked). This process will be referred to as CMP stacking. The resulting data set, called the stacked section, is an approximation for a data set where source and detector positions coincide (zero offset). In this way the volume of the data is reduced and the signal-to-noise ratio is improved. Theoretically the hyperbolic correction is correct for homogeneous media only. In case of velocity variations this correction is invalid and the CMP stacking process will reduce the quality of the final processing result. In practice, especially in 3-D acquisition, it is often very difficult to position sources and receivers such that they have a certain midpoint in common. This additional problem of CMP oriented methods is called the binning problem.

The second step in standard seismic processing is migration of the stacked data. In practice time migration is the most usual method. Here a hyperbolic operator is applied to the stacked data. In this way the data may be focussed correctly, but because Snell's law (refraction) is not taken into account the events are not positioned correctly, when lateral velocity variations are present in the subsurface. The correct way of migration is generally referred to as depth migration. In depth migration Snell's law is incorporated. In addition to a proper focussing of diffraction energy, reflection energy is transferred to their correct spatial position. To do this the global propagation properties of the subsurface must be known. In section 1.4 the macro subsurface model, which defines the propagation properties, will be described in more detail.

By applying migration after CMP stacking at the surface (poststack migration), the limitations of CMP stacking still hold. A way to avoid the problems of CMP stacking is shot record migration. Such a scheme works directly on shot records (prestack migration). Here for each shot record the propagation effects are eliminated by wave field extrapolation. Finally the migrated results for all shot records are summed (stacked) for each depth point, the so called Common Depth Point (CDP) stacking. By working per shot record instead of per CMP the binning problem is avoided. Note that the main difference between poststack and prestack migration is, that in prestack migration the stacking is performed at points located in the subsurface after elimination of the propagation effects, while for poststack migration the stacking is performed at the surface.

In this thesis a method for 3-D depth processing of seismic shot records is presented. In the extrapolation of the shot records Snell's law is properly incorporated. With this scheme accurate 3-D prestack processing becomes feasible with current computer technology. This efficient scheme is outlined in section 1.5.

1.4 MACRO MODEL AND DETAIL

In section 1.2 and 1.3 of this chapter I discussed the basic principles of the seismic exploration method. A seismic wave propagates downward into the subsurface, gets reflected at inhomogeneities and propagates upward to the surface, where it is detected. It is clear that in order to process seismic data we have to deal with two effects, namely propagation and reflection.The subsurface of the earth consists of a number of main layers, that often correspond to different geologic eras. Within these main geologic eras many small layers were deposited. These small layers cause detailed variations in the propagation velocities of the seismic waves. However, the propagation properties of the subsurface can be largely described by the average propagation velocities of the main geologic layers. In figure 1.2 an example of the vertical velocity profile is given. A clear trend can be seen due to the main layers and detailed velocity variations of the fine layering are superimposed.
The model containing the main geological layers with average propagation velocities will be called the macro subsurface model. Peels (1988) demonstrated that even large velocity variations in the detailed structure of the subsurface has no serious effect on the propagation properties of the subsurface.

On the other hand, the reflectivity properties of the subsurface are mainly determined by the detailed velocity variations. The trend information in the macro model mainly determines
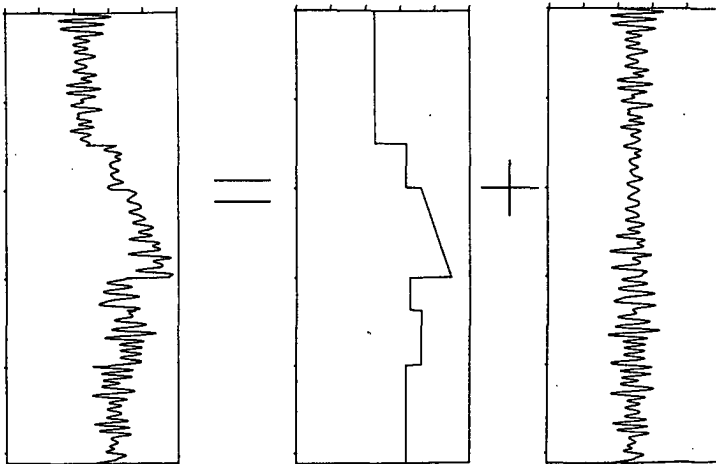
Figure 1.2: An example of a vertical velocity profile of the subsurface. This velocity profile consists of a trend, which determines the propagation properties and detailed velocity variations, which determines the reflectivity properties of the subsurface.

source

0 ×─×─×─×─×─○─×─×─×─×─× ←── detectors for
                                    reflected
                                    wave field

3000 m/s

depth   400

(m)   2000 m/s

                                                  detectors for
800   × × × × × × × × × × ×   ←── propagated
                                                  wave field
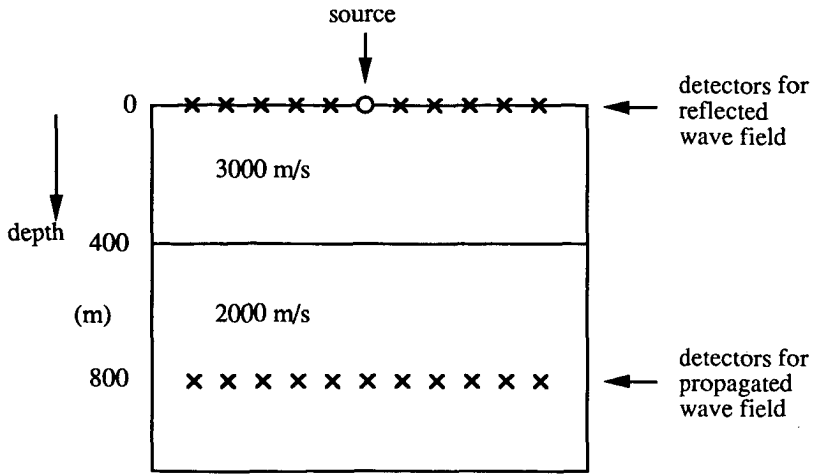
Figure 1.3:   Subsurface model used to describe the effect of different parameterization on the
propagation and reflection properties of the subsurface. The model consists of a single
interface and for a source at the surface both the reflected wave field at z = 0 m and the
propagated wave field at z = 800 m are modeled.

velocity
0   3000

350
depth

400

450

REFLECTION   PROPAGATION

0.0

0.5

1.0

1.5

(s)
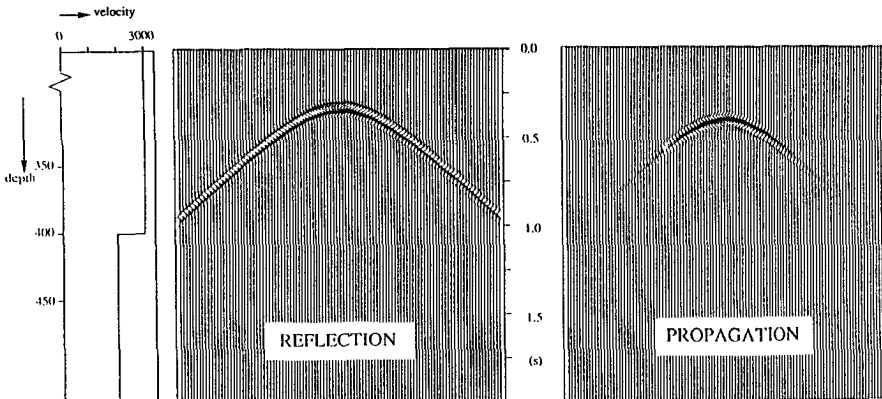
Figure 1.4:   For a blocked subsurface model (a) the reflected wave field at z = 0 m (b) and the
propagated wave field at z = 800 m (c) are modeled.
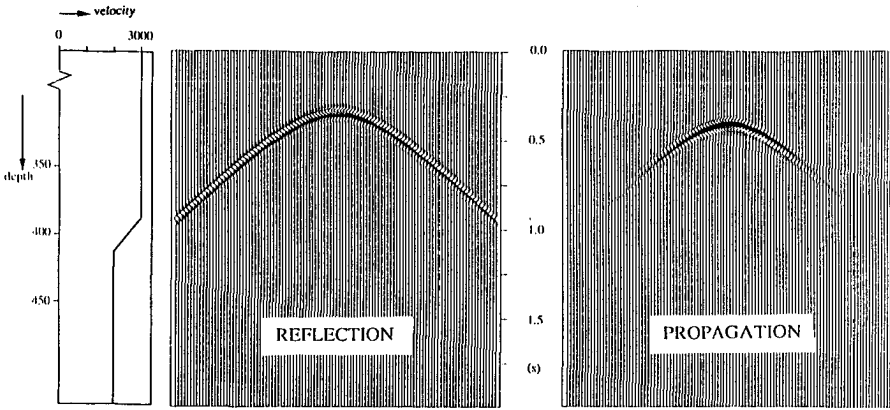
Figure 1.5: The velocity contrast is smoothed linearly over 25 m (a). The reflected (b) and propagated wave fields (c) are modeled.
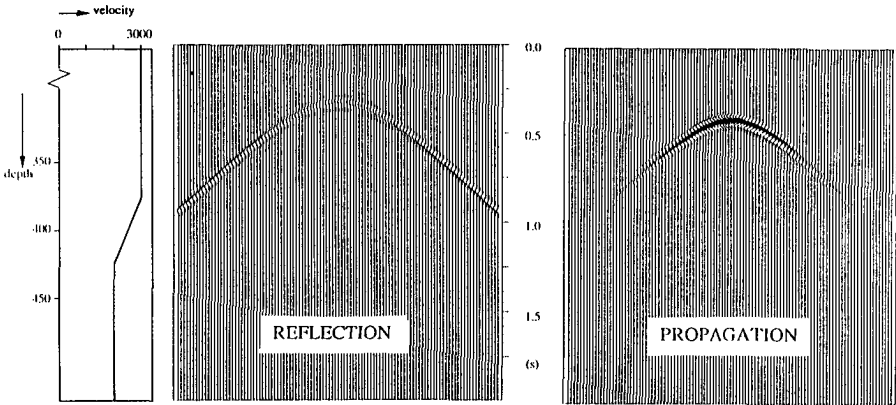
Figure 1.6: The velocity contrast is smoothed linearly over 50 m (a). The reflected (b) and propagated wave fields (c) are modeled.
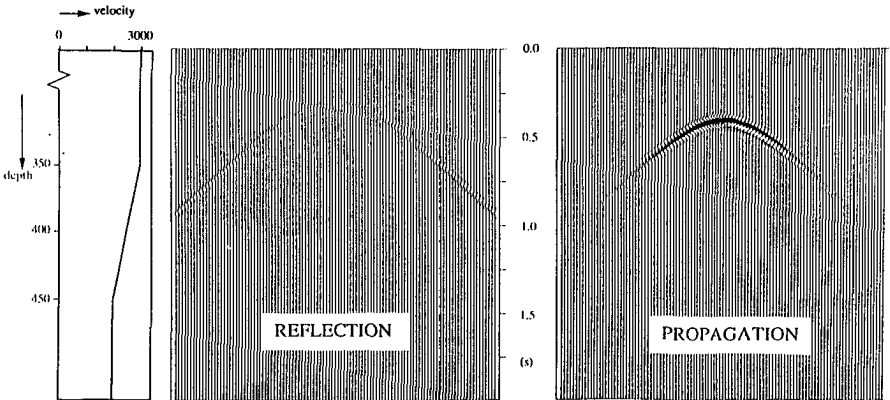
Figure 1.7: The velocity contrast is smoothed linearly over 100 m (a). The reflected (b) and propagated wave fields (c) are modeled.

blocked
·········· smoothed 25 m
····· smoothed 50 m
—–— smoothed 100 m
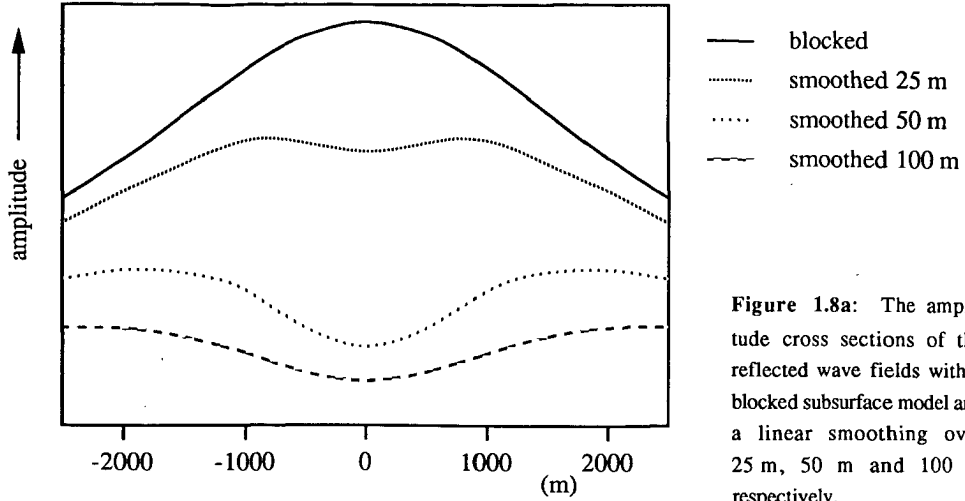
Figure 1.8a: The amplitude cross sections of the reflected wave fields with a blocked subsurface model and a linear smoothing over 25 m, 50 m and 100 m respectively.
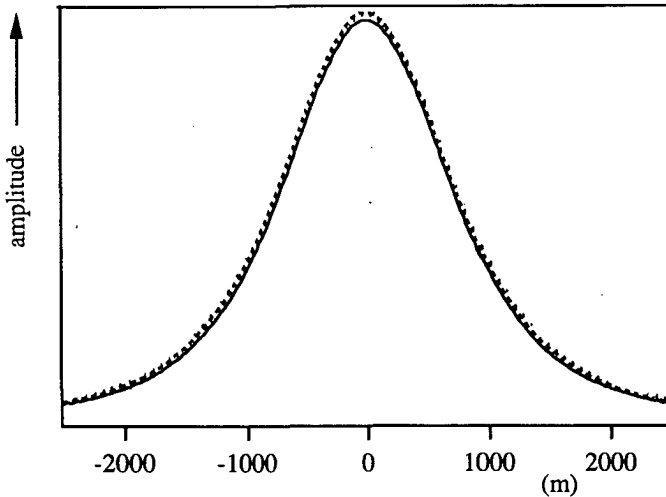
Figure 1.8b: The amplitude cross sections of the propagated wave fields with a blocked subsurface model and a linear smoothing over 25 m, 50 m and 100 m respectively.

the travel times in the seismic data, while the detail has a large effect on the amplitudes in the measurements. The aim of migration is to get a proper image of the reflectivity of the subsurface. In order to obtain a correct image of the reflectivity a crucial step in migration is the elimination of the propagation properties, determined by the macro subsurface model. Because of their different nature, the macro model has to be estimated in a different manner and separately from the detailed information.

Both the macro model and the detail can be described by the velocity and density distribution and no clear separation can be made between trend and detail, but the difference can be expressed by the parameterization of the subsurface model. Using a simple example I will illustrate the effect of different parameterization on the reflectivity and on the propagation of seismic waves. The model, depicted in figure 1.3, consists of two

layers with propagation velocities of 3000 m/s and 2000 m/s respectively. At the surface a point source is located at x = 500 m with a frequency content of 0 to 40 Hz. This means, that for the central frequency of 20 Hz the source field has a wave length of 100 m in the lower layer. In figure 1.4a a vertical velocity profile of the subsurface model is shown. The reflected wave field, measured at the surface, is shown in figure 1.4b. The source wave field at z = 800 m below the layer interface is shown in figure 1.4c. Next the velocity contrast is smoothed over an area of a quarter of the typical wave length (25 m), half the wave length (50 m) and over one wave length (100 m). For these models also the reflection and propagation effects were modeled. In figure 1.5 the results for smoothing over 25 m are shown. Figure 1.5a shows the vertical velocity profile and in figure 1.5b and 1.5c the reflected and propagated wave fields are shown respectively. In the same way in figure 1.6 the results for a model smoothed over 50 m and in figure 1.7 for smoothing over 100 m are shown. Finally in figure 1.8a the amplitude cross sections are shown for the reflected waves and in figure 1.8b for the propagated waves.

From these figures it can be concluded, that the smoothing of the subsurface model has a large effect on the reflectivity. The reflectivity, determined by the detail in the model, is strongly dependent on the local velocity and density contrasts. Therefore in a smoothed subsurface model the reflections are much lower than in a blocked subsurface model.

The type of parameterization has little effect on the wave propagation. There is only a small difference on the propagated wave field for a blocked subsurface model and for the smoothed models. Therefore the macro subsurface model can be characterized by a small number of parameters for calculating the wave propagation.

1.5 OVERBURDEN AND TARGET ZONE

In section 1.3 the aim and basic principles of seismic data processing were explained. Until now shot record migration of 3-D data is not feasible, because of the huge amount of data and the extreme long computation times. By limiting the output of the migration scheme to the detailed reflectivity of just a small part of the subsurface, the target zone, the efficiency can be improved significantly. Such a target-oriented migration scheme makes 3-D prestack processing feasible on current computer systems. In this approach the subsurface is separated into two parts (see figure 1.9).

The part in which the geologists are especially interested is called the target zone. This part of the subsurface can be indicated as a possible candidate for hydrocarbon reserves. The detail of the other part is generally of interest to the geologist. The part of the subsurface that is on top of the target zone is called the overburden. The seismic response of the target zone has thus traveled twice through the overburden. Firstly during the downward
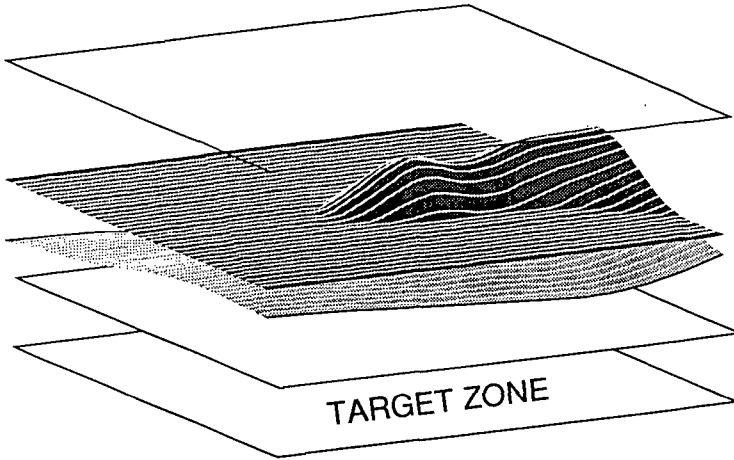
Figure 1.9a: The 3–D subsurface can be separated into two parts, an overburden and a target zone in which the geologist is especially interested.
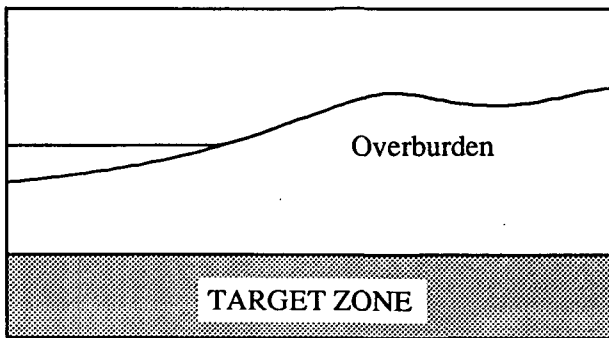
Figure 1.9b: 2–D cross section through the 3–D volume of figure 1.9a.

propagation of the source wave field and secondly during the upward propagation of the reflected waves.

The propagation through the overburden has distorted the image of the target zone considerably. Due to geometrical spreading and refraction at interfaces, the response of the target zone at the surface can often not be easily interpreted. As mentioned before, the

effects of the overburden (= propagation) can be accurately described by the macro subsurface model and, therefore the overburden need not be described in detail. By limiting the output of the migration to a detailed reflectivity image of the target zone, target-oriented migration, 3-D shot record migration becomes feasible on current computers. This approach to 3-D migration is investigated in the TRITON project (TRITON, 1985). This target-oriented scheme consists of a number of separate steps (figure 1.10):
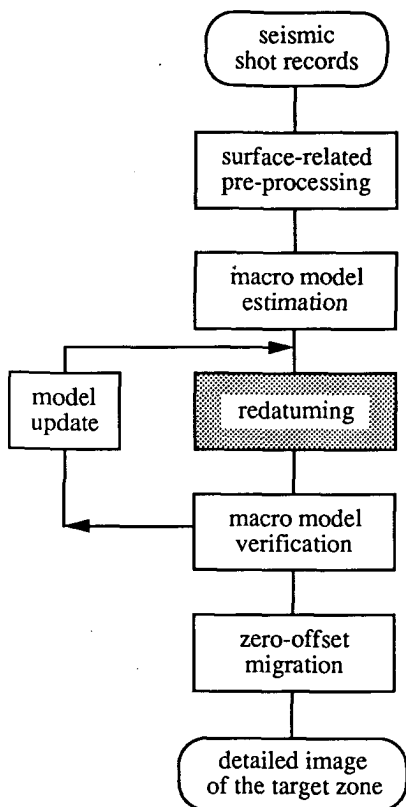
Figure 1.10: Target oriented approach to 3–D migration. This thesis will focuss on the redatuming step in this scheme.

1) *Surface related pre-processing*
Here the surface related multiples are eliminated. After this step the reflecting surface is effectively replaced by a reflection free surface.

2) *Estimation of the macro subsurface model*
There are several ways to estimate the macro model. The best known method are Dix's formula (1955) and the extensions made by Hubral (1976). However, these methods apply only for very simple subsurfaces. The more realistic travel time inversion method is based on parametric inversion (Van der Made, 1988).
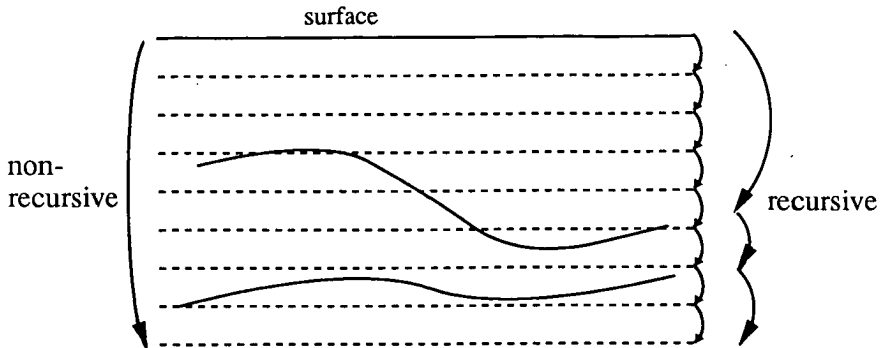
Figure 1.11:   Non-recursive versus recursive wave field extrapolation. The wave field at a certain level can be calculated directly from the wave field at the surface (non-recursive) or via a number of intermediate levels (recursive).

3) *Redatuming of the data at the surface to the upper boundary of the target zone*
In this step the surface data are extrapolated to the target upper boundary and there 'genuine' zero offset data are generated. The distorting propagation effects of the overburden are eliminated in this step. This thesis describes the extraplation step of the 3-D target-oriented migration scheme.

4) *Verification of the macro subsurface model*
After redatuming it is checked whether the used macro subsurface model was correct. Depending on the errors, the data can be corrected (residual NMO correction) or the model can be updated. This method is described by Jeannot et al. (1986) and Cox et al. (1988).

5) *Zero offset depth migration within the target zone*
Finally the zero offset output data of the redatuming scheme are migrated. It results in a detailed depth section of the target zone. An efficient 3-D migration scheme is described Blacquière et al. (1989).

Wave field extrapolation from the surface to the upper boundary of the target zone plays a key role in redatuming. There are two distinct methods of wave field extrapolation, recursive and non-recursive wave field extrapolation (figure 1.11). In non-recursive wave field extrapolation the wave field at a certain depth level is calculated in one step from the wave field at the surface. In recursive extrapolation the wave field is calculated via a number of intermediate levels. For recursive wave field extrapolation with small depth steps the medium is generally assumed to be locally homogeneous, which means that the

used operators can be calculated analytically. Much attention has to be paid to operator aliasing and truncation (see Blacquière et al., 1989). Recursive wave field extrapolation can also be performed via the macro boundaries of the overburden. This type of extrapolation is described by Peels (1988). In non-recursive extrapolation the operators must describe wave propagation through a complex inhomogeneous medium in one step. Therefore in the calculation of these operators modeling algorithms, like e.g. ray tracing, Gaussian beams or finite differences, have to be used (see Kinneging et al., 1989). On the other hand, the extrapolation itself will be very efficient, because it is done in one step. The choice for one of these methods depends highly on the application. In the case, where the wave field does not need to be known in the entire medium, like in redatuming, a non-recursive wave field extrapolation is generally preferred over a recursive one. When also the wave field at the intermediate levels has to be known, as in migration, recursive extrapolation is preferred.

Until now a laterally oriented target zone below an overburden (figure 1.12a) was considered. This is the most common situation and it will be referred to as a *reservoir oriented* target zone. One can also think of a vertically oriented target zone (figure 1.12b) around a possible well location, a *well oriented* target zone. In this way valuable information can be efficiently obtained before the drilling of a well. This information can also be used to verify the correctness of the macro subsurface model, as described by Cox et al. (1988). Hence, the concept of redatuming also applies for a vertical target.
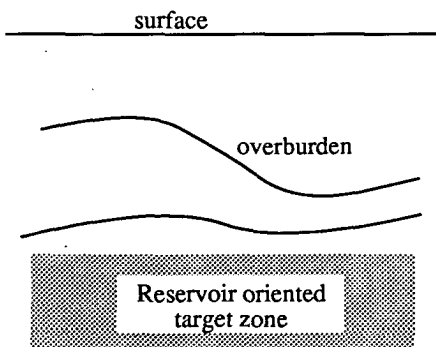
Figure 1.12a: A laterally oriented target zone or a reservoir target zone.
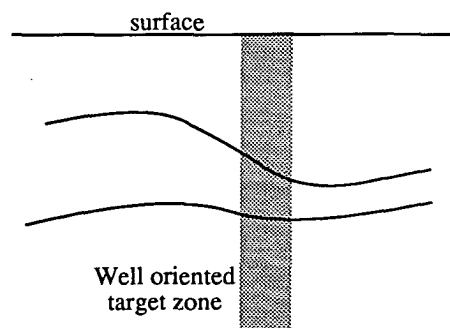
Figure 1.12b: A vertically oriented target zone located around a possible well location (well oriented target zone).

1.6 OUTLINE OF THIS THESIS

Chapter 2 gives the theoretical background to wave field extrapolation and redatuming. The principles of target-oriented processing are formulated in a mathematical sense, using the matrix notation to describe seismic experiments.

In chapter 3 special attention is paid to the design and implementation of 2-D and 3-D non-recursive extrapolation operators. A comparison is made between two methods, namely the "ray tracing method" and the "Gaussian beam" method. With simple extrapolation examples it will be shown that these methods work well. Especially the Gaussian beam method has a good amplitude behavior.

Chapter 4 treats the implementation of the actual redatuming scheme. For the 3-D implementation attention must be paid to efficiency and data flow considerations. If the geometry for land data acquisition is taken into account a very efficient scheme can be developed by using the fact that the detector positions may be common for many shot records.

The results of the redatuming scheme are shown in chapter 5. First the results for numerically modeled input data are shown. Next the results are discussed for input data measured over a scale model in a water tank.

Thirdly the results of redatuming of 2-D field data are shown and compared to the results of full prestack migration. Finally an example is given of shot record redatuming of 3-D modeled data.

In two appendices the Gaussian beam modeling algorithm and a prestack modeling algorithm based on raytracing are discussed.

2

THEORETICAL ASPECTS OF SHOT RECORD REDATUMING

2.1 INTRODUCTION

In seismic redatuming and migration wave field extrapolation plays a very important role. Therefore in this chapter wave field extrapolation, both forward and inverse, will be described in terms of the Kirchhoff (or Helmholtz) and Rayleigh integrals. These integrals are not suited for direct use in seismic applications. Ideally the Kirchhoff integral should be evaluated over a closed surface. In seismics, however, the measurements are only available at the surface of the earth. With some approximations, like neglecting evanescent waves and allowing second order amplitude errors, the integrals can be used also for the seismic situation.

The matrix notation will be introduced to describe a monochromatic physical experiment. This notation holds for both 2-D as well as for 3-D experiments. By using the matrix notation we have a simple and clear formulation, that is suited for the discrete measurements and is close to the actual implementation on a computer.
We will see that the formulation of the redatuming algorithm, for the full multi-shot experiment as well as for the shot record approach, is rather straightforward when the matrix notation is used.

2.2 FORWARD WAVE FIELD EXTRAPOLATION

In general, seismic waves consist of compressional and shear waves. In practice the shear waves are often neglected and the extrapolation of the compressional waves is used. In the DELPHI project (1988) a scheme is proposed to decompose the multi-component seismic data at the surface into separate primary compressional and shear wave fields. Each wave field can then be handled with the same algorithms developed for acoustic processing. In this thesis acoustic waves are handled, but application of the scheme to elastic waves is possible, after decomposition.

Propagation of acoustic waves is described for a source free medium by the well known acoustic wave equation,

$$\rho \nabla \cdot \left[\frac{1}{\rho} \nabla p\,(r,t) \right] - \frac{1}{c^2} \frac{\partial^2 p(r,t)}{\partial t^2} = 0 \quad , \tag{2.1a}$$

where $\rho(r)$ is the mass density distribution,

             $p(r,t)$ is the pressure field at position $r = (x,y,z)$ and time t

and $c(r)$ is the propagation velocity of the acoustic waves.

This wave equation can be transformed to the frequency domain by the Fourier transformation defined as,

$$P(r,\omega) = \int\limits_{-\infty}^{\infty} p(r,t)\, e^{-i\omega t}\, dt \quad , \tag{2.1b}$$

where $P(r,\omega)$ represents the acoustic pressure field in the frequency domain

and $\omega = 2\pi f$ is the circular frequency.

The wave equation in the frequency domain reads

$$\rho \nabla \cdot \left[\frac{1}{\rho} \nabla P\,(r,\omega) \right] + k^2 P\,(r,\omega) = 0 \quad , \tag{2.1c}$$

where $k = \omega/c$ is the wave number.

Now consider the volume V bounded by the closed surface S as depicted in figure 2.1 with the normal vector n pointing outwards. If we assume that volume V is source free we can write for the Kirchhoff integral in the time domain.

$$p(r_A,t) = \int\limits_{-\infty}^{\infty} \oint\limits_{S} \frac{-1}{\rho(r)} \left[p(r,\tau) \frac{\partial g(r,r_A,t-\tau)}{\partial n} - \frac{\partial p(r,\tau)}{\partial n} g(r,r_A,t-\tau) \right] dS\, d\tau \quad , \tag{2.2a}$$

with $r_A = (x_A,y_A,z_A)$ the point inside V for which the wave field is calculated.
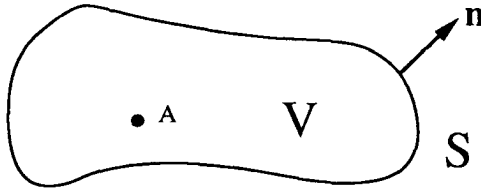
Figure 2.1: The wave field inside a source free volume V can be found by evaluating the Kirchhoff integral over the closed surface S.

The Green's function $g(r,r_A,t)$ is defined by the following equation inside V,

$$\rho \nabla \cdot \left[\frac{1}{\rho} \nabla g\, (r,r_A,t) \right] - \frac{1}{c^2} \frac{\partial^2 g\,(r,r_A,t)}{\partial t^2} = -\rho\delta\,(r-r_A)\,\delta(t) \quad . \tag{2.2b}$$

The differential equation (2.2b) has two types of solutions (forward and backward propagating). In evaluating the expressions for *forward* wave field extrapolation the causal solution of equation (2.2b) will be used,

$$g(r,r_A,t) = 0 \quad \text{for } t < 0 \quad .$$

In the following I will refer to this solution as the *forward propagating* Green's wave field.

The Kirchhoff integral in the frequency domain is often referred to as the Helmholtz integral. In this thesis, however, I will refer to the integrals as Kirchhoff integral in both domains. In the frequency domain the Kirchhoff integral reads,

$$P(r_A,\omega) = \int_S \frac{-1}{\rho(r)} \left[P(r,\omega) \frac{\partial G(r,r_A,\omega)}{\partial n} - \frac{\partial P(r,\omega)}{\partial n} G(r,r_A,\omega) \right] dS \quad , \tag{2.3a}$$

where the forward propagating Green's function $G(r,r_A,\omega)$ in the frequency domain is defined by,

$$G(r,r_A,\omega) = \int_{-\infty}^{\infty} g(r,r_A,t)\, e^{-i\omega t}\, dt \quad , \tag{2.3b}$$

with $g(r,r_A,t)$ being the causal Green's function defined above. Note that $G(r,r_A,\omega)$ satisfies the following wave equation,

$$\rho \nabla \cdot \left[\frac{1}{\rho} \nabla G\,(r,r_A,\omega) \right] + k^2 G\,(r,r_A,\omega) = -\rho\delta\,(r-r_A) \quad . \tag{2.3c}$$

The Green's function $G(\mathbf{r},\mathbf{r}_A,\omega)$ describes the pressure at $\mathbf{r}$ for the wave field from a point source at $\mathbf{r}_A$. For a homogeneous medium the forward propagating solution of equation (2.3c) in the frequency domain reads,

$$G(\mathbf{r},\mathbf{r}_A,\omega) = \frac{\rho}{4\pi} \frac{e^{-ik|\mathbf{r}-\mathbf{r}_A|}}{|\mathbf{r}-\mathbf{r}_A|} \quad . \tag{2.3d}$$

In the following I will consider again arbitrarily inhomogeneous media. Note also that the Green's function is defined by equation (2.2b) or (2.3c) with the medium inside volume V equal to the actual medium. Outside volume V the medium can be chosen freely.

The Kirchhoff integral states that the wave field $P(\mathbf{r}_A,\omega)$ at any point inside a source free volume V can be calculated from the pressure field $P(\mathbf{r},\omega)$ and its normal derivative at the closed surface S around that volume V.

In seismics, however, measurements are never available on a closed surface. From the wave field at the earth's surface the field at any point in the subsurface must be calculated. Therefore consider the geometry of figure 2.2, consisting of an infinite surface S_0 and a hemisphere S_1 with radius R going to infinity. The Sommerfeld radiation condition, which is described by a.o. Bleistein (1984), states that the contribution of the Kirchhoff integral over S_1 vanishes. So the Kirchhoff integral may be replaced by the integral over S_0 only,

$$P(\mathbf{r}_A,\omega) = \int_{S_0} \frac{-1}{\rho} \left[P \frac{\partial G}{\partial n} - \frac{\partial P}{\partial n} G \right] dS_0 \quad . \tag{2.4}$$
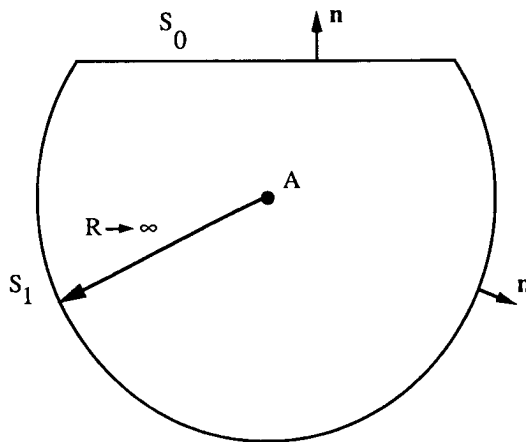

Figure 2.2: Geometry to calculate the Kirchhoff integral for the seismic situation.

In the DELPHI project (1988) a preprocessing method is proposed for decomposition and multiple elimination at the surface. The result of this step is that the reflecting surface is effectively replaced by a homogeneous upper half space; in this way the surface S_0 can be assumed reflection free.

Berkhout and Wapenaar (1989) show that for the geometry of figure 2.2 and a reflection free surface the *one-way* Rayleigh integral can be derived from the Kirchhoff integral (2.4). At the (reflection free) surface the pressure wave field is split into downgoing (P^-) and upgoing (P^+) waves

$$P = P^+ + P^- \text{ at } S_0 \ . \tag{2.5a}$$

The Green's wave fields can be decomposed in the same way into an upgoing and a downgoing part. For the Green's function the entire upper half space, including the surface is also chosen to be reflection free, so the Green's wave field at the surface has an upgoing part only (the source of G^- is at A *below* S_0):

$$G = G^- \text{ at } S_0 \ . \tag{2.5b}$$

Berkhout and Wapenaar (1989) show that, when the Green's wave field and the actual pressure field at S_0 have the same propagation direction, the Kirchhoff integral vanishes. For a Green's wave field and a pressure wave field with opposite propagation directions the terms do not vanish. (This important property will also be used later on in the derivation for inverse wave field extrapolation).

In this way the Kirchhoff integral can be simplified to the one-way Rayleigh I integral,

$$P(r_A,\omega) = 2\int\int_{x \ y} \left[\frac{-1}{\rho(r)} \frac{\partial P^+(r,\omega)}{\partial z} \ G^-(r,r_A,\omega) \right]_{z=z_0} dx \ dy \ , \tag{2.6}$$

or the one-way Rayleigh II integral,

$$P(r_A,\omega) = 2\int\int_{x \ y} \left[\frac{1}{\rho(r)} P^+(r,\omega) \frac{\partial G^-(r,r_A,\omega)}{\partial z} \right]_{z=z_0} dx \ dy \ . \tag{2.7}$$

For a complete derivation of these one-way Rayleigh integrals the reader is referred to Berkhout and Wapenaar (1989).

The Rayleigh integrals (2.6) and (2.7) state that the pressure wave field $P(r_A, \omega)$ at any point in the subsurface can be calculated from the downgoing part of the pressure field at the surface. This calculation is called *forward* wave field extrapolation, because the direction of wave field extrapolation is the same as the direction of wave propagation at z_0. Relations (2.6) and (2.7) are valid for arbitrarily inhomogeneous media. The only assumption is that at $z = z_0$ the wave fields may be split into downgoing and upgoing waves.

Note the important role of the Green's function in the Rayleigh integral. In principle, the Green's function can be generated by any available modeling scheme. In chapter 3 much attention is paid to an efficient calculation of the Green's function.

2.3 INVERSE WAVE FIELD EXTRAPOLATION

For inverse wave field extrapolation the wave field must be extrapolated in the direction opposite to the wave propagation. This means *towards* (secondary) sources located in the subsurface.

This makes a different approach to the Kirchhoff integral necessary (Wapenaar et al., 1989). In the expressions for forward extrapolation the causal solution of equation (2.2b) for the Green's function was used. For inverse extrapolation the anti-causal or backward propagating solution will be used. In the frequency domain this anti-causal Green's function is the complex conjugate of the causal solution in case of loss-less media. Note that this backpropagating Green's function represents a wave field propagating towards 'source' point A at $r = r_A$.

The Kirchhoff integral, that uses this backpropagating Green's function reads,

$$P(r_A, \omega) = \oint_S \frac{-1}{\rho} \left[P \frac{\partial G^*}{\partial n} - \frac{\partial P}{\partial n} G^* \right] dS \quad , \tag{2.8}$$

where the integral is again evaluated over a closed surface S around a source free volume V.

Because we want to extrapolate towards (secondary) sources in the subsurface, a hemi-sphere of infinite extent would contain the sources and can thus not be used. Therefore consider the geometry depicted in figure 2.3 to evaluate the Kirchhoff integral, where the (secondary) sources are located below surface S_1.

The Kirchhoff integral (2.10) is written in three main parts,

$$P(r_A, \omega) = P_0(r_A, \omega) + P_1(r_A, \omega) + P_\infty(r_A, \omega) \quad , \tag{2.9a}$$

with

$$P_0(r_A,\omega) = \int\limits_{S_0} \frac{-1}{\rho}\left[P\frac{\partial G*}{\partial n} - \frac{\partial P}{\partial n}G*\right] dS_0 \quad , \tag{2.9b}$$

$$P_1(r_A,\omega) = \int\limits_{S_1} \frac{-1}{\rho}\left[P\frac{\partial G*}{\partial n} - \frac{\partial P}{\partial n}G*\right] dS_1 \quad , \tag{2.9c}$$

and

$$P_\infty(r_A,\omega) = \int\limits_{S_\infty} \frac{-1}{\rho}\left[P\frac{\partial G*}{\partial n} - \frac{\partial P}{\partial n}G*\right] dS_\infty \quad . \tag{2.9d}$$

Now the separate contributions over the three parts of surface S will be investigated more closely. First the contribution over S_∞ will be examined. Letting the distance r from A to S_∞ go to infinity, both P and G* decrease in the order of r^{-1}, whereas the size of surface S_∞ increases in the order r. This means that expression (2.9d) decreases in the order r^{-1} for $r \to \infty$. So when the surfaces S_0 and S_1 are approaching infinity the integral over S_∞ (2.9d) vanishes.

(secondary) sources
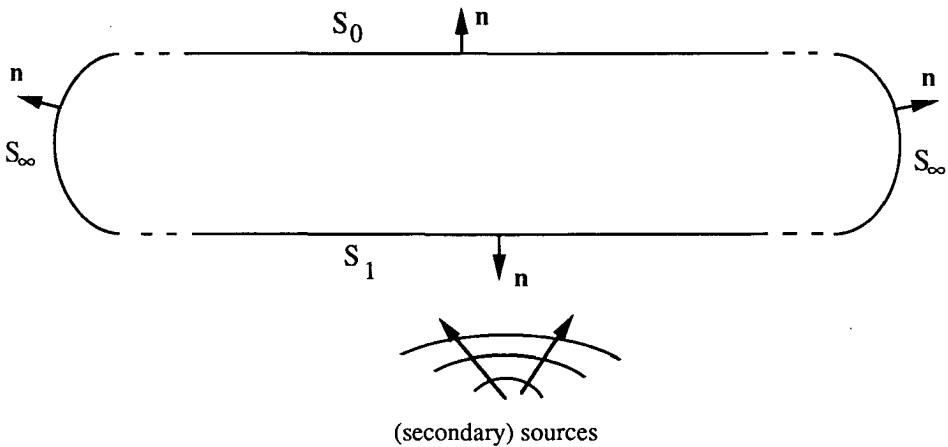
Figure 2.3: Geometry to derive the expressions for inverse wave field extrapolation.

Next, at the surfaces S_0 and S_1 the wave field and the Green's function are split into upgoing and downgoing parts (see figure 2.4). The actual wave field consists of an up- and downgoing part at both S_0 and S_1 (figure 2.4a):
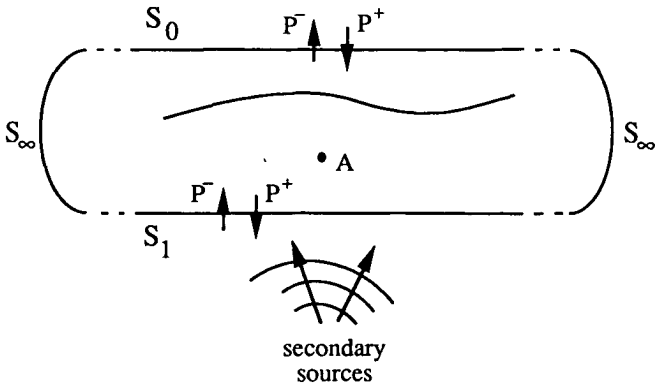
**Figure 2.4a:** The wave field can be split into upward and downward propagating parts at S_0 and S_1.
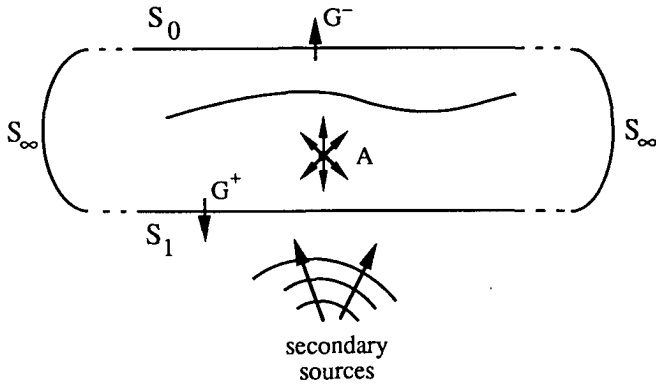
**Figure 2.4b:** The Green's function is upgoing at S_0 and downgoing at S_1.
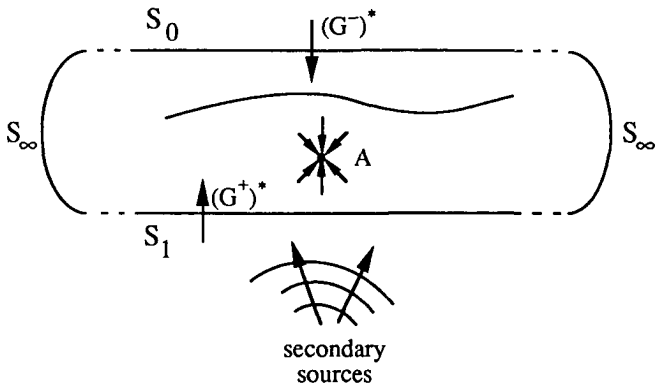
Figure 2.4c: The backpropagating Green's function is downgoing at S_0 and upgoing at S_1.

$P = P^+ + P^-$ at S_0 and S_1 .

The medium outside volume V is chosen reflection free for the Green's function, which means that the Green's function only has an upgoing part at S_0 and a downgoing part at S_1 (figure 2.4a):

$$G = G^- \text{ at } S_0$$

and $\quad G = G^+$ at S_1 .

The backpropagating Green's function is therefore downgoing at S_0 and upgoing at S_1 (figure 2.4c). Using the property that the Kirchhoff integral vanishes (Berkhout and Wapenaar, 1989), when the wave field and the Green's function have the same propagation direction at the integration surface and the evanescent waves are neglected, the integrals (2.9b) and (2.9c) can be written as,

$$P_0(r_A, \omega) = \int_{S_0} \frac{-1}{\rho} \left[P^- \left(\frac{\partial G^-}{\partial n} \right)^* - \frac{\partial P^-}{\partial n} \left(G^- \right)^* \right] dS_0 \tag{2.10a}$$

$$P_1(r_A, \omega) = \int_{S_1} \frac{-1}{\rho} \left[P^+ \left(\frac{\partial G^+}{\partial n} \right)^* - \frac{\partial P^+}{\partial n} \left(G^+ \right)^* \right] dS_1 \quad . \tag{2.10b}$$

Further note that the part of the Green's function that is upgoing at source point A (part 1 in figure 2.5a) contributes to the upgoing reconstructed wave field in A. The part of the Green's function that is downgoing at source point A (part 2 in figure 2.5a) contributes to the reconstruction of the downgoing wave field in A. When point A is chosen infinitely close to surface S_1 and the medium below S_1 is chosen reflection free for the Green's function, the part of the Green's function, that is downgoing in point A, has no contribution at S_0. Therefore integral (2.10a) only reconstructs an upgoing wave field at point A, so

$$P_0(r_A, \omega) = P_0^-(r_A, \omega) \quad . \tag{2.11}$$

The Green's function at S_1 consists of two parts (figure 2.5b), a direct component (G_D^+) and a component (G_S^+), that was scattered by inhomogeneities in volume V. It can be seen that the direct component of the Green's function contributes to the downgoing wave field at A, while the scattered component contributes to the upgoing wave field at A, so

$$P_1(r_A, \omega) = P_1^+(r_A, \omega) + P_1^-(r_A, \omega) \tag{2.12a}$$

with

$$P_1^+(r_A,\omega) = \int_{S_1} \frac{-1}{\rho} \left[P^+ \left(\frac{\partial G_D^+}{\partial n} \right)^* - \frac{\partial P^+}{\partial n} \left(G_D^+ \right)^* \right] dS_1 \quad .$$

(2.12b)

$$P_1^-(r_A,\omega) = \int_{S_1} \frac{-1}{\rho} \left[P^+ \left(\frac{\partial G_S^+}{\partial n} \right)^* - \frac{\partial P^+}{\partial n} \left(G_S^+ \right)^* \right] dS_1 \quad .$$

(2.12c)
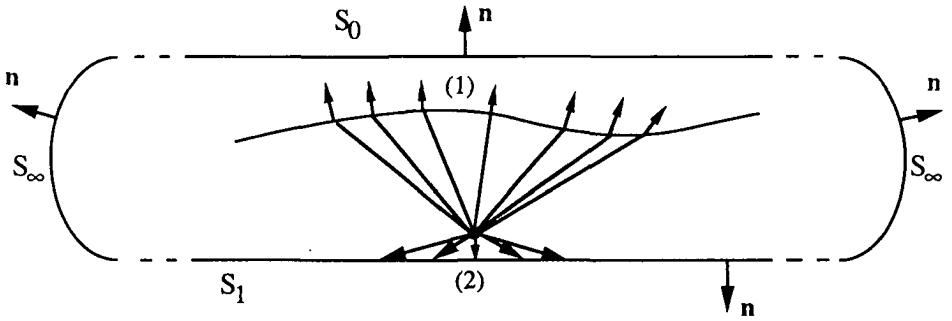
Figure 2.5a: The part of the Green's function that is upgoing at point A reconstructs the upgoing wave field in A. The part of the Green's function that is downgoing at A reconstructs the downgoing wave field in A.
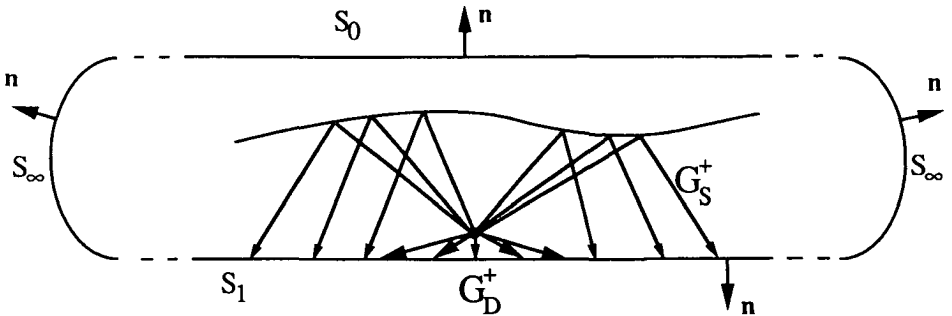
Figure 2.5b: The Green's function at S_1 consists of a direct component G_D^+ and a scattered component G_S^+.

In inverse wave field extrapolation we are only interested in reconstruction of the upgoing wave field in A. Therefore integral (2.12b) is not of interest. For the *upgoing* wave at r_A we write $P^-(r_A,\omega) = P_0^-(r_A,\omega) + P_1^-(r_A,\omega)$ with P_0^- and P_1^- determined by the equations (2.10a) and (2.12c). Note that the latter term contains the product of the scattered field P^+ and the scattered Green's function G_S^+. By omitting this term a second order amplitude error is made (proportional to R^2, where R is the reflectivity of reflectors inside volume V).

In the same way as described in section 2.2 for the forward problem, the Kirchhoff integral for the inverse problem (2.10a) can be transformed into one-way Rayleigh integrals as well. The Rayleigh I integral for inverse extrapolation then reads,

$$P^-(r_A,\omega) \approx 2 \int_x \int_y \left[\frac{-1}{\rho(r)} \frac{\partial P^-(r,\omega)}{\partial z} \left(G^-(r,r_A,\omega) \right)^* \right]_{z=z_0} dx\, dy \qquad (2.13)$$

and the Rayleigh II integral,

$$P^-(r_A,\omega) \approx 2 \int_x \int_y \left[\frac{1}{\rho(r)} P^-(r,\omega) \left(\frac{\partial G^-(r,r_A,\omega)}{\partial z} \right)^* \right]_{z=z_0} dx\, dy \quad . \qquad (2.14)$$

These Rayleigh integrals state that the upgoing wave field at any point A in the subsurface can be (approximately) derived from the upgoing wave field at the surface (pressure or velocity).

I will summarize the assumptions made in (2.13) and (2.14). In the derivation the evanescent waves are neglected and the medium is considered to be lossless. It is assumed that the effects of medium losses are taken into account in a separate deconvolution process. By neglecting the integral over the lower boundary of the source free volume V, second order amplitude errors are made. Note that in current seismic processing these approximations are always made (explicitly or implicitly).

Finally by going from the Kirchhoff integral to the Rayleigh integrals a plane surface is assumed. Peels (1988) compares the use of the Kirchhoff and Rayleigh integrals for non-planar surfaces. His numerical results confirm that in case of strong lateral topography variations the Rayleigh integral breaks down and the Kirchhoff integral should be used.

The Green's function plays a central role, both in the expressions for forward extrapolation (equations 2.6 and 2.7) and in the expressions for inverse extrapolation (equations 2.13

and 2.14). In inhomogeneous media Green's functions (i.e. monopole responses) can be computed by a numerical forward modeling scheme. In chapter 3 much attention is paid to an efficient calculation of these Green's functions.

2.4   MATHEMATICAL DESCRIPTION OF A SEISMIC EXPERIMENT

In the acoustic one-way version of a seismic experiment a source transmits acoustic waves into the earth. These waves propagate downward, get reflected and propagate upward to the surface, where they are detected. In order to perform data processing on seismic measurements these effects must be described in a more quantitative way.

In section 2.2 wave propagation is described in terms of the Kirchhoff and Rayleigh integrals. In this section a convenient notation will be introduced to describe wave propagation, reflection and detection as a series of matrix multiplications. This matrix notation, as introduced by Berkhout (1985) and extended to 3-D by Kinneging et al. (1989), can be used to describe the seismic experiment.

First consider the matrix notation for the 2-D case. The 2-D Rayleigh II integral reads (for notational convenience I leave out the frequency ω),

$$P^+(x_A,z_A) = \int_{-\infty}^{\infty} \frac{2}{\rho(x,z_0)} P^+(x,z_0) \frac{\partial G^-(x,z_0,x_A,z_A)}{\partial z_0} \, dx \quad . \tag{2.15}$$

The 2-D Green's function $G^-(x,z_0,x_A,z_A)$ describes the response at (x,z_0) of a line source at (x_A,z_A). In discrete form this integral reads,

$$P^+(x_i,z_A) = \sum_{k=-\infty}^{\infty} P^+(x_k,z_0) \frac{\partial G^-(x_k,z_0,x_i,z_A)}{\partial z_0} \frac{2\Delta x}{\rho(x_k,z_0)} \quad , \tag{2.16}$$

where $x_k = k \, \Delta x$ is the lateral coordinate at the surface

             $x_i = i \, \Delta x$ the lateral coordinate at $z = z_A$

and Δx is the spatial sampling interval.

Note that the one-way version of the reciprocity theorem states,

$$G^+(x_i,z_A,x_k,z_0) = G^-(x_k,z_0,x_i,z_A) \quad . \tag{2.17a}$$

Let us now define the Green's matrix $G^+(z_A,z_0)$, with at the kth column and the ith row,

$$\left[G^+(z_A,z_0) \right]_{ik} = G^+(x_i,z_A,x_k,z_0) \quad . \tag{2.17b}$$

Furthermore, matrix $M(z_0)$ is a diagonal matrix with at the kth diagonal element,

$$\left[\mathbf{M}(z_0)\right]_{kk} = \frac{2\Delta x}{\rho(x_k, z_0)} \quad . \tag{2.17c}$$

Using equations (2.17a) through (2.17c), equation (2.16) can now be written as a matrix multiplication,

$$\vec{\mathbf{P}}^+(z_A) = \mathbf{W}^+(z_A, z_0)\, \vec{\mathbf{P}}^+(z_0) \quad , \tag{2.18}$$

with

$$\mathbf{W}^+(z_A, z_0) = \left[\partial_{z_0} \mathbf{G}^+(z_A, z_0)\right] \mathbf{M}(z_0) \quad .$$

Here the ith element of the vector $\vec{\mathbf{P}}^+$ contains the monochromatic downgoing part of the acoustic pressure field at $x = x_i = i\,\Delta x$ as visualized in figure 2.6a.

In the forward extrapolation matrix $\mathbf{W}^+(z_A, z_0)$ the column index represents the coordinates at the surface $z = z_0$ and the row index represents the coordinates at the subsurface level $z = z_A$ (see figure 2.6b).
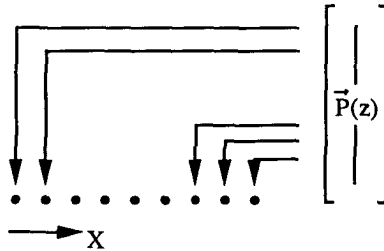
Figure 2.6a: Each element of the data vector $\vec{\mathbf{P}}(z)$ corresponds to one lateral coordinate.
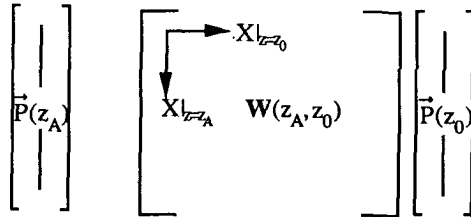
Figure 2.6b: The colums of $\mathbf{W}(z_A, z_0)$ correspond to the surface coordinate. The rows correspond to the coordinate at the target level.

Berkhout (1985) shows that with this notation also reflection of acoustic waves can be written as a matrix multiplication,

$$\vec{P}^-(z) = R(z)\,\vec{P}^+(z) \quad . \tag{2.19}$$

A seismic experiment can now be written in the matrix notation as,

$$\vec{P}^-(z_0) = D(z_0) \sum_{m=1}^{\infty}\left[W^-(z_0,z_m)\,R(z_m)\,W^+(z_m,z_0)\right] \vec{S}^+(z_0) \quad , \tag{2.20}$$

with

$$W^-(z_0,z_m) = \left[\partial_{z_m} G^-(z_0,z_m)\right] M(z_m) \quad ,$$

$$G^-(z_0,z_m) = \left[G^+(z_m,z_0)\right]^T$$

and $\vec{S}^+(z_0)$ the monochromatic downgoing source wave field at the surface.

For one depth level z_m this description is visualized in figure 2.7. The source wave field at the surface, $\vec{S}^+(z_0)$, propagates down into the subsurface, described by extrapolation matrix $W^+(z_m,z_0)$. At the different impedance contrasts in the subsurface the acoustic waves get reflected ($R(z_m)$) and the reflected waves propagate back to the surface, described by $W^-(z_0,z_m)$. At the surface the waves get detected. The influence of the detector pattern can be described by the detector matrix $D(z_0)$.
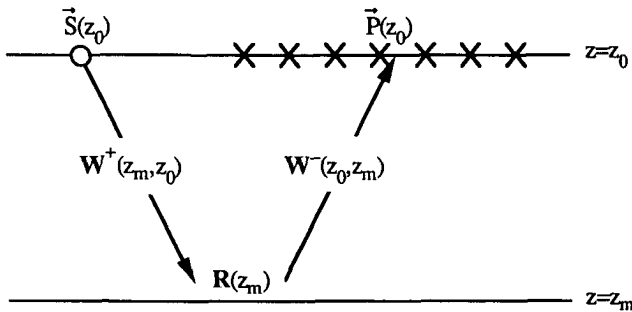
Figure 2.7: Schematic representation for one depth level of a seismic experiment in the matrix notation.

Equation (2.20) describes a single experiment. When we place the vectors $\vec{P}$ and $\vec{S}$ of the different single experiments in the columns of the matrices P and S we can thus describe the full multi-shot experiment in the matrix notation as,

$$\mathbf{P}^-(z_0) = \mathbf{D}(z_0) \sum_{m=1}^{\infty} \left[\mathbf{W}^-(z_0,z_m) \, \mathbf{R}(z_m) \, \mathbf{W}^+(z_m,z_0) \right] \mathbf{S}^+(z_0) \quad . \tag{2.21}$$

For a locally reacting reflector matrix $R(z)$ will be a diagonal matrix with the reflection coefficients on the diagonal elements. In general a reflector will not be locally reacting and then the reflection can be described as a spatial convolution, $R(z)$ will in that case have the form of a band matrix.

In figure 2.8 the representation of the monochromatic multi-experiment data matrix $P(z_0)$ is visualized. By making different cross sections through this data matrix, different data gathers can be found.

The columns of the data matrix represent, as mentioned, the monochromatic single shot experiments or Common-Shot-Gathers. The rows of this matrix represent the detected wave field at one receiver position for all shots, a Common-Receiver-Gather.

Furthermore the diagonals represent the Common-Offset-Gathers with at the central diagonal the zero offset data. Finally the anti-diagonals represent the well known Common-Midpoint-Gathers.
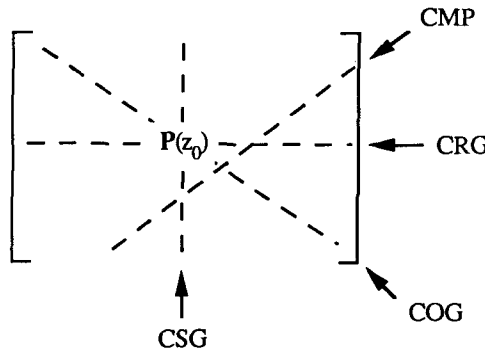
Figure 2.8: Representation of the monochromatic multi-experiment data matrix $P(z_0)$ with the different gathers.

The use of the matrix notation has the advantage, that it is a simple method to describe a seismic experiment. Furthermore, it is very close to implementation on a digital computer.

In addition the method is very well suited to describe wave theory based data processing techniques, like migration and redatuming.

In the following I will show that the matrix notation is also suited for 3-D. Analogous to equation (2.16) the discrete version of the Rayleigh II integral in 3-D reads,

$$P^+(x_i,y_j,z_A) = \sum_{k=-\infty}^{\infty} \sum_{\ell=-\infty}^{\infty} P^+(x_k,y_\ell,z_0) \frac{\partial G^-(x_k,y_\ell,z_0,x_i,y_j,z_A)}{\partial z_0} \cdot \frac{2\Delta x\, \Delta y}{\rho(x_k,y_\ell,z_0)} \cdot \quad (2.22)$$

For 3–D the one-way version of the reciprocity theorem states,

$$G^+(x_i,y_j,z_A,x_k,y_\ell,z_0) = G^-(x_k,y_\ell,z_0,x_i,y_j,z_A) \quad . \quad (2.23a)$$

Analogous to the derivation of the 2–D matrix notation we define a sub-matrix $G^+_{j,\ell}(z_A,z_0)$ with at the kth column and the ith row,

$$\left[G^+_{j,\ell}(z_A,z_0) \right]_{ik} = G^+(x_i,y_j,z_A,x_k,y_\ell,z_0) \quad (2.23b)$$

and the diagonal sub-matrix $M_{\ell,\ell}(z_0)$ with at the kth diagonal element,

$$\left[M_{\ell,\ell}(z_0) \right]_{kk} = \frac{2\Delta x\Delta y}{\rho(x_k,y_\ell,z_0)} \quad . \quad (2.23c)$$

Expression (2.22) can be reformulated as

$$\vec{P}^+_j(z_A) = \sum_{\ell=-\infty}^{\infty} W^+_{j,\ell}(z_A,z_0)\, \vec{P}^+_\ell(z_0) \quad , \qquad j = 1, 2, \dots , J \quad (2.24)$$

with

$$W^+_{j,\ell}(z_A,z_0) = \left[\partial_{z_0} G^+_{j,\ell}(z_A,z_0) \right] M_{\ell,\ell}(z_0) \quad ,$$

where　　　ℓ represents the y-coordinate $y_\ell = \ell\, \Delta y$ at $z = z_0$
and　　　j the y-coordinate $y_j = j\, \Delta y$ at $z = z_A$.

Equation (2.24) can be simplified from a notational point of view by writing the summation over the y-coordinate as a matrix multiplication (see Kinneging et al., 1989),

$$\vec{P}^+(z_A) = W^+(z_A,z_0)\, \vec{P}^+(z_0) \quad , \quad (2.25a)$$

where

$$
\vec{P}^+(z_0) = \begin{bmatrix} \vec{P}^+_1(z_0) \\ \vec{P}^+_2(z_0) \\ \cdot \\ \vec{P}^+_{\ell}(z_0) \\ \cdot \\ \vec{P}^+_L(z_0) \end{bmatrix} , \ \vec{P}^+(z_A) = \begin{bmatrix} \vec{P}^+_1(z_A) \\ \vec{P}^+_2(z_A) \\ \cdot \\ \vec{P}^+_j(z_A) \\ \cdot \\ \vec{P}^+_J(z_A) \end{bmatrix}
\tag{2.25b}
$$

$$
W^+(z_A,z_0) = \left[\partial_{z_0} G^+(z_A,z_0) \right] M(z_0) \ ,
\tag{2.25c}
$$

$$
G^+(z_A,z_0) = \begin{bmatrix} G^+_{1,1}(z_A,z_0) & G^+_{1,2}(z_A,z_0) & - & - & G^+_{1,L}(z_A,z_0) \\ G^+_{2,1}(z_A,z_0) & G^+_{2,2}(z_A,z_0) & - & - & G^+_{2,L}(z_A,z_0) \\ \cdot & \cdot & - & - & \cdot \\ G^+_{J,1}(z_A,z_0) & G^+_{J,2}(z_A,z_0) & - & - & G^+_{J,L}(z_A,z_0) \end{bmatrix} ,
\tag{2.25d}
$$

with the submatrices $G^+_{j,\ell}$ defined by equation (2.23b) and

$$
M(z_0) = \begin{bmatrix} M_{1,1}(z_0) & O & - & - & O \\ O & M_{2,2}(z_0) & - & - & O \\ \cdot & \cdot & - & - & \cdot \\ O & O & - & - & M_{L,L}(z_0) \end{bmatrix}
\tag{2.25e}
$$

with the submatrices $M_{\ell,\ell}$ defined by (2.23c) and O is the null matrix.

Note that the matrix notation of equation (2.25a) is exactly the same as the 2-D matrix notation (2.18) when a more general interpretation is given to the elements in the matrix. In figure 2.9 the interpretation for the 3-D matrix notation is illustrated.

The data vector $\vec{P}(z)$ is constructed by placing the vectors for 2-D data at each y-value one after another in one vector for 3-D data. So the index of each element in this vector represents a 2-D coordinate in x and y, instead of just the lateral x position. The extrapolation matrix consists of sub-matrices, each describing a "2-D extrapolation" of lines in the x direction for different y coordinates at the surface (y_ℓ) and at the subsurface level (y_j).
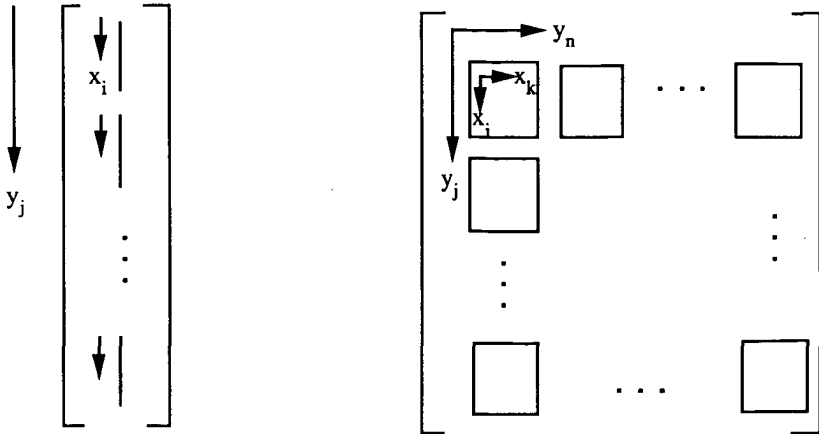
Figure 2.9: Interpretation of the 3–D matrix notation for the data vector and the extrapolation matrix.

The column indices of matrix $W^+(z_A,z_0)$ represent one surface coordinate (x_k and y_ℓ) and the row indices represent one subsurface coordinate (x_i and y_j).

The matrices describing 3-D reflection and the 3-D (multi-shot) seismic experiment can be derived in the same way as the matrices for a 2-D seismic experiment.
All these matrices can be manipulated in exactly the same way as the matrices for 2-D data and therefore the formulation of e.g. migration and redatuming (see next section) in the matrix notation holds for 2–D as well as for 3–D data.

2.5 THEORY OF REDATUMING

The concept of redatuming, which means transforming seismic data as if it were measured at another depth level, is also described by Berryhill (1984). Schultz and Sherwood (1980) already mention in their paper on 2-D prestack depth migration the possibility of generating poststack data at a certain target level and continuing the processing with poststack migration. Applications of redatuming are the elimination of the effects of an overburden with strong lateral velocity variations, like in layer replacement (Yilmaz and Lucas, 1985 and Berryhill, 1986). These methods all perform the redatuming by alternately downward extrapolation of detectors and sources. Extensions of these methods to 3-D need a reordering of the data between these steps, because the huge amount of data can not be kept in memory. Such a reordering would slow down the process enormously. In this section I

will describe the theory of shot record redatuming as introduced by Berkhout (1984) and used by Peels (1988) and Kinneging et al., (1989).

Using the matrix notation as described in the previous section a multi-experiment seismic measurement can be described as,

$$\mathbf{P}^-(z_0) = \mathbf{D}(z_0) \left[\sum_{m=1}^{\infty} \mathbf{W}^-(z_0,z_m) \, \mathbf{R}(z_m) \, \mathbf{W}^+(z_m,z_0) \right] \mathbf{S}^+(z_0) \ . \tag{2.26}$$

Let the upper boundary of the target zone be at $z = z_M$. In that case it is useful to rewrite equation (2.26) as,

$$\mathbf{P}^-(z_0) \quad = \mathbf{D}(z_0) \left[\sum_{m=1}^{M-1} \mathbf{W}^-(z_0,z_m) \, \mathbf{R}(z_m) \, \mathbf{W}^+(z_m,z_0) \right] \mathbf{S}^+(z_0)$$

$$+ \, \mathbf{D}(z_0) \left[\mathbf{W}^-(z_0,z_M) \, \mathbf{X}(z_M) \, \mathbf{W}^+(z_M,z_0) \right] \mathbf{S}^+(z_0) \ , \tag{2.27a}$$

with

$$\mathbf{X}(z_M) = \sum_{n=0}^{\infty} \mathbf{W}^-(z_M,z_{M+n}) \, \mathbf{R}(z_{M+n}) \, \mathbf{W}^+(z_{M+n},z_M) \ , \tag{2.27b}$$

where

$$\mathbf{W}^-(z_0,z_{M+n}) = \mathbf{W}^-(z_0,z_M) \, \mathbf{W}^-(z_M,z_{M+n}) \ , \tag{2.27c}$$

and

$$\mathbf{W}^+(z_{M+n},z_0) = \mathbf{W}^+(z_{M+n},z_M) \, \mathbf{W}^+(z_M,z_0) \ . \tag{2.27d}$$

The first part of equation (2.27a) describes the response of reflections of interfaces within the overburden ($z_0 < z < z_M$) and the second part of (2.27a) describes the response at the surface of the reflections in the target zone ($z \geq z_M$).

Here $\mathbf{X}(z_M)$ represents the multi-experiment impulse response ($\doteq$ a perfectly deconvolved seismic data set) at $z = z_M$ of the target zone;

$\mathbf{W}^+(z_M,z_0)$ describes the propagation effects of the source wave field $\mathbf{S}^+(z_0)$ to the upper boundary of the target zone

and $\mathbf{W}^-(z_0,z_M)$ describes the propagation effects of the reflected waves from the upper boundary of the target zone to the surface.

Given expression (2.27) redatuming can now be defined as a technique which estimates $\mathbf{X}(z_M)$, given the seismic data at the surface. To do this the distorting effect of wave

propagation through the overburden, described by $W^+(z_M,z_0)$ and $W^-(z_0,z_M)$ must be eliminated using the macro subsurface model of the overburden. It can be seen that, in elimination of these propagation effects, time shifts are involved, that cause the reflections of the overburden (first part of (2.27a)) to occur at negative times after redatuming. Therefore these reflections can easily be separated from reflections of the target zone itself. Thus they will be ignored in the following derivations.

The response at the surface of the target zone can be described by,

$$P^-(z_0) = \left[W^-(z_0,z_M)\, X(z_M)\, W^+(z_M,z_0) \right] S^+(z_0) \quad . \tag{2.28}$$

For simplicity I write for the source data matrix $S^+(z_0)$,

$$S^+(z_0) = S(\omega)\, I \quad , \tag{2.29a}$$

where I is the identity matrix

and $S(\omega)$ is the signature of the source.

For the following I will assume that a separate deconvolution is performed for the source wavelet $S(\omega)$ together with the absorption and for the detector geometry, which means;

$$D(z_0) = I \quad . \tag{2.29b}$$

The response at the surface of the target zone after deconvolution can then be described by,

$$P^-(z_0) = \left[W^-(z_0,z_M)\, X(z_M)\, W^+(z_M,z_0) \right] \quad . \tag{2.30}$$

Hence it is assumed that for each experiment a dipole source is positioned at one surface location and that the source signature is equal for all experiments.

From expressions (2.28) and (2.29) it can be easily seen that redatuming can be written as,

$$X(z_M) = F^-(z_M,z_0)\, P^-(z_0)\, F^+(z_0,z_M) \quad , \tag{2.31a}$$

with

$$F^-(z_M,z_0) = \left[W^-(z_0,z_M) \right]^{-1} \quad , \tag{2.31b}$$

and

$$F^+(z_0,z_M) = \left[W^+(z_M,z_0) \right]^{-1} \quad . \tag{2.31c}$$

Inspection of equation (2.31a) shows that the matrix multiplication with $F^-(z_M,z_0)$ acts upon the columns of $P^-(z_0)$, which means a lowering of the detectors from the surface to

the target upper boundary. On the other hand the multiplication of $P^-(z_0)$ with $F^+(z_0,z_M)$ acts upon the rows of $P^-(z_0)$, which means a lowering of the sources from the surface to the upper boundary of the target zone.

Therefore conventionally a redatuming consists of three main steps (see e.g. Berryhill, 1986):

– First the data measured at the surface are inversely extrapolated to the new datum (in our case the upper boundary of the target zone).

– Secondly the data are reordered from Common-Shot-Gathers into Common-Receiver-Gathers. Using the reciprocity property now the shots are located at the target upper boundary and the receivers are located at the surface.

– Finally the data are inversely extrapolated from the surface to the new datum.

For 3–D application, the reordering in the second step should be avoided. Therefore, in this thesis a shot record redatuming scheme is described. The redatuming can be written in the following steps,

$$P^-(z_M) = F^-(z_M,z_0)\, P^-(z_0) \quad , \tag{2.32a}$$

$$X(z_M) = P^-(z_M)\, F^+(z_0,z_M) \quad . \tag{2.32b}$$

These steps mean:

– Inverse extrapolation of the wave field measured at the surface, described by (2.32a), like in the conventional redatuming scheme.

– The upgoing reflected wave field at $z = z_M$, $P^-(z_M)$, is deconvolved for the downgoing incident wave field, which is described by (2.32b).

From equations (2.32) the shot record redatuming scheme can be derived. Using data vector $\vec{P}_j^-(z_0)$, we can write for shot record redatuming,

$$\vec{P}_j^-(z_M) = F^-(z_M,z_0)\, \vec{P}_j^-(z_0) \quad , \tag{2.33a}$$

$$<X(z_M)>_j = \vec{P}_j^-(z_M) \left[\vec{F}_j^+(z_0,z_M) \right]^T \tag{2.33b}$$

$$X(z_M) = \sum_j <X(z_M)>_j \quad , \tag{2.33c}$$

where   index j stands for the shot number,

           $\vec{P}_j^-(z)$ is the jth column of $P^-(z)$,

           $[\vec{F}_j(z_0,z_M)]^T$ is the j-th row of $F^+(z_0,z_M)$

and $<X(z_M)>_j$ is the result of redatuming of shot j.

The approach of the shot record redatuming versus full multi-experiment redatuming is illustrated in figure 2.10. In the upper part of this figure the deconvolution is done per shot record. The result for each shot record is an underdetermined estimate of the impulse response $X(z_M)$, namely $<X(z_M)>_j$. After stacking all single fold redatuming results as described by (2.33c) the final result $X(z_M)$ is obtained, which is exactly the same as would have been obtained by full multi-experiment redatuming, which is illustrated in the lower part of figure 2.10.
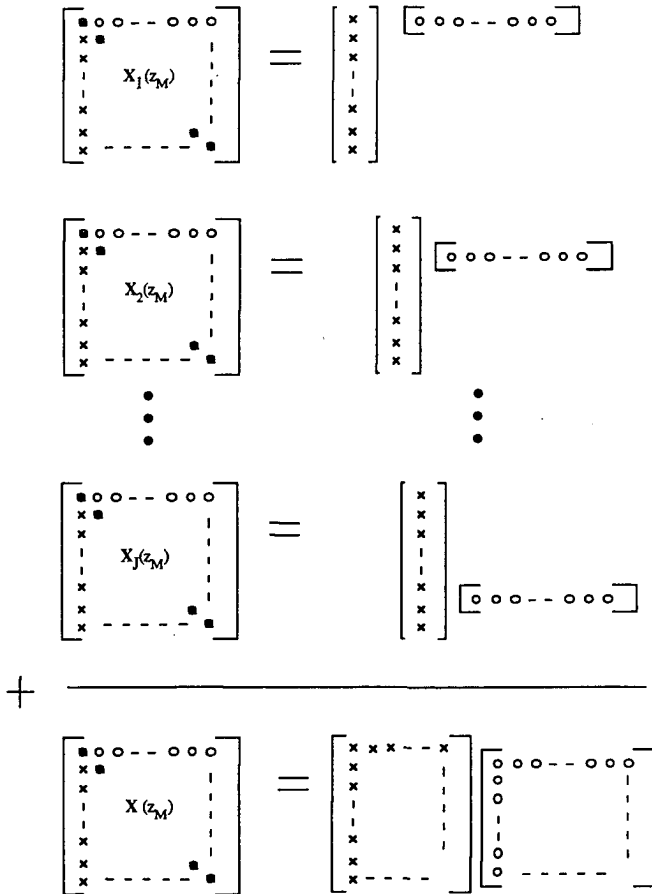
Figure 2.10: Schematic representation of full multi-experiment redatuming versus single-experiment redatuming followed by CDP stacking.

We have seen that conventional redatuming involves a reordering of the data from Common-Shot-Gathers into Common-Receiver-Gathers. In 2-D this can be avoided, because then a monochromatic prestack data set can be kept in memory easily. For 3-D the size of such a data set would be too large to keep in memory. In that case reordering of the data would require much additional disk I/O, which would slow down the redatuming enormously. Therefore in 3-D the redatuming should preferably be performed per shot record. Another important advantage of shot record redatuming in 2–D and in 3–D is the ability to study redatumed single shot gathers and Common Depth Point gathers. These CDP gathers represent the redatumed (unstacked) data for one depth point and all shots.

Finally I want to make a remark on the inverse extrapolation operators (equations (2.33b) and (2.33c)). It is not practical to obtain these operator matrices by a direct inversion of the forward extrapolation matrices. As shown in section 2.3 these inverse extrapolation operators can also be obtained in a direct way (equation (2.14)). In matrix notation these operators read,

$$\mathbf{F}^-(z_M, z_0) = \left[\partial_{z_0} \mathbf{G}^+(z_M, z_0) \right]^* \mathbf{M}(z_0) \quad , \tag{2.34a}$$

$$\mathbf{F}^+(z_0, z_M) = \left[\partial_{z_M} \mathbf{G}^-(z_0, z_M) \right]^* \mathbf{M}(z_M) \quad . \tag{2.34b}$$

where we made again use of the one-way version of the reciprocity theorem.

In chapter 3 an efficient implementation of these 3–D extrapolation operators is described.

3

2–D AND 3–D OPERATOR DESIGN FOR WAVE FIELD EXTRAPOLATION

3.1 INTRODUCTION

In the previous chapter the theory of wave field extrapolation (both forward and inverse) was discussed. It was concluded, that the role of the Green's function is crucial. It was also shown that Green's functions can be obtained by any numerical modeling algorithm. Because the Green's functions define the extrapolation operators, the modeling scheme must be able to model *propagation* correctly. The requirements for modeling *reflections* are less important. Ideally the Green's functions can be calculated using a finite difference or finite element algorithm. Those methods make 'true amplitude' extrapolation possible. For application in 3-D wave field extrapolation however these algorithms would be far too expensive. The amount of computation time as well as the memory requirements of the scheme would be enormous in 3-D. Therefore other modeling schemes must be used. This chapter concentrates on two modeling schemes, that are suited for 3-D extrapolation, i.e. ray tracing and Gaussian beams. These two methods are able to model propagation effects reasonably well and, with an efficient implementation, they are very suited for non-recursive wave field extrapolation in 3-D.

In section 3.2 the implementation aspects of Green's functions modeled with ray tracing as well as Gaussian beams are discussed.

In section 3.3 applications of extrapolation with these two methods will be illustrated with some examples. Finally in section 3.4 various methods of operator development will be reviewed and their strong and weak points will be discussed.

3.2 REVIEW OF OPERATOR CALCULATION

In this chapter two methods are discussed to calculate Green's functions, used in wave field extrapolation operators. These two methods, based on ray tracing and on Gaussian beam modeling, are most suited for non-recursive extrapolation operators in 3-D. In this section first a number of methods will be reviewed to compute extrapolation operators and it will be shown that for different applications different methods should be used.

There are two important groups of operators, namely recursive and non-recursive extrapolation operators. In recursive wave field extrapolation the wave field at a certain level is calculated via a number of intermediate levels. In the group of recursive operators again a subdivision can be made, namely extrapolation with small constant depth steps and extrapolation via the macro boundaries of the subsurface model.

Recursive wave field extrapolation via a large number of small depth steps is most suited when the wave field must be known at the intermediate levels, like in migration, where a reflectivity image of the total subsurface is calculated. The method is less suited for redatuming, where one is interested in the wave field at a limited number of subsurface points only. In the second type of recursive wave field extrapolation the wave field at a certain level is calculated via a number of macro boundaries. Applications of these operators can be found in 'true amplitude' 2-D redatuming. At this moment the calculation of these operators is not efficient enough to be of practical use in 3-D.

The second large group of extrapolation operators is the non-recursive operator type. Here the wave field at a certain depth level (e.g. the upper boundary of the target zone) is calculated in one step from the wave field at the surface. For these operators it is not possible to consider the subsurface to be homogeneous and therefore analytical computation of the operators is (in most cases) not possible. To obtain these operators, a numerical modeling scheme can be used to calculate the Green's functions. There are several algorithms to model these Green's functions. Very accurate methods are the finite difference and finite element methods, that are based on discrete versions of the acoustic or elastic wave equation. These methods can be applied both recursively and non-recursively. This method gives very accurate amplitudes of the Green's functions and therefore it is suited for 'true amplitude' extrapolation. A disadvantage of these methods is that the wave field needs to be calculated for a dense grid of subsurface points and a small sampling interval in time. This causes very large computation times and also much computer memory is required. The method will therefore in the near future be restricted to 2-D 'true amplitude' migration and not for 2-D or 3-D redatuming. Other methods for modeling the Green's functions are ray tracing and Gaussian beam modeling, as discussed in this

chapter. The concept of using ray tracing for calculation of extrapolation operators is also used by Beydoun and Keho (1987) and Keho and Beydoun (1988) in a time domain implementation of a Kirchhoff migration scheme. These schemes are efficient and can easily be used in 3-D wave field extrapolation. In section 3.3 it has been shown, that the Gaussian beam method is better than the ray tracing method with respect to the amplitude behavior. The ray tracing method suffers from shadow zones in the subsurface, for which no rays can be found. In the Gaussian beam method the response is calculated through superposition of the contributions of different beams, such that also in shadow zones a response is found. On the other hand it is very useful, that much research has been done in the past on 2-D and 3-D ray tracing algorithms. Commercially available ray tracing packages can easily be used for the modeling of Green's functions.

In table 3.1 a summary is given of different methods for calculating extrapolation operators, their typical application area and some of their main characteristics.

Table 3.1: Overview of different types of extrapolation.

	recursive		recursive and non-recursive	non-recursive	
method	small steps	macro steps	finite difference / element	ray tracing	Gaussian beams
application	migration	2–D 'true-amplitude' redatuming	2–D 'true-amplitude' migration (complicated)	2–D and 3–D redatuming	2–D and 3–D redatuming
pros / cons	accurate efficient migration	accurate expensive	accurate very expensive	amplitude problems efficient commercial package	accurate efficient memory expensive

3.3 OPERATOR CALCULATION

In this section I will describe the calculation of extrapolation operators (i.e. the Green's functions). These calculation methods will be illustrated and compared with the aid of some some examples. In chapter 4 the application of these operators in a shot record redatuming scheme is described and various aspects of the implementation of such a scheme in 3-D are discussed. Not just the implementation of the redatuming scheme must be efficient, but also the methods for calculating the operators must be very efficient in both computation

time and in computer memory usage. The methods must be able to generate operators for any irregular shooting geometry. In the practice of data acquisition it is often impossible to position sources and receivers on a regularly spaced acquisition grid. One tries to make the actual acquisition geometry as regular as possible, but there will always be irregularities, e.g. due to roads and buildings in land data acquisition or due to cable feathering in the marine case. Most migration methods however assume that the acquisition is done on a regular grid. Therefore the data is often transferred to a regular grid. Generally this process contaminates the data and reduces the quality of the migration result. By calculating the extrapolation operators for irregular acquisition geometries this problem is avoided and no interpolation of the data has to be performed.

As shown in section 2.4 wave field extrapolation, forward and inverse, can be described in the matrix notation as a matrix multiplication,

$$\vec{P}^{+}(z_M) = W^{+}(z_M, z_0)\, \vec{P}^{+}(z_0) \tag{3.1a}$$

and

$$\vec{P}^{-}(z_M) = F^{-}(z_M, z_0)\, \vec{P}^{-}(z_0) \tag{3.1b}$$

with the forward extrapolation operator (see equation 2.28c),

$$W^{+}(z_M, z_0) = \left[\partial_{z_0} G^{+}(z_M, z_0) \right] M(z_0) \tag{3.2a}$$

and for the inverse extrapolation matrix (see equation 2.37a),

$$F^{-}(z_M, z_0) = \left[\partial_{z_0} G^{+}(z_M, z_0) \right]^{*} M(z_0) \quad , \tag{3.2b}$$

where $G^{+}(z_M, z_0)$ is the downgoing component of the Green's matrix which is defined in equations (2.35) and (2.27a),

$M(z_0)$ is defined in equation (2.27b),

$\vec{P}^{+}(z_0)$ and $\vec{P}^{+}(z_M)$ are the downgoing wave fields at $z = z_0$ and $z = z_M$ respectively

and $\vec{P}^{-}(z_0)$ and $\vec{P}^{-}(z_M)$ are the upgoing wave fields at $z = z_0$ and $z = z_M$ respectively.

The most important part of the calculation of the wave field extrapolation operators is the computation of the Green's matrices. One column of matrix $G^{+}(z_M, z_0)$ describes the monochromatic downgoing response at $z = z_M$, due to a point source at $z = z_0$. This means that matrix $G^{+}(z_M, z_0)$ can be obtained through a numerical modeling of the wave fields at $z = z_M$ for point sources located at $z = z_0$. The computation of one column of $G^{+}(z_M, z_0)$

corresponds to the monochromatic modeling of the wave field for a source at the lateral position at the surface, corresponding to the column-index. Note that the reciprocity principle states that the rows of the Green's matrix G^+ are equal to the columns of G^-, so

$$G^+(z_M, z_0) = \left[G^-(z_0, z_M) \right]^T .$$ (3.3)

It is also possible to calculate the Green's wave fields $G^-(z_0, z_M)$. This is the upgoing response at the surface due to sources located at $z = z_M$. For the modeling of the Green's wave fields the macro subsurface model is needed. I will assume here that the macro subsurface model is known. It is possible to estimate such a macro model by methods as described by Van der Made (1988), Jeannot et al. (1986) or Cox et al. (1988).

Using the macro model the extrapolation operators can be calculated separately from the actual redatuming of the data. For this calculation also the shooting geometry at the surface and the desired geometry at the upper boundary of the target zone is needed besides the macro model. This means that the data is not involved in the first phase of operator computation. In the second phase of extrapolation or redatuming the macro subsurface model is not needed anymore and the operators are read from disc. Storing the extrapolation operators for all frequencies between these two phases, however, would require too much disk space. The size of the extrapolation operator in the frequency domain is

$$N_0 = N_a * N_t * N_f ,$$

with N_0 the number of complex samples in the operator,

            N_a the total number of acquisition points at the surface,

            N_t the number of points at the upper boundary of the target zone

and N_f the number of frequencies to be handled.

For an indication of the size of the operator consider the following numerical example, with 5000 acquisition points, 10,000 points at the upper boundary of the target zone and 500 frequency samples. For this example the extrapolation operator would consist of $25 \cdot 10^9$ complex samples, which is 200 Gbyte of information. It is clear that it is unpractical to store such an amount of data on disc. Not only the large amount of required disc space is a problem, also the relatively slow disc I/O would slow down the processing considerably. It is therefore necessary to reduce this data volume.

Until now no remarks have been made on the modeling algorithm, that will be used to calculate 3-D extrapolation operators. In this thesis two methods for modeling the Green's functions will be used. The first method is based on ray tracing followed by an interpolation of the operator and the second method is based on the Gaussian beam method.

3.3.1   The ray tracing method   -

First the ray tracing method for modeling the Green's wave field will be considered. To calculate the wave field at $z = z_N$ due to a source at the surface $z = z_0$, a fan of rays is calculated from the source location (figure 3.1). For each ray Snell's law is applied at layer interfaces in the subsurface model until the rays end at depth $z = z_N$. Normally from the initial set of rays, calculated for a range of take-off angles at the surface, the rays are searched, that connect the source location at the surface and the detector location at the upper boundary of the target zone. This search is often the most time consuming part of a ray tracing scheme. Ray tracing is a high-frequency approximation, where the energy is considered to propagate along the rays. Along the calculated ray, parameters of the wave field are calculated, such as travel time and amplitude. Amplitude effects, like geometrical spreading and transmission losses, are incorporated. The seismic response (here the Green's function) at point $r_{ij} = (x_i, y_j, z_M)$ at the upper boundary of the target zone due to a source at $r_{kl} = (x_k, y_l, z_0)$ at the surface can then be calculated from these parameters by,

$$G^+(r_j, r_k, \omega) = A(r_j, r_k)\, e^{-i\omega T}(r_j, r_k) \quad , \tag{3.4}$$

where $G^+(r_j, r_k, \omega)$ is the downgoing monochromatic Green's function at the target level (r_j) due to a source at the surface (r_k) (figure 3.2),

   $A(r_j, r_k)$ is the amplitude along the ray

and $T(r_j, r_k)$ is the travel time along the ray from r_k to r_j with the smallest travel time (first arrival).
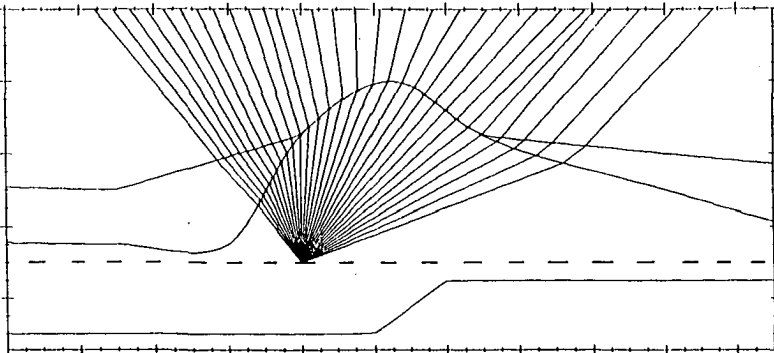

Figure 3.1: For each Green's source location a fan of rays is calculated.
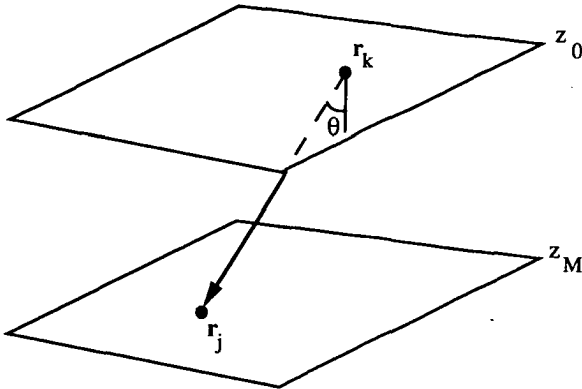
Figure 3.2: Geometry of Green's function $G^+(r_j, r_k, \omega)$.

In equation (3.4) only the first arriving waves are used. In general these waves properly describe wave propagation through the macro subsurface model. In case of a complicated macro model the propagation can not be described with the first arriving waves only. In that case also other rays from r_k to r_j must be incorporated and these separate contributions should be summed.

For a detailed description of the ray tracing method, that is used for the operators in this thesis, one is referred to Sierra (1987). Because ray tracing is not properly based on the wave equation the amplitude behavior (especially at caustics) is worse than can be expected from wave equation based modeling algorithms. Another problem of ray tracing are shadow zones. For certain parts of the subsurface, where there should be a seismic response due to diffractions, no rays can be found. On the other hand, ray tracing is an efficient method and in general, when propagation of seismic waves is modeled without reflections, the method works satisfactorily.

When ray tracing modeling is used to calculate extrapolation operators, the rays must be calculated from all source locations at the surface to all detector locations at the upper boundary of the target zone. Each ray corresponds to one element of the Green's matrix in equation 3.2. Note that, because of the reciprocity property, the source may also be chosen at the target level and the detectors at the surface. In order to reduce the amount of ray tracing for the operator calculation, the rays are not calculated for all source and detector points. For a coarse grid at the surface the rays are calculated to points at the upper boundary of the target zone. The rays for this coarse operator grid are called the 'basic rays'. The amplitudes and travel times, needed to calculate the Green's function, are

obtained by means of an interpolation of these 'basic rays'. By assuming the wave front at the surface to be locally plane around the ray (the far field or Fraunhofer approximation) the travel time of the ray at the actual acquisition point can be obtained by a simple correction. In 3-D this correction is given by (see figure 3.3):

$$\Delta T = \frac{\sin \theta_g}{V_0} \left[(x_a - x_g) \cos \psi_g + (y_a - y_g) \sin \psi_g \right] \ , \tag{3.5}$$

where $\quad (x_a, y_a)$ is the location of the acquisition point,

$\quad\quad\quad \Delta T$ the correction to the travel time of the 'basic ray',

$\quad\quad\quad (x_g, y_g)$ the location at the surface of the 'basic ray',

$\quad\quad\quad \theta_g$ the dip angle at the surface of the 'basic ray',

$\quad\quad\quad \psi_g$ the azimuth angle at the surface of the 'basic ray'

and $\quad\quad V_0$ the propagation velocity of the upper layer of the macro subsurface model.
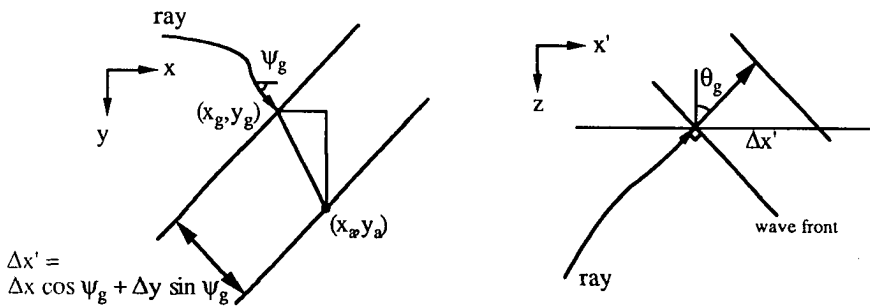
Figure 3.3:   Geometry for calculating the 3-D Fraunhofer correction to the travel time.
a) Top view
b) Side view

This local plane wave approximation assumes no amplitude variations along the plane wave front in the vicinity of the 'basic ray'. Note that this interpolation can very easily be performed for any irregular acquisition geometry. Other methods of interpolating the travel times and amplitudes for the irregular acquisition grid are also possible, like a spline's interpolation. Here a polynomial function is used to describe the travel time and amplitude as function of the surface coordinate. For the 2-D examples cubic splines were used to calculate the operator, but for 3-D this method is not further evaluated. In figure 3.4 the local plane wave correction of the operator is schematically depicted. The operator parameters are calculated through a correction of the parameters of the nearest 'basic ray'.
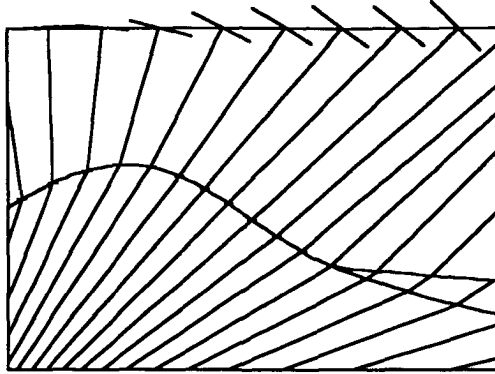
Figure 3.4: Principle of operator interpolation to the acquisition grid with the ray tracing method and the local plane wave assumption.

The operator parameters T and A are stored in two two-dimensional arrays. The two axes of these arrays represent the positions at the upper boundary of the target zone and the acquisition positions at the surface.

Given the Green's functions the final step to compute extrapolation operators is given by equations (3.2a) and (3.2b). With the local plane wave assumption the z-derivative of the Green's function can be approximated. Thus the element at k–th row and the j–th columns of the forward extrapolation operator becomes,

$$W^+(z_M, z_0)_{jk} \approx -\frac{i\omega \cos\theta}{V_0} G^+(r_j, r_k, \omega) \frac{2 \Delta x \Delta y}{\rho(r_k)} \quad, \tag{3.6}$$

with θ the dip angle of the ray at the surface

           V_0 the propagation velocity in the upper layer of the macro subsurface model

and $\rho(r_k)$ the density at $r_k = (x, y, z_0)$.

3.3.2   The Gaussian beam method

The second method, that is suited for calculating non-recursive extrapolation operators is Gaussian beam modeling. In appendix A of this thesis the Gaussian beam method for modeling wave fields is explained in more detail, but here the main principles will be summarized. In the same way as in ray tracing a fan of rays is calculated for a number of take-off angles. In the Gaussian beam method the wave field is not supposed to propagate solely along the ray. The Gaussian beam method is based on a high-frequency

approximation of the wave equation in a ray centered coordinate system. Here the acoustic energy propagates along a beam, of which the ray forms the center. The amplitude of the contribution of a beam decreases with the distance to the central ray according to a Gaussian function. For each beam a number of characteristic parameters are calculated along the ray. From these parameters the contributions to the complex valued 'travel times' of each beam in a certain acquisition point can be calculated according to,

$$T(s,n) = \int_{s_0}^{s} \frac{ds}{v(s)} + \frac{1}{2v(s)} K(s) \, n^2 \quad , \tag{3.7a}$$

where $T(s)$ is the complex valued 'travel time',

         s measures the arclength along the central ray from an arbitrary reference point s_0,

         n is the distance of the acquisition point perpendicular to the ray from s,

         $v(s)$ is the propagation velocity along the ray

and $K(s)$ can be interpreted as a measure of the curvature of the phase front of the beam.

The contribution of each beam to the complex valued 'amplitude' is given by,

$$A(s,n) = \sqrt{\frac{v(s)}{q(s)}} \, \exp\left[-\frac{n^2}{L^2(n)} \right] \quad , \tag{3.7b}$$

where $A(s,n)$ is the complex valued 'amplitude',

         $q(s)$ represents the geometrical spreading

and $L(n)$ represents the effective half-width of the beam.

The complex operator parameters T and A are stored in two complex valued three-dimensional arrays. The three axes represent the positions at the upper boundary of the target zone, the acquisition positions at the surface and the beam number. To obtain the total response of the Green's function with the Gaussian beam method the contributions of all beams have to be summed for each detector position,

$$G^+(r_j, r_k, \omega) = \sum_{beams} A_b(r_j, r_k) \, e^{-i\omega T_b(r_j, r_k)} \tag{3.8}$$

with $A_b(r_j, r_k)$ the complex valued amplitude contribution of beam b in point $r_j = (x, y, z_M)$ due to a point source in $r_k = (x, y, z_0)$

and $T_b(r_j, r_k)$ the complex valued 'travel time' contribution of beam b.

Here I described the Gaussian beam method to calculate the Green's wave field at the upper boundary of the target zone for a source at the surface. Because of the reciprocity property the source and detector positions can be interchanged. Further note, that in the Gaussian beam method the Green's function is interpolated between the beams in a natural way, based on the wave equation. Because the acquisition geometry at the surface is in general irregular, it is more practical to perform the interpolation in the Gaussian beam method at the surface and to place the sources at the upper boundary of the target zone. In figure 3.5 the principle of the Gaussian beam method is illustrated. For a certain acquisition point each beam gives a contribution to the total response. Because in the Gaussian beam method the energy is not supposed to propagate solely along a ray but in a beam no amplitude problems will occur at caustics. Also in shadow zones a response is found for the Gaussian beam method in contrast to the ray tracing method. It is therefore expected that the amplitude behavior of the Gaussian beam method is better than the amplitude behavior of the ray tracing method.
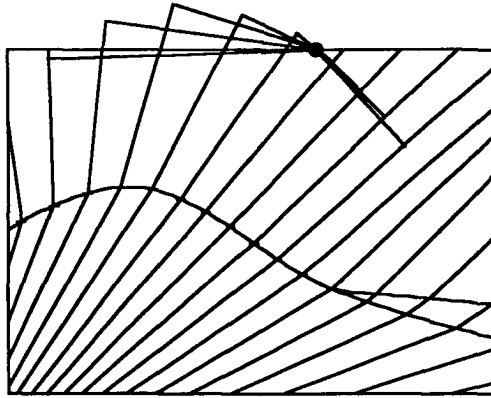

Figure 3.5: Principle of operator interpolation to the acquisition grid with the Gaussian beam method.

I have now described two methods for calculating Green's functions, ray tracing and Gaussian beam modeling, separately. There is however a large resemblance between these two methods. In the figures 3.6 and 3.7 the general scheme of operator design is shown. Both methods, ray tracing and Gaussian beams, are different implementations of this general scheme. As the first step in the scheme a set of 'basic rays' are calculated (figure 3.6). In the ray tracing method these 'basic rays' were calculated for a coarse operator grid at the surface, while the central rays of the Gaussian beams form also a set of 'basic rays'.
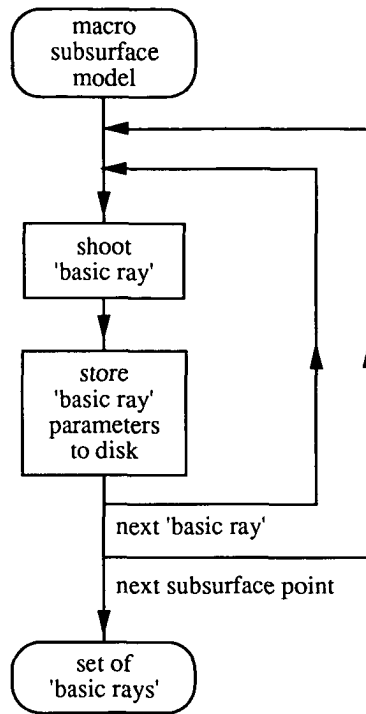
Figure 3.6: The main steps in the first phase of the general scheme for operator design.

In the next step (the first block in figure 3.7) from these 'basic rays' frequency independent operator parameters, travel times and amplitudes, are calculated for the irregular acquisition geometry and the final monochromatic operator is calculated from these operator parameters. Note that although the two methods differ with respect to the meaning and use of the rays calculated in the first phase, there is an important analogy. The rays form in each method a basis from which during a second phase the actual extrapolation operator is constructed for an irregular grid.
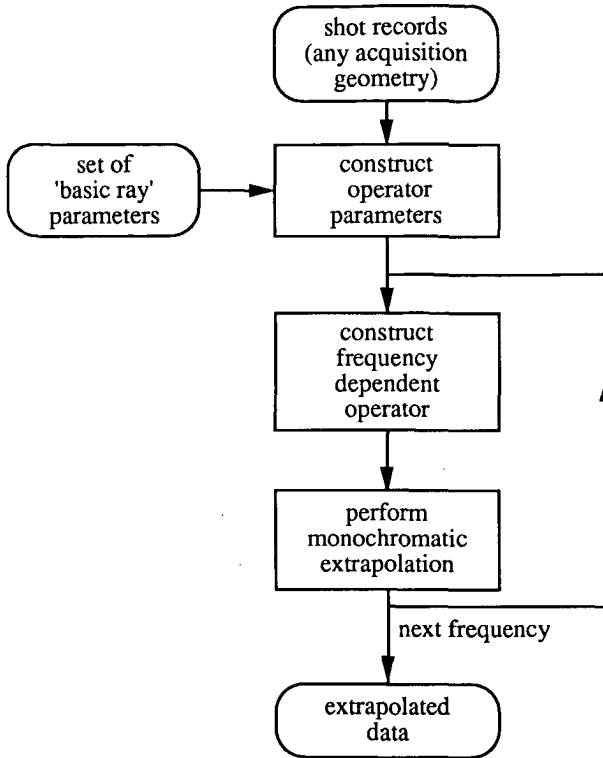
Figure 3.7: The main steps in the second phase of the general scheme for operator design just before the actual extrapolation.

3.4 EXAMPLES OF INVERSE WAVE FIELD EXTRAPOLATION

I will now demonstrate non-recursive wave field extrapolation with operators based on ray tracing and on the Gaussian beam method. Both methods will be used to extrapolate inversely 2-D zero offset data, that were modeled using the exploding reflector assumption with a finite difference modeling scheme. In figure 3.8 the 2-D subsurface model that was used for this example is shown. Here a faulted structure is placed beneath a salt dome. The zero offset data, that were generated for the reflections of the faulted reflector, are displayed in figure 3.9. Note that the reflections of the overlying layers were not modeled in this example. From these data it is very difficult to recognize the faulted structure. Due to propagation through the overburden the image is heavily distorted.
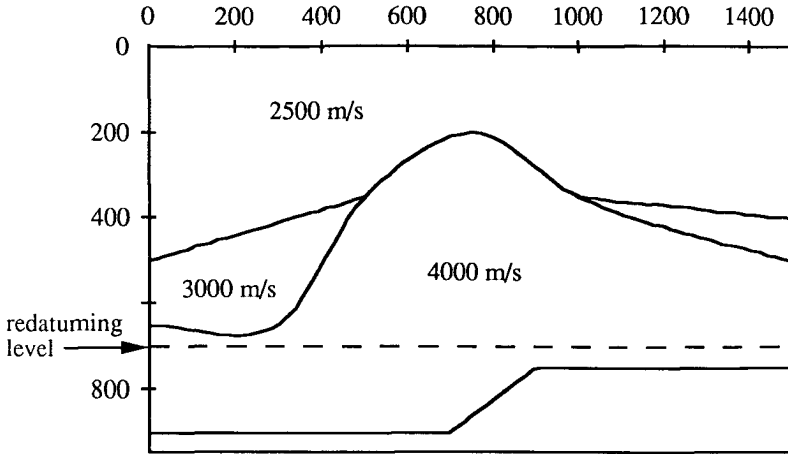
**Figure 3.8**: 2-D subsurface model.
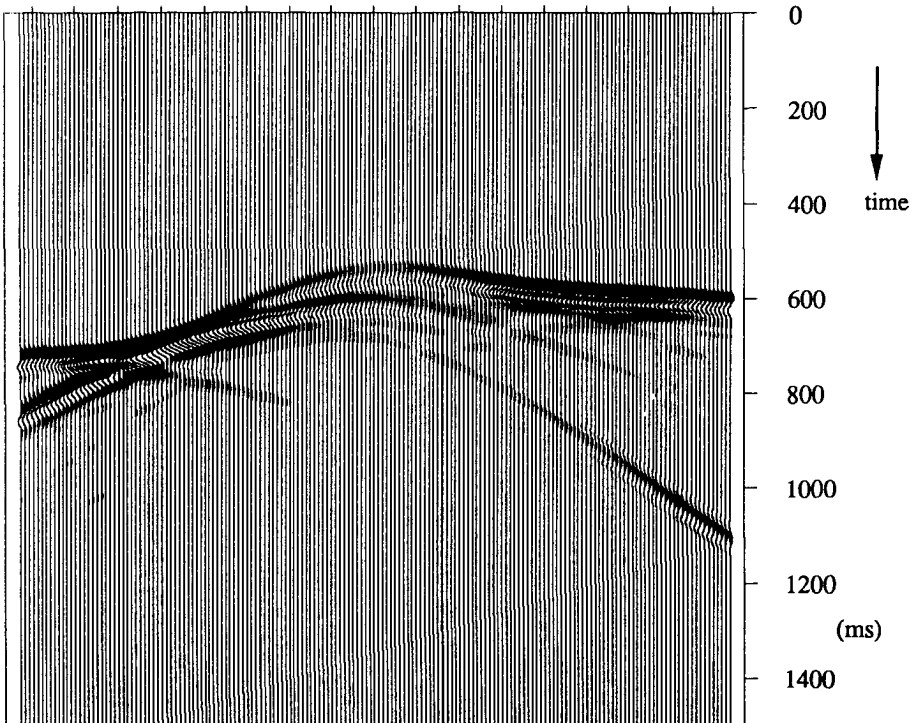
Figure 3.9:   2-D zero offset data from the lower reflector in figure 3.6, modeled with an acoustic finite difference scheme.
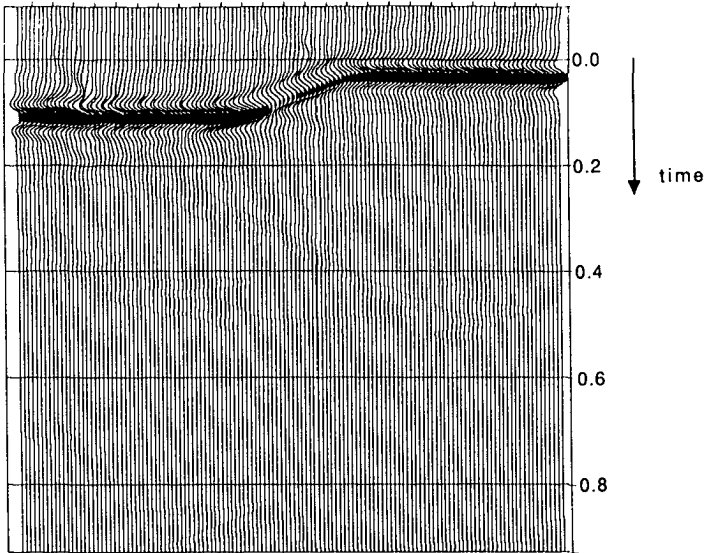
Figure 3.10: Result after inverse wave field extrapolation with the ray tracing method for operator design.

With the ray tracing method the operators were calculated for inverse extrapolation from the surface to a depth of 700 m, just above the faulted structure. In figure 3.10 the result after inverse extrapolation with the ray tracing method is shown. The propagation effects of the overburden are eliminated and the positioning of the reflector is correct, both in the lateral as in the temporal direction. A shadow zone at the left side of the new datum causes a discontuity in the inversely extrapolated result.

Using the Gaussian beam method for inverse wave field extrapolation the amplitude behavior is much better. The result is shown in figure 3.11. Just like the ray tracing method the position of the reflector is correct here. We see that the amplitude is smoother than for the ray tracing. This is because the Gaussian beam method is based on the wave equation and does not suffer from shadow zones or instabilities. Also in the data extrapolated with the Gaussian beam method amplitude variations are present along the reflector. Some of the reflection energy from the lower reflector is not measured at the surface. The absence of some of this enery causes the amplitude variations, especially for the dipping part of the reflector.
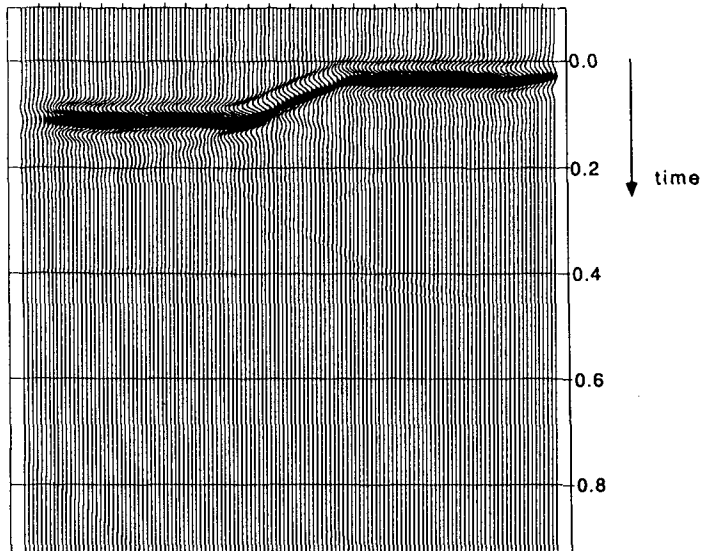
Figure 3.11: Result after inverse wave field extrapolation with the Gaussian beam method for operator design.

The second example is a 3-D inverse wave field extrapolation. Here we only used the ray tracing based operators. In figure 3.12 the 3-D inhomogeneous subsurface model is shown that was used for this example. With a recursive Kirchhoff modeling scheme zero offset
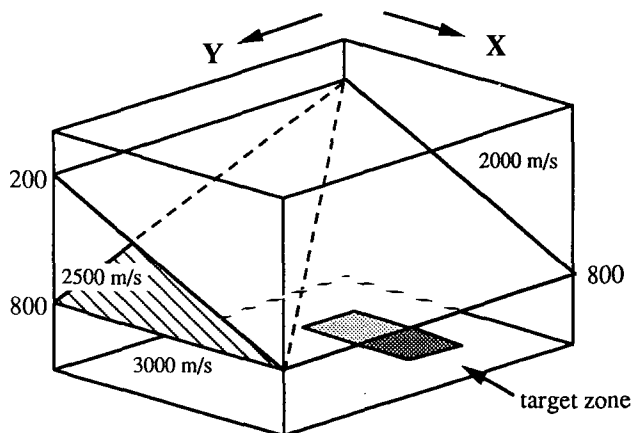
Figure 3.12: 3-D subsurface model with a reflector of limited length at the target zone.

data were generated at the surface for a reflector of limited extend at a depth of 1000 m (see figure 3.12). Two cross sections of the data at the surface are shown in figure 3.13. In figure 3.14 the result after 3-D inverse wave field extrapolation to z = 1000 m is shown. The lateral positioning (both in the X as in the Y direction) of the reflector is correct and the event aligns correctly at t = 0 s.
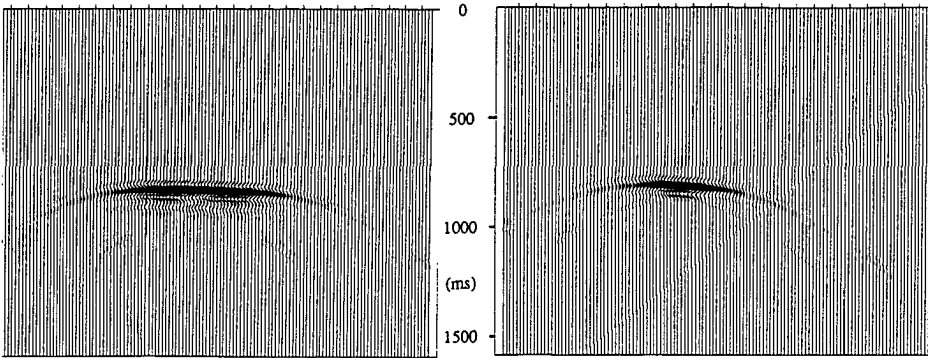
Figure 3.13: Two cross sections through the zero offset data at the surface, modeled with a Kirchhoff summation method.
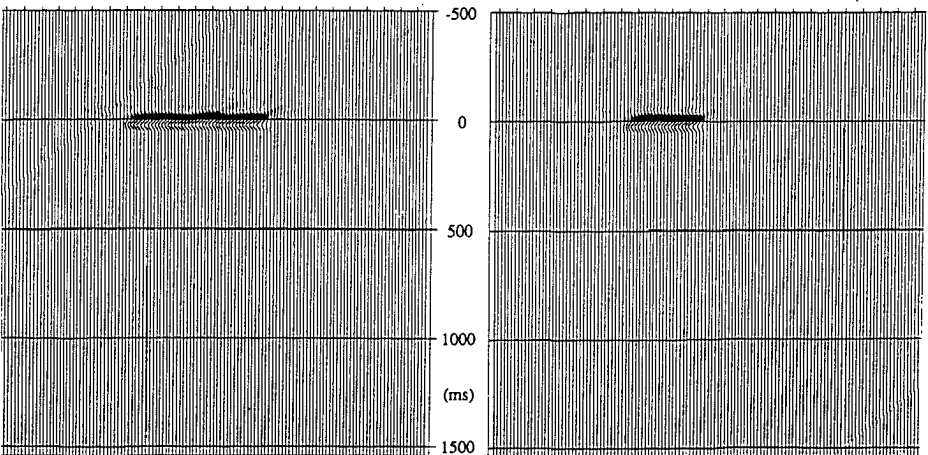
Figure 3.14: Two cross sections through the data after 3-D inverse wave field extrapolation.

In conclusion, a non-recursive wave field extrapolation scheme is developed, that is efficient with respect to computation time and disc I/O. It is possible to use this scheme to extrapolate through strongly inhomogeneous media for both 2-D and 3-D applications. These operators are especially suited for implementation in a 3-D shot record redatuming scheme.

4

IMPLEMENTATION OF 3–D
REDATUMING

4.1 INTRODUCTION

In this chapter the implementation of the shot record redatuming will be discussed. In chapter 2 the theory of shot record redatuming was summarized and the basic steps in the scheme were given. It is however very important for the efficiency of the scheme how it is practically implemented, like the nesting of the different loops in the scheme. A major concern is the enormous amount of data, that must be processed. Special attention is paid to minimize the number of time consuming I/O operations in the scheme. Finally it will be shown that the shot record redatuming scheme is extremely well suited for multi-processor computer systems. Some benchmarks show a very effective computer usage on vector processors and also on a parallel computer with 4 CPU's.

4.2 DATA VOLUMES INVOLVED IN THE SHOT RECORD REDATUMING

In this section the data volumes, that are involved in 3-D shot record redatuming, will be discussed. First, let us consider an example of a 3-D acquisition geometry for land data as depicted in figure 4.1. Typically, the geophones are located on 5 or 6 parallel lines of about 100 geophones each. The spacing between the geophones is in the order of 25 m and between the lines a couple of hundred meters. The sources are located on lines, that are perpendicular to the lines of the geophones, with a source spacing of 25 m and a line
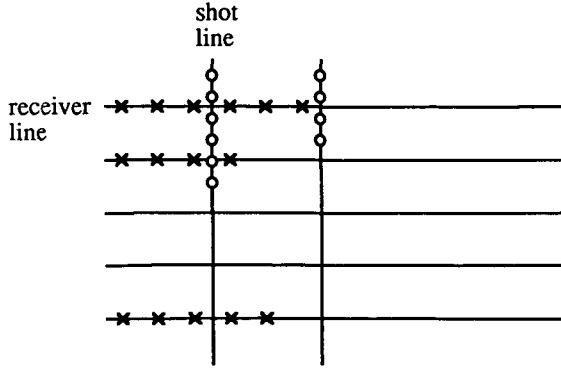
Figure 4.1: Typical shooting geometry for 3-D land data acquisition.

spacing of hundreds of meters. These numbers are just used as an indication. In practice the choice of the different spacings can vary with the requirements and the local situation. In this geometry the detector spacing is dense in one direction (the in-line direction) and coarse in the other direction (the cross-line direction), while on the opposite, the source spacing is dense in the cross-line direction and coarse in the in-line direction. For this geometry a regular grid of midpoints of sources and receivers exists, which is convenient for CMP oriented processing techniques. In the practice of land data acquisition it is often impossible to locate sources and receivers on such a regular acquisition grid. Especially in densely populated areas, e.g. in Western Europe, the acquisition geometry is irregular due to roads, buildings, canals, etc.

For all single shot experiments along one source line the same set of detectors is used. Moving to the next line of sources, a number of detectors is added on one side of the detector lines and a number of detectors is removed from the other side. For the efficiency of the shot record redatuming scheme described in this thesis it is very important, that the same detector stations are used (located at the same surface positions) for a large number of single shot experiments. For 3-D marine data acquisition the situation is different (see figure 4.2). Both the sources (air guns) and the receivers (hydrophones) are towed by one or more vessels. At present 4 or 5 parallel cables, containing the hydrophones, can be towed simultaneously. During the sailing of the ship the experiments are performed, which means that the complete line is moved between the different shots. The movement of the cable causes variations in the hydrophone positions (cable feathering). For marine data the property of coincident receiver positions for different shots can therefore not be used.
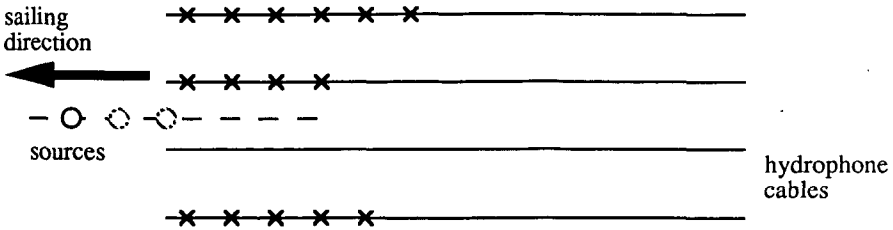
Figure 4.2: Typical shooting geometry for 3-D marine data acquisition.

In order to have an estimate for the sizes of the data volumes involved in 3-D shot record redatuming, I will use an average size of a 3-D survey. Consider the next 3-D survey:

N_s	(= 5000)	shot records
N_c	(= 500)	detectors per single experiment
T	(= 5 s)	registration time
Δt	(= 4 ms)	time sampling interval
$f_{min} \rightarrow f_{max}$	(10 – 60 Hz)	frequency range

From these figures the size of some other parameters can be calculated:

$$N_t = \frac{T}{\Delta t} \quad (= 1250) \qquad \text{number of times samples}$$

$$\Delta t \quad (= 4 \text{ ms}) \qquad \text{time sampling interval}$$

$$N_f \quad \frac{(f_{max} - f_{min})}{\Delta f} \quad (= 250) \text{ number of frequency samples}$$

The size of one shot record in the time domain thus becomes for this numerical example,

$$N_c * N_t * 4 \text{ byte} = 2.5 \text{ Mbyte}$$

and in the frequency domain,

$$N_c * N_f * 8 \text{ byte} = 1.0 \text{ Mbyte} \quad .$$

Note that the data volume in the frequency domain is smaller than the volume in the time domain, because the Nyquist frequency is larger than the highest frequency of interest. This is one of the advantages of redatuming in the frequency domain above time domain processing. The total volume of the 3-D data set in this example is 12.5 Gbyte in the time domain and 5 Gbyte of data in the frequency domain. This enormous amount of data has to

be processed properly. However, by working per monochromatic shot record the amount of data used at one time is limited to just 4 kbyte.

Another important data volume in the redatuming scheme is the extrapolation operator. In chapter 2 it is shown, that the monochromatic extrapolation operator could be written in the form of a complex valued matrix. This matrix consists of N_s columns, where N_s is the number of locations at the surface, and N_t rows, with N_t the number of locations at the upper boundary of the target zone. Let N_t be 10,000 points, then for extrapolation of the source wave field ($N_s = 1$) of one single experiment the size of the extrapolation operator equals,

$1 * N_t * 8$ byte $= 80$ kbyte of data   .

The extrapolation operator for inverse extrapolation of the detected wave field ($N_s = N_c$) from the surface to the target upper boundary has the size of

$N_c * N_t * 8$ byte $= 40$ Mbyte   .

It is clear that the size of the extrapolation operators is much larger than the size of the data of a single shot experiment. However, for land data it can be seen that the same extrapolation operator can be used for a large number of single shot experiments, because the detector stations coincide. Even by moving from one source line to another most of the elements of the extrapolation operator stay the same.

The size of the monochromatic extrapolation operator is about 40 Mbyte, so the operator size for all frequencies would be 10 Gbyte. It is clear that storage of the complete extrapolation operator for all frequencies is not practical. By limiting the storage to some frequency independent operator parameters, like travel time and amplitude, this size can be reduced considerably to,

$N_s * N_t * 2 * 4$ byte   ,

where N_s is the *total* number of used surface positions.

Over a complete survey the total number of surface locations on land will be in the order of 5000. In that case the storage size of the extrapolation operator equals 400 Mbyte, still being a very large data volume.

In the previous chapter a method was outlined, where the operator was calculated by means of ray tracing followed by interpolation to the densely spaced irregular acquisition grid. Such a scheme has the advantage of reducing even more the number of parameters, from which the actual operator can be computed. Other advantages are the support of irregular

shooting geometries and the reduction of the computation time needed for ray tracing. The size of the data volume of operator storage now becomes,

$$N_r * N_t * N_p * 4 \text{ byte} \quad ,$$

with N_r the number of rays, that were calculated for each point at the upper boundary of the target zone and N_p the number of parameters, that has to be stored for each ray.

In practice it is possible to obtain good operators even when the number of 'basic rays' is one percent of the number of acquisition points at the surface for a 3-D operator. On the other hand for these parameters the emergence angles at the surface of the rays have to be stored beside the travel time and amplitudes. Using these figures ($N_r = 50$ and $N_p = 4$) the total data volume to store the extrapolation operator on disc becomes 8 Mbyte, which is very acceptable in 3-D processing. It is therefore advantageous to perform the *operator* interpolation just before the actual redatuming of the shot records, instead of directly after the ray tracing and storing that result.

4.3 DIFFERENT ALGORITHMS

In the previous section an overview was given of the enormous data volumes involved in 3-D shot record redatuming. Especially the size of the extrapolation operator is very large and needs special attention concerning I/O and calculation time. Therefore the structure of the redatuming algorithm depends highly on the operator size and how the operator changes during the processing. For this reason different processing structures are proposed for land data and for marine data. The basic principles of the redatuming scheme, described in this thesis, are processing per shot record and per frequency component. In the structure of redatuming these principles result in two loops, a shot record loop and a frequency loop. The processing steps in the scheme are operator calculation, forward extrapolation of the source wave field, inverse extrapolation of the detected wave field, deconvolution of the upgoing waves with the downgoing waves at the upper boundary of the target zone and the CDP stacking. Here the operator calculation can be separated into a frequency independent operator interpolation and the actual computation of the frequency dependent operator from the operator parameters. Thus two essentially different structures can be designed as shown in figure 4.3, which perform the same redatuming algorithm. The difference between these structures is the nesting of the shot loop and the frequency loop. It turns out to be best to use the scheme with the frequency loop *outside* the shot record loop (figure 4.3a) for land data processing, while the scheme with the frequency loop *inside* the shot record loop (figure 4.3b) can be best used in marine data processing.
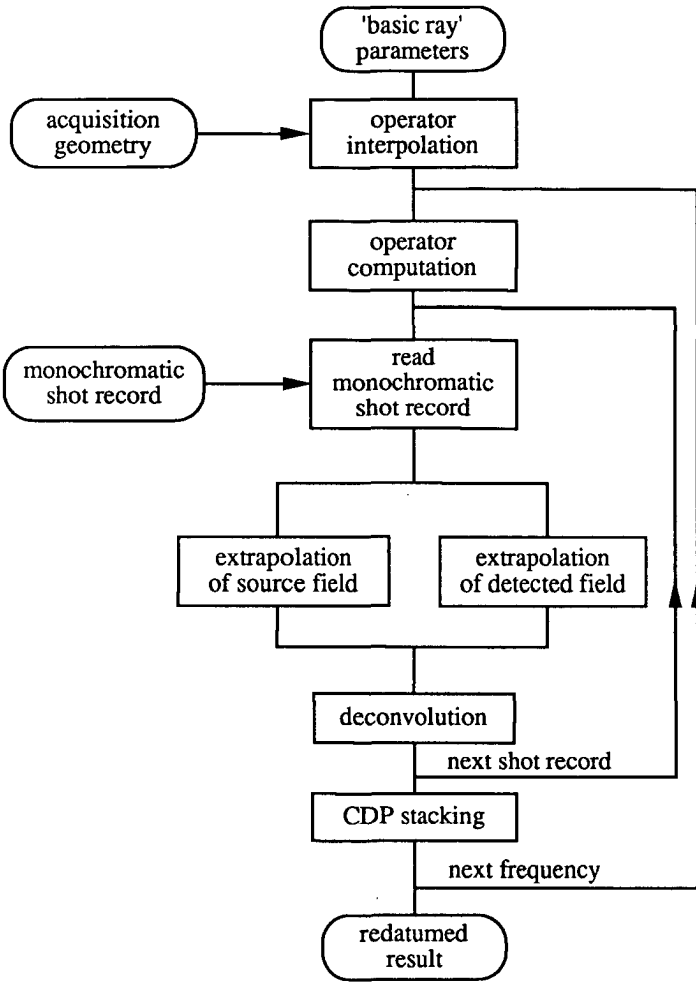
Figure 4.3a: Structure of the redatuming algorithm with the frequency loop *outside* the shot record loop.

Let us first consider the case of redatuming land data. As mentioned before, the property that (most of) the extrapolation operator elements stay the same for different shot records is very important. By making the shot record loop the most inner loop of the main scheme, it is possible to keep the extrapolation operator (unchanged) in memory for a large number of shot records. The different elements of the extrapolation operator are in this way calculated only once and no extra disc I/O is needed. If some detector positions change for different shots only a small number of the elements has to be replaced by new elements.
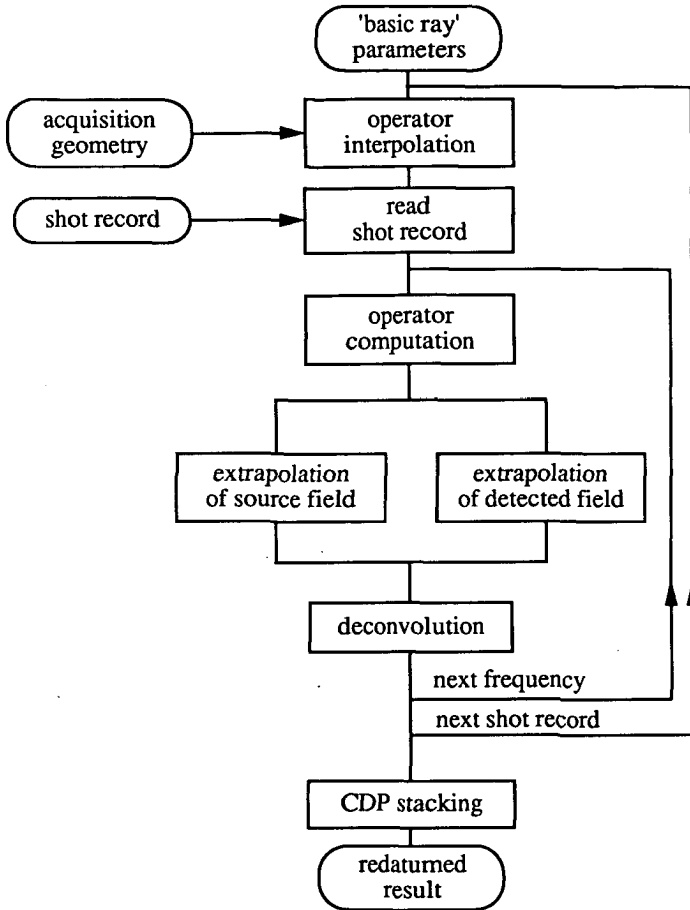
Figure 4.3b: Structure of the redatuming algorithm with the frequency loop *inside* the shot record loop.

Ideally the frequency independent part of the operator calculation is placed outside the frequency loop. In section 4.2 it is argued that the operator parameters calculated by ray interpolation would amount to about 400 Mbyte of data. It is very inconvenient to keep this amount of data in memory during the entire redatuming process, but also storage of these operator parameters on disc can require much disc space and disc I/O. At the cost of some extra computation time these problems can be avoided. The operator interpolation can also be done inside the frequency loop, just before calculation of the frequency dependent

operator elements. The disc I/O and storage is then limited to the parameters of the 'basic rays'. On the other hand the operator interpolation is now performed N_f times instead of just once. From these considerations we arrive at the redatuming scheme for land data, that is depicted in figure 4.4. The required computer memory for this scheme is mainly determined by the size of the extrapolation operator. This size is limited, because the redatuming is performed per shot record. For the numerical example used in this chapter the size is about 40 Mbyte. On most of the current computer systems the memory size is often a couple of hundred Mbytes, so this size will give no problems in most cases. If the scheme has to be adjusted for smaller memory requirements, the operator size should be
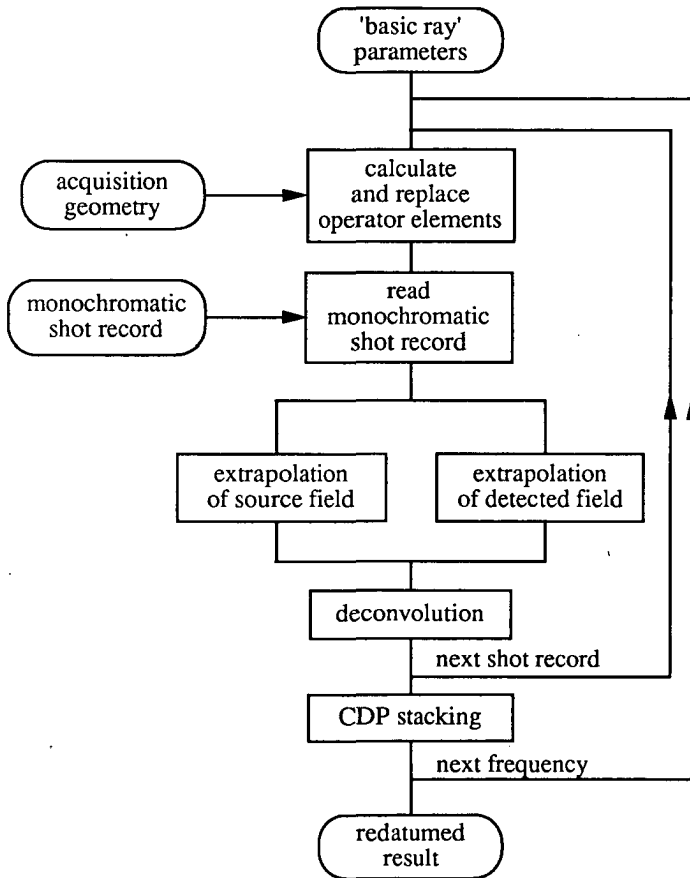
Figure 4.4:   Structure of the redatuming algorithm with the operator interpolation directly before the monochromatic extrapolation.

reduced. This can be done by redatuming to separate parts of the target level. Because of the property of coincident operator elements, here the shot record loop also has to be the inner loop in the main scheme. The cost of this extra loop is caused by extra transfers of the shot records from disc to memory. To keep the amount of shot records, that are processed at a time, limited the scheme can also be performed per cluster of shot records, e.g. one tape of data. Thus the general structure of the redatuming scheme for land data is shown in figure 4.5.
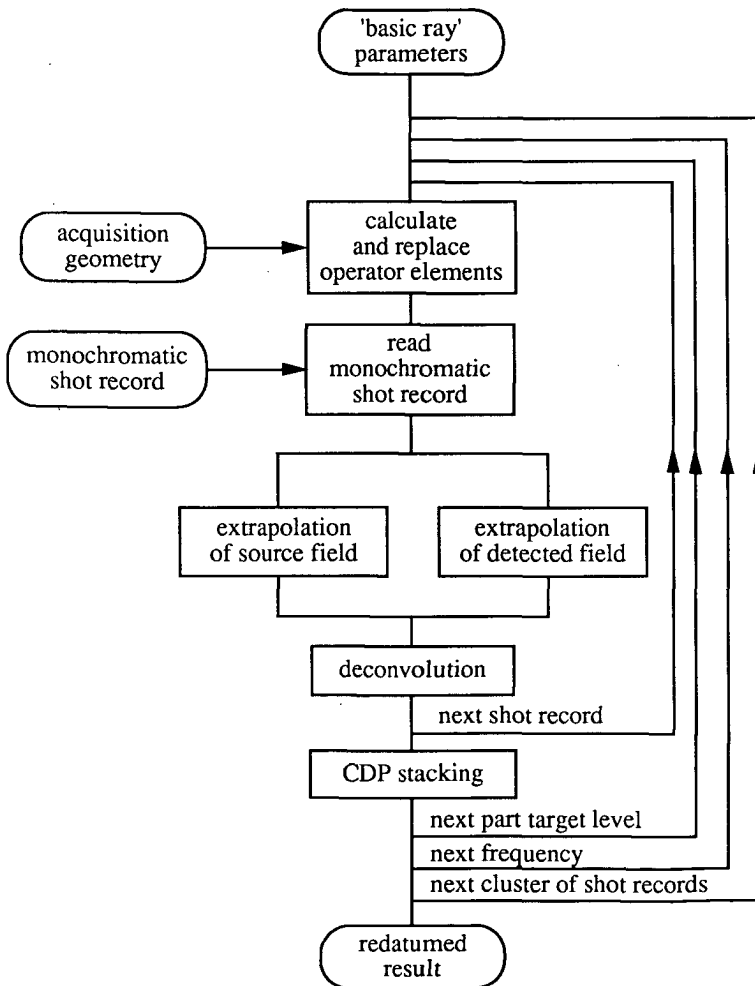

Figure 4.5: General structure of the redatuming algorithm for land data.

For marine data it is not possible to use the coincident detector positions due to cable feathering. In principle the detector positions are different for all single shot experiments. For this case the calculation of the extrapolation operator will be the most time consuming step in the redatuming scheme. Given the travel time T_{ki} and the amplitude A_{ki} for a certain pair of one detector point and one target point, the element of the operator can be written as (see also equations (2.26), (2.27), (3.5) and (3.6)),

$$W_{ki}^+ (z_A,z_0,\omega) = - \frac{2i\omega \cos \theta_{ki}}{\rho_k V_k} A_{ki}\, e^{-i\omega T_{ki}} \Delta x \Delta y \quad , \tag{4.1}$$

with   column-index k the position at the surface,

                     row-index i the position at the target level,

                     ω (= $2\pi f$) the circular frequency,

                     V_k the propagation velocity of position k at the surface,

and ρ_k the density of position k at the surface.

In this equation the calculation of the complex exponential function will take most of the computer time. However from the extrapolation operator for circular frequency ω, the operator for the following frequency $\omega + \Delta\omega$ can be derived using the following recurrent relation,

$$W^+(z_A,z_0,\omega + \Delta\omega)_{ki} = \frac{\omega + \Delta\omega}{\omega} W^+(z_A,z_0,\omega)_{ki}\, C_{ki} \quad , \tag{4.2}$$

with $C_{ki} = e^{-i\Delta\omega T_{ki}}$.

Note that in this relation the complex exponential factor C_{ki} is independent from the frequency and needs to be evaluated once. It can therefore be expected that relation (4.2) can be evaluated much faster than relation (4.1). To illustrate this a simple benchmark is performed. In figure 4.6 the different methods are shown that are compared in this benchmark. In figure 4.6a the scheme is shown for computing the extrapolation operator using the complex exponential function. Here the frequency dependent operator is calculated directly from the operator parameters T and A. The nesting of the loops is here of minor importance, as long as the length of the inner loop is long enough to enable efficient vectorization. For the benchmark the following values for the loop sizes were used,

N_s	= 100,	number of surface positions,
N_t	= 100,	number of target positions,
and N_f	= 100,	number of frequencies.

For these numbers it took 5.20 seconds CPU time to execute the scheme of figure 4.6a on a Convex C1 computer.
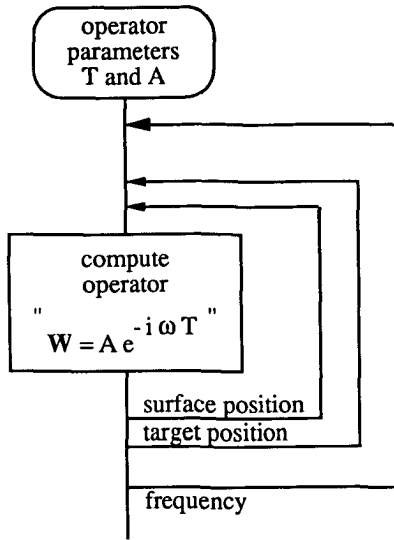
Figure 4.6a: Strucuture of the benchmark with operator computation by an complex exponential function (method 1).
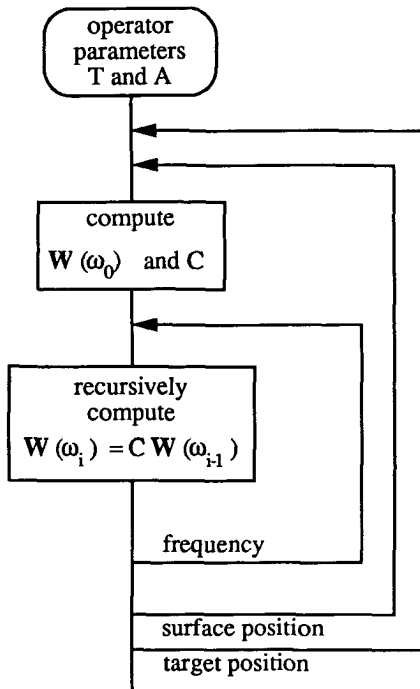

Figure 4.6b: Structure of the benchmark with operator computation by recursive formula 4.2 (method 2).
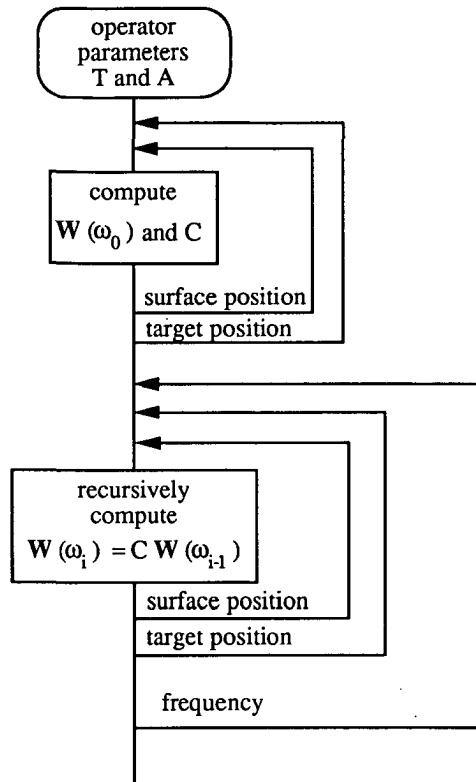
Figure 4.6c: Structure of the benchmark with operator computation by recursive formula 4.1 and position loops inside the frequency loop (method 3).

For the structure, where the frequency dependent operator is calculated recursively for the different frequencies, two different schemes were used, as shown in figures 4.6b and 4.6c. In figure 4.6b the frequency loop is chosen to be the innermost loop of the scheme. For the numbers mentioned above this scheme was performed in 3.88 seconds of CPU time on the Convex. It is clear that this method of calculating the operator is more efficient than the method using the complex exponential function. Note however, that the scheme of figure 4.6b can not be vectorized, because the inner frequency loop contains a recursive operation. Even when the inner loop is run in the scalar mode of the computer this scheme is faster than the scheme of figure 4.6a. In order to make optimum use of a vector computer the frequency loop was interchanged with the loops of surface and target positions, as depicted in figure 4.6c. Note, that in this scheme the complex exponential

factor C_{ki} must be saved for all elements of the extrapolation matrix during execution of the scheme. The scheme of figure 4.6c, executed on the Convex, took only 1.43 seconds, which is much faster than the original method of calculating the extrapolation operator. In table 4.1 the results of this benchmark are summarized.

Table 4.1: Operator calculation with the complex exponential function or by a recurrent relation.

	method	CPU-time (seconds)	relative speed (to method 1)
1	complex exponential	5.20	1.00
2	recursive relation (ω-loop inside)	3.88	1.40
3	recursive relation (ω-loop outside)	1.43	3.65

In the numerical example for 3-D processing, used earlier in this chapter, the size of the matrix of recursion factors C_{ki} would be 40 Mbyte. This extra memory requirement can be reduced by placing the frequency loop inside the loop for the target positions in figure 4.6c. Moving the frequency loop inside the innermost loop is also possible. Then the extra memory requirement would be just 8 bytes (one complex variable), but it was shown, that in that case the innermost loop can not be vectorized anymore on vector computers. The benchmark shows that even in that case this way of operator calculation is still faster than calculation of the complex exponential, but no efficient use is made of the computer capacities.

I finish this section with the remark that both structures are from algorithmic point of view the same. Just the implementation differs, depending on the type of data acquisition. The examples of shot record redatuming given in this thesis are all performed with the structure for land data redatuming.

4.4 BENCHMARKING AND PARALLELISM

With the redatuming algorithm, that is described in this thesis, some benchmarks were performed on different computers. First the performance of the scheme is examined, when the number of detectors, shots and points on the upper boundary of the target zone, are varied. In figure 4.7 the results of this test are shown. While one parameter was varied the other two parameter were fixed to 300. It can be seen that the algorithm is linear in all parameters. Because the algorithm is linear the results of the benchmark have not to be

examined for all parameters, when comparing different computers. The different computers, for which the results are compared, are

Convex C1	vector	1 CPU
Alliant	vector	1 – 4 CPU's
Gould SEL	scalar	1 CPU
Masscomp	scalar	1 CPU

Furthermore for the Convex C1 also the benchmark was performed, where the matrix multiplication in the wave field extrapolation was used from an optimized library instead of the normal vectorized Fortran code. In table 4.2 the results are given in the number of CPU-seconds and the performance is rated, normalized to the slowest computer (Masscomp).
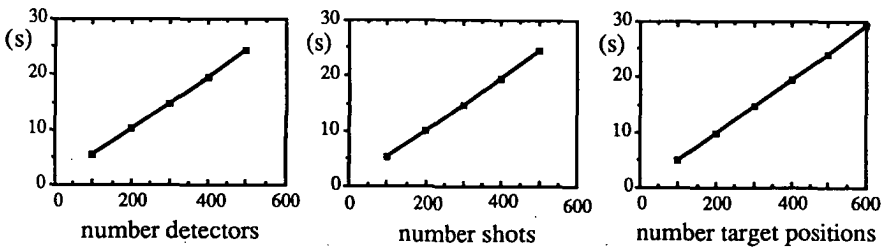

Figure 4.7: Computation time on a Convex C1 as function of processing parameters.

Table 4.2: Benchmark on different computers.

	CPU time (seconds)	Performance
Convex (Fortran) (1 CPU)	46.4	39.8
Convex (veclib) (1 CPU)	14.8	124.6
Alliant (1 CPU)	64.2	28.7
Alliant (2 CPU's)	34.1	54.1
Alliant (4 CPU's)	19.3	95.6
Gould SEL	1042.2	1.8
Masscomp	1844.7	1.0

From this table it can be seen that the scheme can be vectorized very well. Another important observation is that it is very advantageous to use optimized libraries for matrix multiplication, when they are available. In this case the program speeded up by another factor of 3 on the same computer, when the library function was used. It should be noted that for larger vector lengths this improvement will in general be less significant.

Now let us look at the parallelism in the redatuming scheme. In figure 4.8 the redatuming scheme of figure 4.3a is depicted in a different way. Here the loops of the scheme, that can be performed independently from the others, are shown parallel. As can be seen the redatuming scheme consists of a lot of independent modules. Therefore redatuming is very well suited for parallel processing. As a first initial step the highest level of independency is the redatuming of the monochromatic components. There is no interaction between the processing of the different frequencies. One lower level of independency is the monochromatic redatuming of each single experiment. The time consuming extrapolation and deconvolution of the data can be carried out independently for each monochromatic shot record. In the CDP stacking the results of the independent processes come together again. The lowest level of independency can be found within the extrapolation of the shot records, which is not explicitly shown in figure 4.8. This extrapolation is implemented as a matrix multiplication per frequency component on parallel computers. Such a matrix multiplication can be implemented automatically as a parallel process.

The redatuming scheme has been tested without any modification on an Alliant computer with 4 processors. At that moment it was not possible to indicate to the compiler at what level the parallel processing should occur. This meant, that the compiler vectorized the innermost loop (dot product of the data vector and a row of the extrapolation matrix) and automatically parallelized the second innermost loop (rows of the extrapolation matrix). It is clear that this will not give the optimum result, because parallel processing is most efficient as the separate parallel jobs each are as long as possible, which means the outermost loop in the scheme. In table 4.3 the result of this benchmark is shown.

It can be seen that the benchmark speeded up by a factor of 3.3 to 3.5, when the number of CPU's increased from 1 to 4. This meant that the efficiency of the parallel algorithm (2 innermost loops) is over 80% of the maximum possible speed-up of 4. This efficiency is very high. By parallelizing more outer loop it is expected that the efficiency will approach 100% (speed-up by a factor of 4).
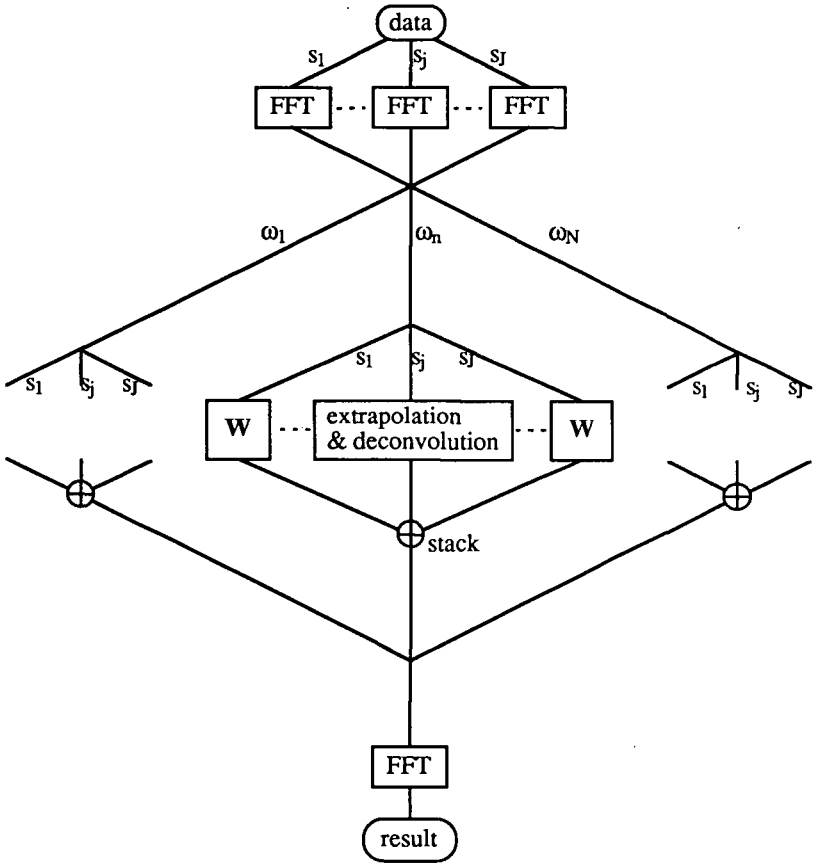
Figure 4.8: Parallelism in the redatuming scheme.

Table 4.3: Parallel processing of the redatuming scheme.

vector length	1 CPU	2 CPU's	4 CPU's	speed-up (4 CPU's)
100	22.6	11.5	6.3	3.5
200	43.9	23.1	13.0	3.4
300	64.2	34.1	19.3	3.3
400	84.6	45.0	25.4	3.3
500	105.0	55.8	31.5	3.3

5

EXAMPLES OF SHOT RECORD REDATUMING

5.1 INTRODUCTION

In the previous chapters various aspects of non-recursive wave field extrapolation and shot record redatuming were discussed. In chapter 2 the general theory of extrapolation and redatuming was discussed and in chapters 3 and 4 aspects of operator calculation and the implementation of these operators in a 3-D redatuming scheme were discussed. In this chapter some examples of shot record redatuming are shown. In section 5.2 the different steps of shot record redatuming are illustrated with a simple example of 2-D data, modeled with a finite difference algorithm. Here also the total TRITON processing scheme is demonstrated with an example of a subsurface model with a complex target zone. It is shown, that after redatuming and zero-offset migration a detailed depth section of the target zone is obtained. In section 5.3 the use of the redatuming scheme on 2-D data, measured over a scale model in a watertank, is shown. These data were measured for Marathon Oil Company by the Seismic Acoustic Laboratory in Houston, Texas. Because of the complicated structure of this model, conventional processing techniques, based on CMP stacking, fail to image the model correctly. In section 5.4 an example is shown of 2-D field data from the Nederlandse Aardolie Maatschappij (N.A.M.). Finally in section 5.5 an example of 3-D shot record redatuming is given. The data for this example were generated by a modeling algorithm, that is based on ray tracing and is described in appendix B of this thesis.

5.2 REDATUMING OF FINITE DIFFERENCE DATA

In this section two examples are presented of redatuming of shot records, that were modeled with an acoustic finite difference algorithm. In the first example also the intermediate steps of the redatuming scheme will be shown. Consider the subsurface model shown in figure 5.1a. In this model a reflection-free surface was used, so no surface related multiples are present in the data. At the surface of this model data are generated and a shot record redatuming is performed to a depth of 700 m. This level is just above the faulted reflector at 800 m depth. In figure 5.1b the acquisition configuration of this
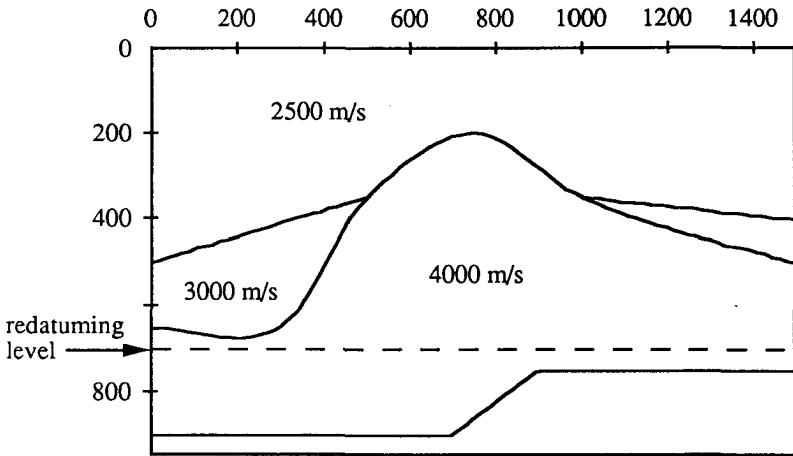
Figure 5.1a: 2–D subsurface model for example 1 with the target level at z = 700 m.
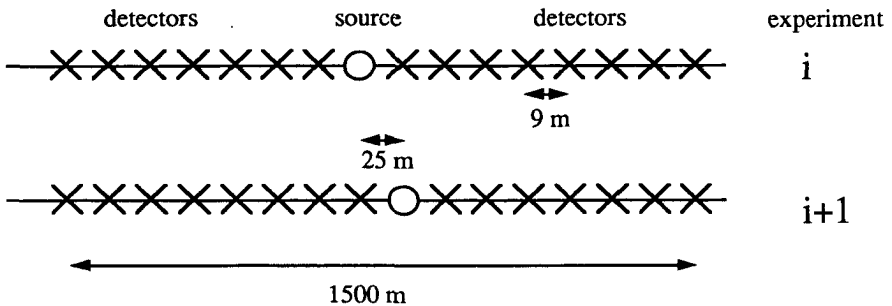
Figure 5.1b: Acquisition configuration for example 1.
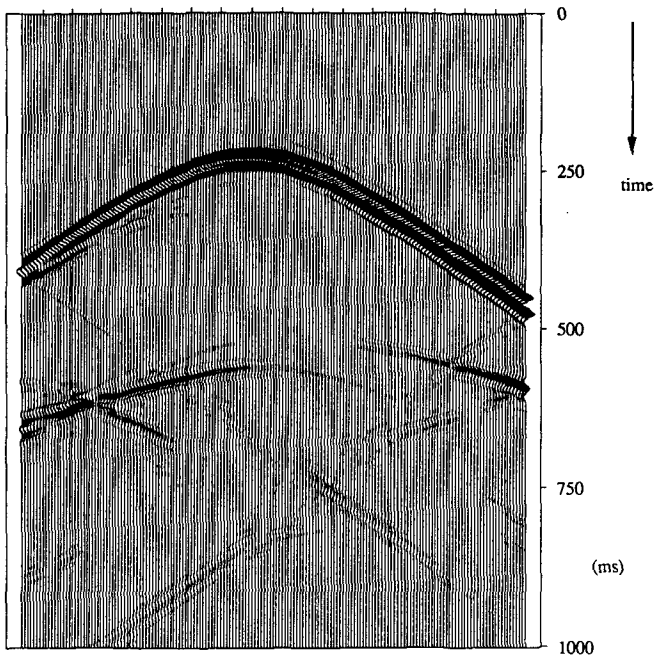
Figure 5.2: Shot record for a source location x = 500 m in the model of figure 5.1a.

example is given. The receivers were located on a fixed grid along the surface with a receiver spacing of 9 m. The source spacing for this example is 25 m. In figure 5.2 one of the shot records at the surface is shown. The source was located at a lateral position of 500 m. In the data no direct wave, that propagates directly from source to receiver, was modeled. Clearly the reflections from the overburden can be recognized from about 200 ms to 500 ms. The reflection from the faulted interface in the target zone can be found at an arrival time of about 600 ms. In figure 5.3a the zero offset data at the surface from the lower reflector is shown. This zero offset data is directly modeled using the exploding reflector model and the reflections of the overburden are left out. This zero offset data is the best result that can be reached using conventional CMP stacking. In figure 5.3b the zero offset data is shown as if it was measured at the upper boundary of the target zone. This is the best result that can be expected from redatuming, if all other processing parameters were ideal (infinite acquisition surface, true amplitude extrapolation operators, etc.). From this the important role of redatuming becomes clear.

Next I will show the intermediate results of each step in the redatuming process for this example. These intermediate steps are shown in the time domain. The redatuming itself
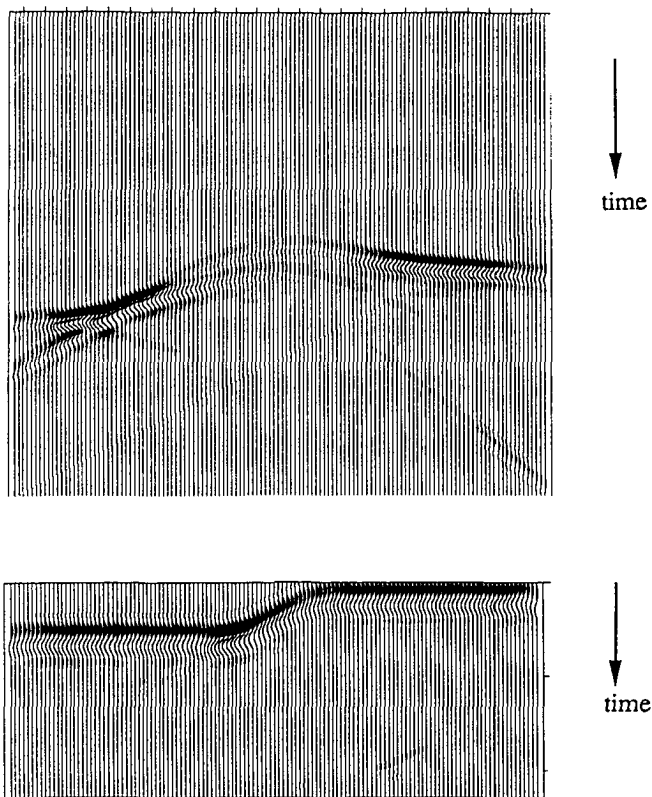
Figure 5.3:   Directly modeled zero offset response of the lower reflector (a) at the surface and (b) at the target level.

however is performed per monochromatic component. The first step in the shot record redatuming is the inverse extrapolation of the detected wave field from the surface to the upper boundary of the target zone. This step is described per monochromatic component by equation (2.36a),

$$\vec{P}_j^-(z_M) = \mathbf{F}^-(z_M, z_0)\, \vec{P}_j^-(z_0) \quad , \tag{5.1a}$$

where $\vec{P}_j^-(z_0)$ is a vector containing the upgoing wave field at the surface of shot record j,

$\mathbf{F}^-(z_M, z_0)$ is the inverse wave field extrapolation operator from the surface z_0 to the upper boundary of the target zone z_M

and $\vec{P}_j^-(z_M)$ is the upgoing wave field at z_M due to source j.
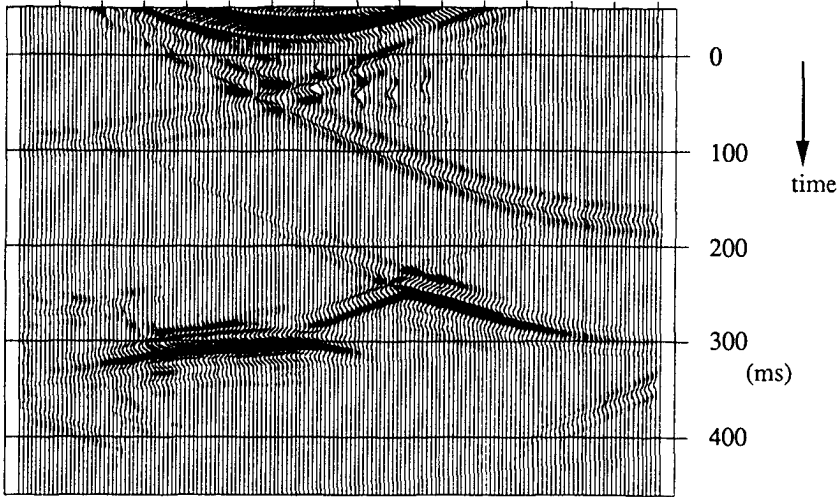
Figure 5.4: Inversely extrapolated data at z = 700 m of the shot record of figure 5.2.

The result of this step, applied to the shot record of figure 5.2, is shown in figure 5.4. In the upper part of this figure (t < 200 ms) the response of the overburden can still be seen. The response of the target zone (220 ms < t < 400 ms) is after inverse wave field extrapolation already much clearer than in the shot record at the surface (figure 5.2).

The second step of the shot record redatuming scheme is related to the extrapolation of the source wave field from the surface to the upper boundary of the target zone. This step involves the calculation of $\vec{F}_j^+(z_0,z_M)$ which contains the elements of the j-th row of $F^+(z_0,z_M)$, the inverse wave field extrapolation operator from z_M to z_0. This step accounts for a stabilized inversion of the incident source wave field at the upper boundary of the target zone. In figure 5.5 the incident source wave field at the upper boundary of the target zone is shown. From this figure it is clear, that ray tracing was used to calculate the extrapolation operator. Due to inhomogeneities in the overburden shadow zones occur at the left part of the subsurface in this example. Because of these shadow zones the source wave field at the upper boundary of the target zone is discontinuous. The correct incident wave field should contain diffraction instead of this discontinuity. If the Gaussian beam method would have been used to compute the operator the correct source wave field should have been approximated much better.
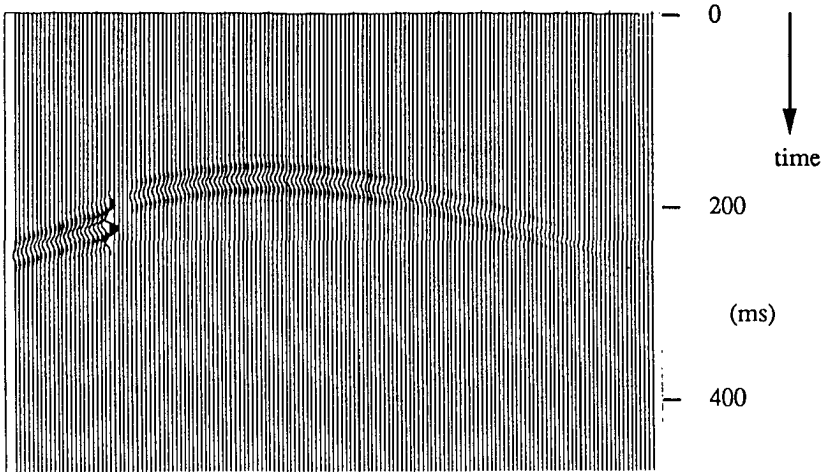
Figure 5.5: Illuminating source wave field at z = 700 m calculated with ray tracing.

The third step in the shot record redatuming scheme is the "deconvolution" of the upgoing reflected wave field at the upper boundary of the target zone (equation 2.36c),

$$<X(z_M)>_j = \vec{P}_j^-(z_M) \left[\vec{F}_j^+(z_0,z_M) \right]^T \ , \tag{5.1b}$$

where $<X(z_M)>_j$ is an underdetermined estimate of the impulse response $X(z_M)$ of the target zone.
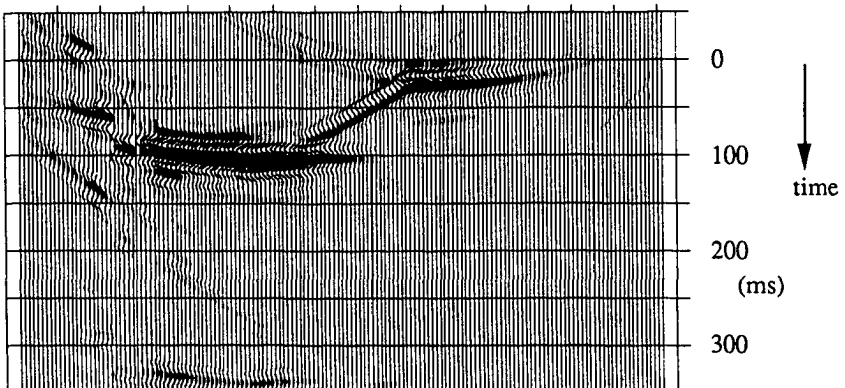
Figure 5.6: Result of deconvolution of the upgoing reflected wave field (figure 5.4) with the downgoing source wave field (figure 5.5).

In figure 5.6 the zero offset traces of this single fold redatuming result are shown after a Fourier transformation from the frequency domain to the time domain. The discontinuity on the left side of this figure is directly caused by the discontinuity in the source wave field (figure 5.5). Note that even this single fold result can be qualitatively interpreted quite well, although no conclusions on the exact location of the fault can be made. One of the advantages of shot record redatuming over the conventional prestack redatuming techniques is the intermediate results for each shot record, that are available and can be investigated. This investigation of intermediate results gives a much better control over the redatuming process.

The final step to obtain the impulse response at the upper boundary of the target zone is the Common Depth Point (CDP) stacking (equation 2.36d),

$$X(z_M) = \sum_j <X(z_M)>_j \; .$$

(5.1c)

By combination of all shot records secondary sources are constructed at the upper boundary of the target zone. In figure 5.7 the result of the CDP stacking is shown. Destructive interference causes, that the discontinuity effects of ray tracing operators and edge effects in each single fold redatuming result are cancelled. The final result shows no discontinuities anymore. However, the artifacts of the ray tracing operators, at the left side of the reflector remains. The edge effect at the right side of the zero offset section is caused by the finite difference modeling scheme, due to the boundaries of the computational
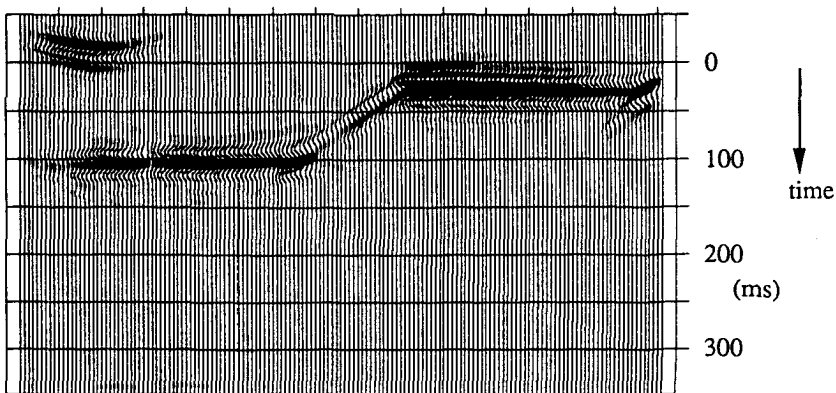

Figure 5.7: Redatuming result after CDP stacking zero offset data at z = 700 m.
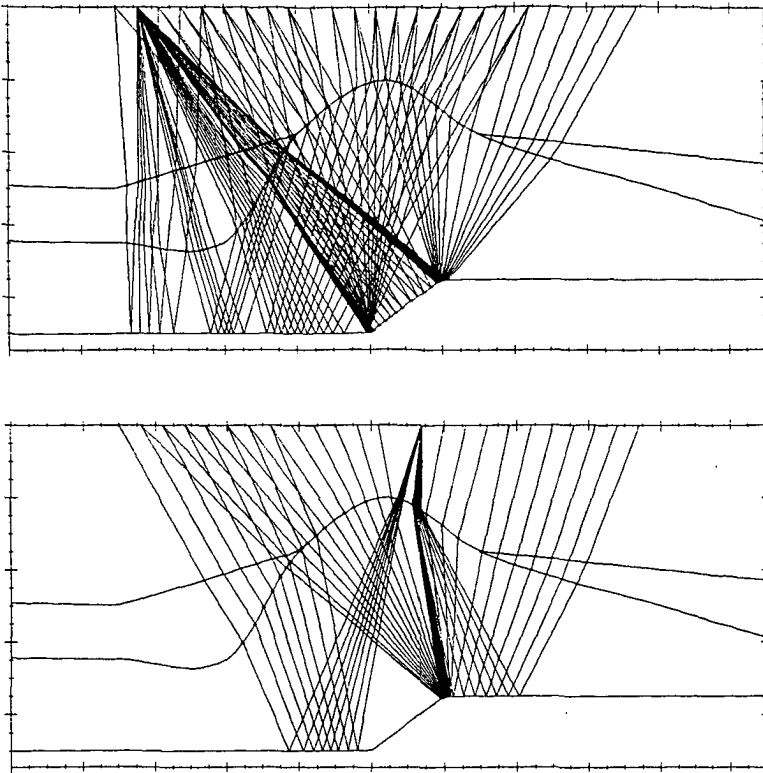
Figure 5.8:   For sources at the left side of the model of figure 5.1a the reflection of the flank of the
lower interface are detected at the surface. For sources at the right side the reflections are
not detected at the surface.

subsurface model. It can also be seen that the reflections of the dipping part of the lower
reflector have a smaller amplitude. From simple geometrical considerations (see the rays in
figure 5.8) it can be seen that most of the energy reflected from this part of the interface
was not measured by the acquisition geometry. The event at negative time on the left side
of figure 5.7 is caused by the lowest interface in the overburden.

For the second example of shot record redatuming the subsurface model was used, that is
shown in figure 5.9a. The surface of this model is chosen pressure free, which causes
strong surface related multiples in the data. In figure 5.9b the acquisition geometry is
schematically depicted. Again the receivers were located on a fixed grid with a spacing of
10 m. The shot spacing was also 10 m, so in total 200 shot records of 200 traces each are
modeled using a finite difference modeling scheme. In this model a complicated target zone
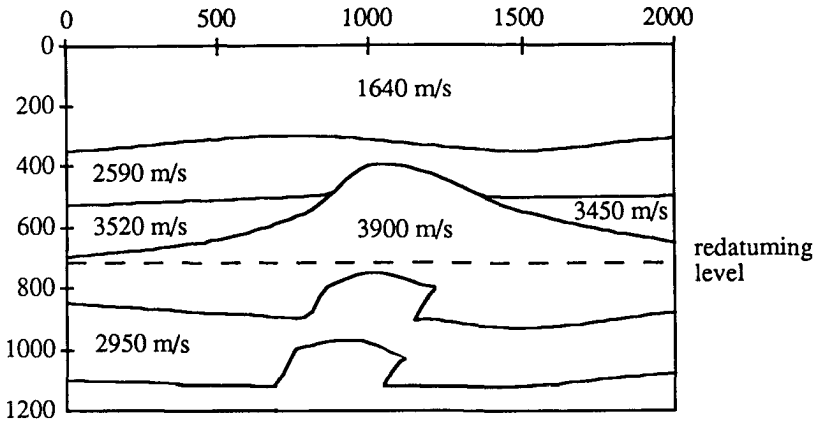
Figure 5.9a: 2–D subsurface model for example 2 with a complicated target zone.
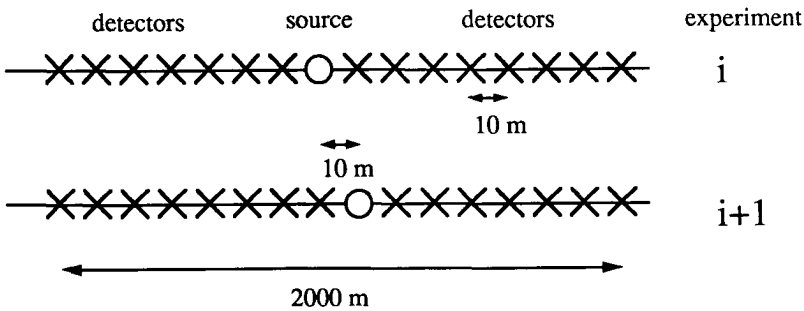

Figure 5.9b: Acquisition configuration for example 2.

is present below 700 m depth, while also the overburden contains strong lateral velocity variations. In figure 5.10a a shot record is shown for this model for a source at 1200 m. Conventional processing would fail for these data, which makes depth migration necessary. With surface related preprocessing, described by Verschuur et al. (1988), the multiples were eliminated and a multiple free shot record for x = 1200 m is shown in figure 5.10b.

Using a well-oriented redatuming to a vertical target zone the macro subsurface model can be estimated, as described by Cox et al. (1988). The estimated macro subsurface model for the overburden in this example is shown in figure 5.11. Comparing this result with the true
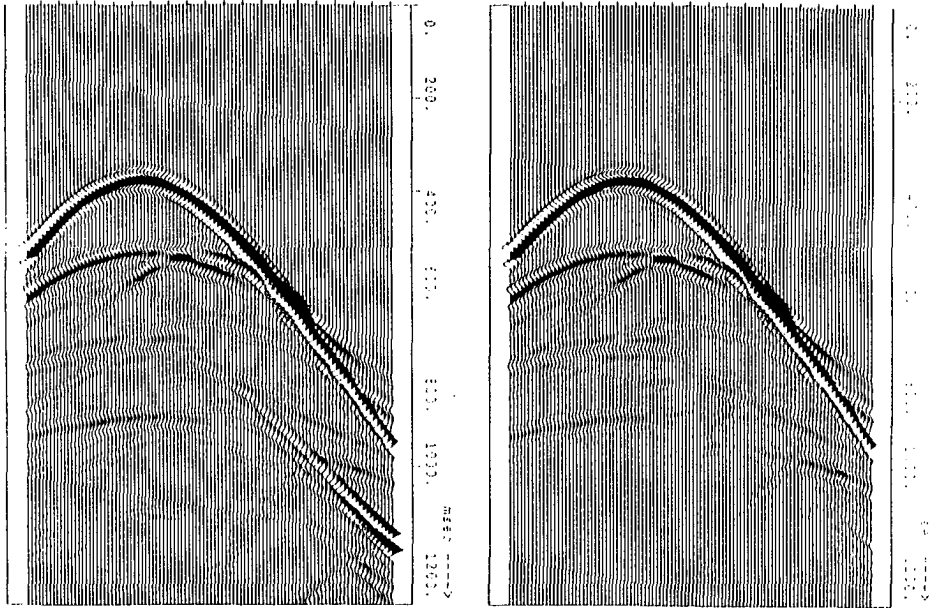
Figure 5.10: Shot record for a source location of x = 1200 m
a: with surface related multiples
b: after multiple elimination.

Figure 5.10: Shot record for a source location of x = 1200 m
a: with surface related multiples
b: after multiple elimination.
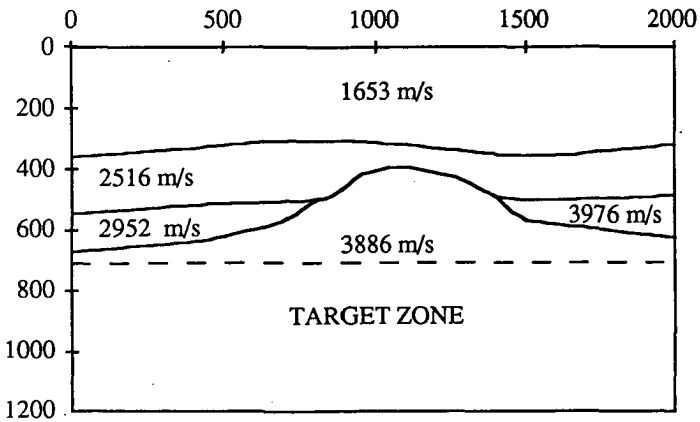
**Figure 5.11**: Estimated macro subsurface model for example 2.
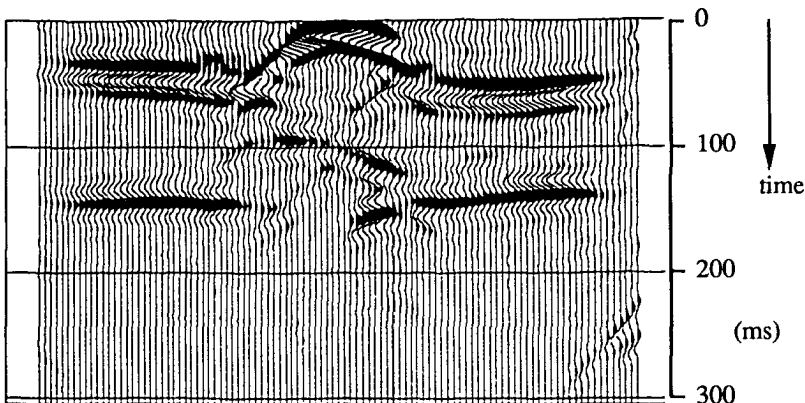
Figure 5.12a: Zero offset data at the target level after redatuming with the true model.
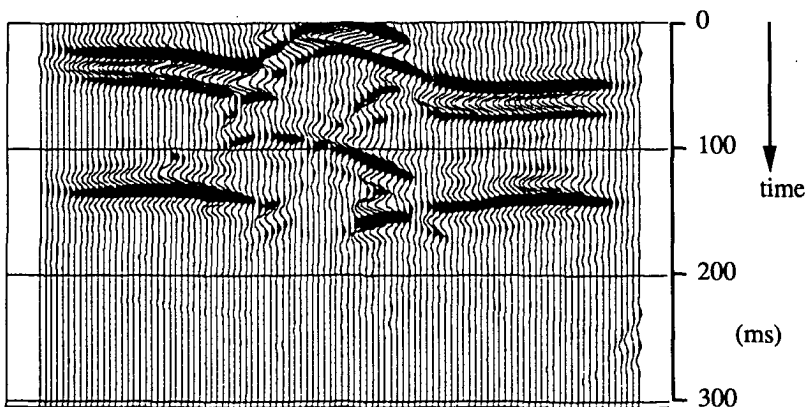

Figure 5.12b: Zero offset data at the target level after redatuming with the estimated model.

model (figure 5.9), it can be seen that the model is estimated very well. For thick layers the velocities match very well with the true velocities, while for the thin layers in the model the propagation velocities cannot be estimated just as good. Note that because with this method the propagation properties of the subsurface are estimated directly, velocity and thickness errors made for shallow layers are compensated by the estimated velocities in the deeper layers. To show that the estimated macro model correctly describes the propagation properties of the subsurface, a shot record redatuming is performed to the upper boundary of the target zone with both the true model and the estimated macro model. In figure 5.12a
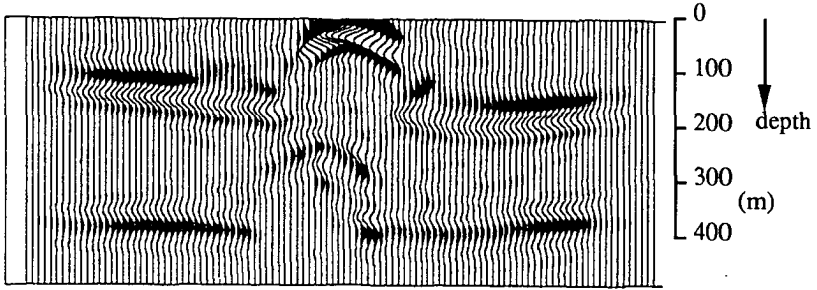
Figure 5.13: Result after migration within the target zone.

the result of redatuming to 730 m with the true subsurface model and in figure 5.12b the result of redatuming with the estimated model is given. Comparing these two figures shows a very good resemblance. This proves, that the estimated macro subsurface model correctly describes the propagation properties of the overburden and therefore it can be used to compute the non-recursive extrapolation operators for redatuming.

Because of the complex structure of the target zone, from the zero offset data at the upper boundary of the target zone no accurate interpretation can be made. To obtain a detailed depth image of the target zone zero offset migration must be performed on these data. Using the method described by Blacquière et al. (1989) the zero offset data are migrated and the result is shown in figure 5.13. Note the good match between the model of the target zone and the migration result.
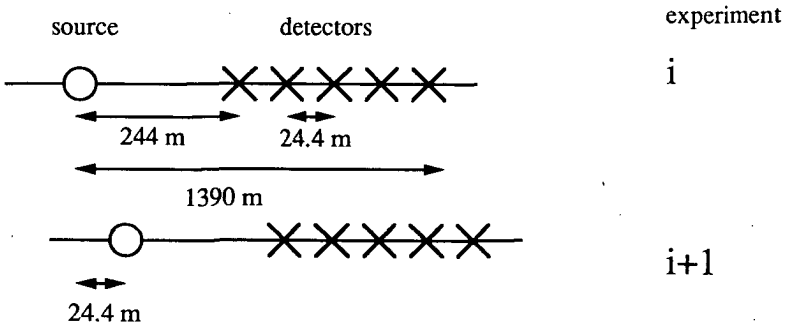

Figure 5.14: Acquisition configuration for the watertank measurement.

5.3   REDATUMING OF 2-D WATERTANK DATA

In this section the redatuming is described of data measured in a watertank over a physical scale model. This model was especially designed by Marathon Oil Company to give serious problems, using conventional CMP oriented techniques. Especially, the ability of depth migration to recover the model's structure was to be tested with these data. Other experiments with these data are described by Postma and Jeannot (1988). In figure 5.14 the end-of-spread acquisition configuration for these data are shown. This configuration is summarized in table 5.1.

Table 5.1: Shooting geometry of the watertank data from Marathon Oil Comp.

Number of shots	296
Shot spacing	24.384 m
Number of detectors per shot	48
Detector spacing	24.384 m
Near offset	243.84 m
Far offset	1389.9 m
Registration time	2 s
Time sampling interval	4 ms

In figure 5.15 some of the shot records, measured over this model, are depicted. Using the focussing analysis method, described by Cox et al. (1989) the macro subsurface model for these data was determined, which is displayed in figure 5.16. The interfaces within the target zone are indicated by dashed lines. Using this macro subsurface model also a redatuming is performed to a depth level at 2200 m below the faulted structure. In figure 5.17 the result of this redatuming is shown. The fault blocks at 3000 m depth are recovered by the redatuming process. Due to the velocity contrast at this faulted interface the lower reflector is not yet perfectly flat in the zero offset data at 2200 m depth. This example shows that with shot record redatuming it is possible to eliminate the effects of a complex inhomogeneous overburden, which heavily distorts the image at the surface of the target zone.
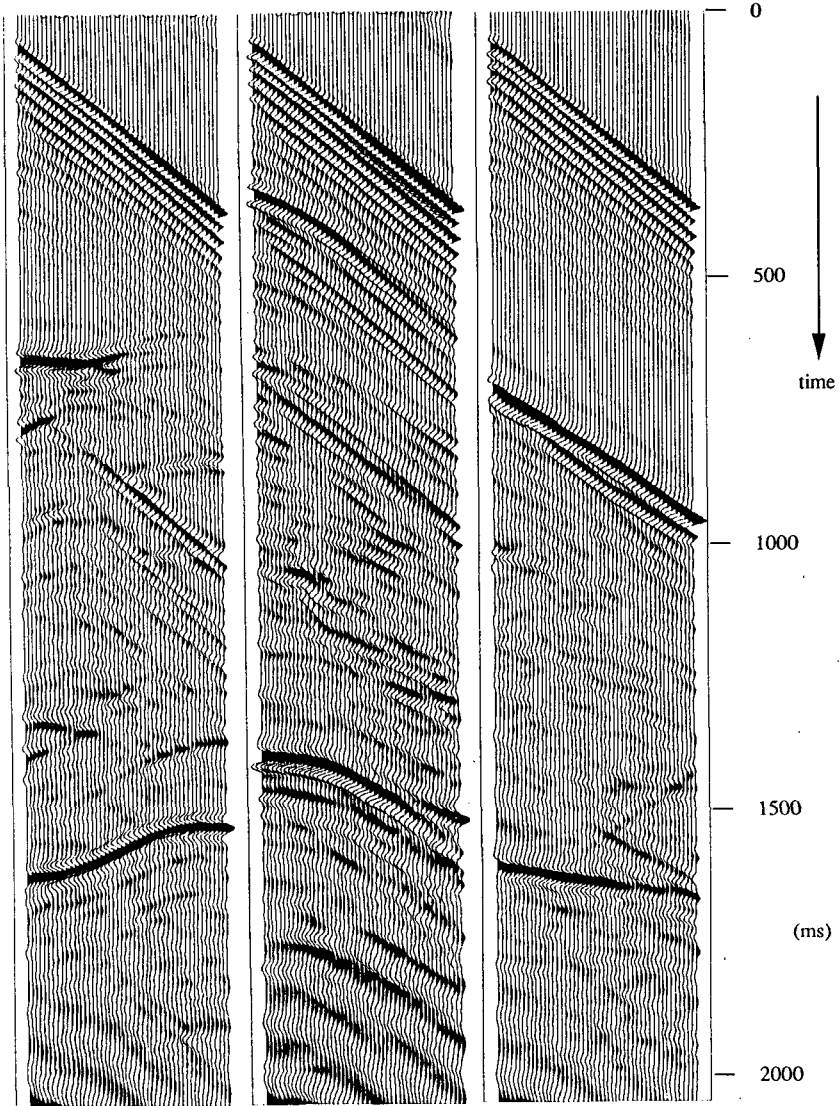
Figure 5.15: Three shot records measured in a watertank (courtesy Marathon Oil Comp.).
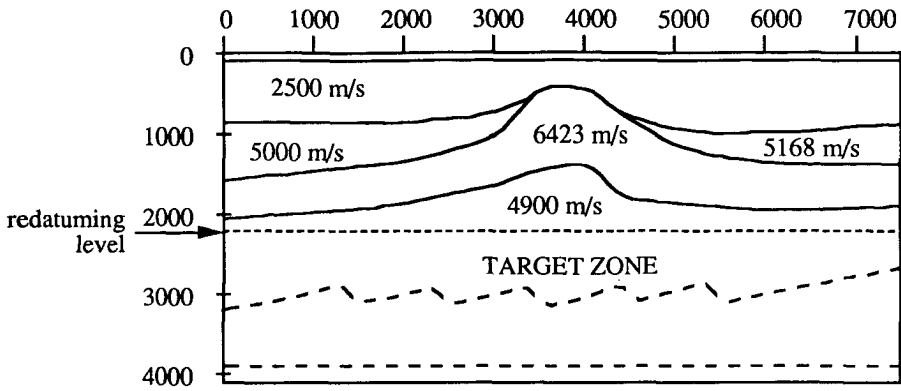
**Figure 5.16**: Estimated macro subsurface model for watertank data.
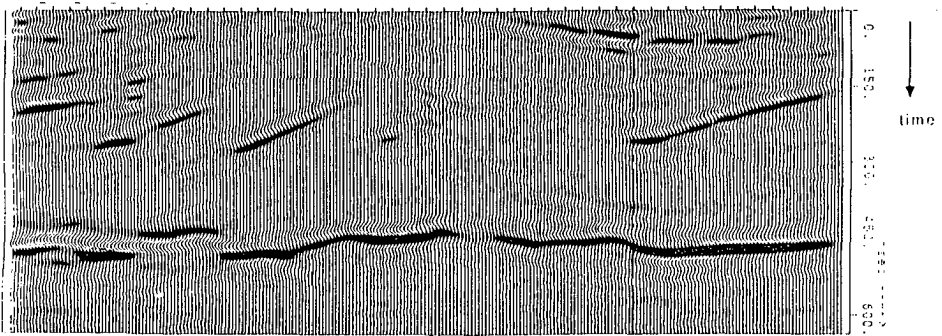
Figure 5.17: Result of redatuming to z = 2200 m.

5.4 REDATUMING OF 2-D FIELD DATA

Using the redatuming scheme, that is outlined in this thesis also a field data set was processed. These data are supplied to us by the Nederlandse Aardolie Maatschappij (N.A.M.). The data was measured on land along a line of about 10 km length. In table 5.2 the geometry of this data set are given.

Table 5.2: Shooting geometry of the field data from N.A.M.

|	
Number of shots	342
Shot spacing	30 m
Number of detectors per shot	120
Detector spacing	30 m
Gap	330 m
Near offset	165 m
Far offset	1935 m
Registration time	4 s
Time sampling interval	4 ms
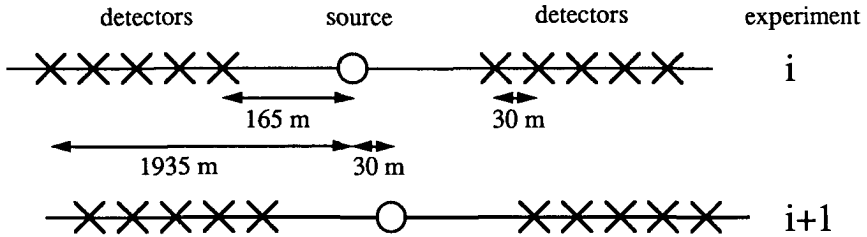
Figure 5.18: Acquisition geometry for field data.

In figure 5.18 this general shooting configuration is depicted. For a number of shots small deviations from this general shooting pattern were made. In figure 5.19 three shot records are shown. Here most of the ground-roll energy is filtered out and also a correction was made for amplitude deviations in the data. It is expected that this pre-processing of the data will have little effect on the redatuming results. With the method described by Van der Made (1988) the macro subsurface model for these data was estimated and this macro model is shown in figure 5.20. In the third layer of the macro model a lateral velocity
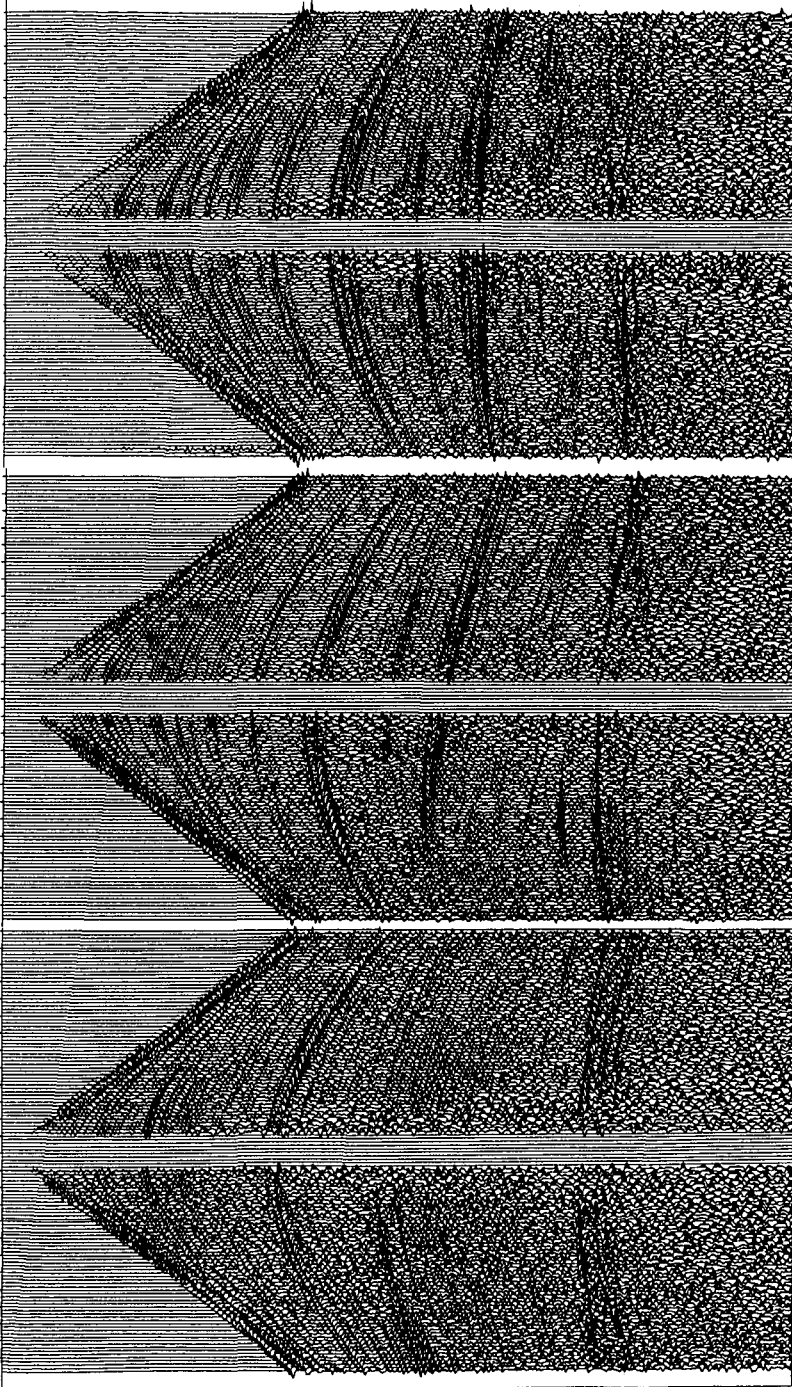
Figure 5.19: Three shot records of field data (courtesy Nederlandse Aardolie Maatschappij).
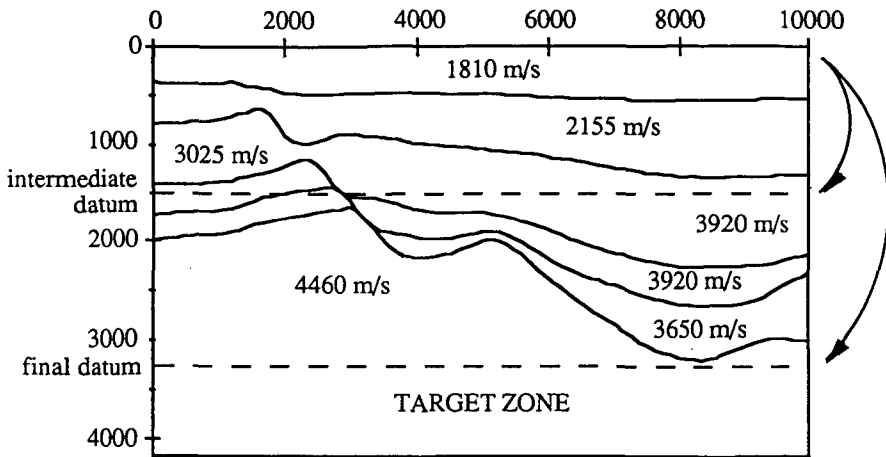
Figure 5.20: Macro subsurface model field data.

gradient was incorporated from 3025 m/s at the left side to 3920 m/s on the right side. The target zone in these data is indicated below 3250 m depth. Furthermore in figure 5.21 a stacked section of the data is shown. The strong reflector in the target zone can be found at about 2300 ms. With the macro model of figure 5.20 first a redatuming of the shot records was performed to a depth of 1500 m. In figure 5.22 the zero offset data, obtained by this redatuming are shown. Here clearly the structure of the salt dome at x = 5000 m and z = 2000 m can be recognized, while also steeply dipping events are imaged good. In these zero offset data the reflector in the target zone has disappeared from the data. Apparently no reflector is present at the expected two-way travel time of 900 ms after redatuming. In order to find the cause of the disappearance a few shot records were extracted from the spatial impulse response at 1500 m depth. In figure 5.23 shot records are shown for (secondary) source locations (x,z) = (4500 m, 1500 m), (x,z) = (6000 m, 1500 m) and (x,z) = (7500 m, 1500 m). In these shot records the reflector in the target can be recognized very clearly. It can be seen that these reflections are found at the offset traces and do not occur at the zero offset traces. In figure 5.24 also some common offset gather at 1500 m depth are shown for offsets of 600 m, 900 m. The reflections just beneath the new datum are moved by the redatuming to the zero offset traces and are not present in these common offset gathers. However, later reflections can be recognized very clearly in these gathers. In the surface data the near offset traces were not measured. By wave field extrapolation the reflections in the offset traces will move to near offset traces and by constructive interference the zero offset response is found in the redatuming scheme. From
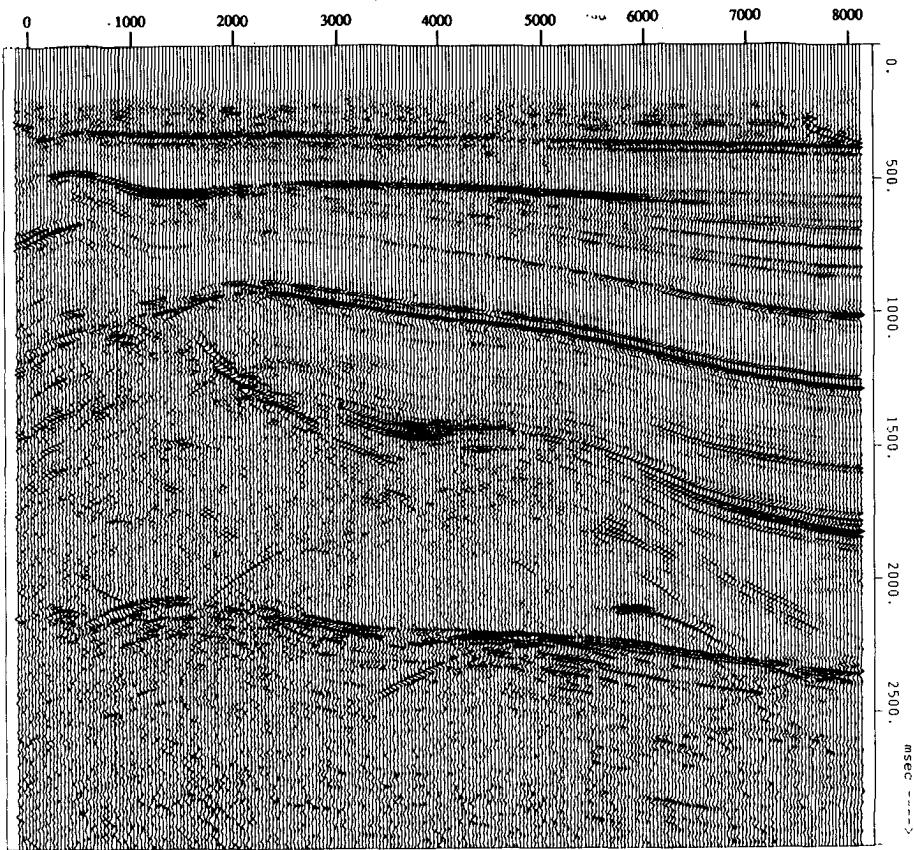
Figure 5.21: CMP stack of field data.

these experiments it can be concluded that for redatuming to the datum at 1500 m depth the reflections from 3500 m depth have not yet fully moved to the near offset traces, which were 'empty' in the surface data. It is clear that for the late reflections in the redatuming result also the common offset sections after redatuming must be examined. From these data it can be decided what following processing has to be done on the redatumed result.

The first option is to perform a zero offset migration of the data at the upper boundary of the target zone. This step can be done when all information of the target zone is contained in the zero offset traces at the upper boundary of the target zone. For the above example a
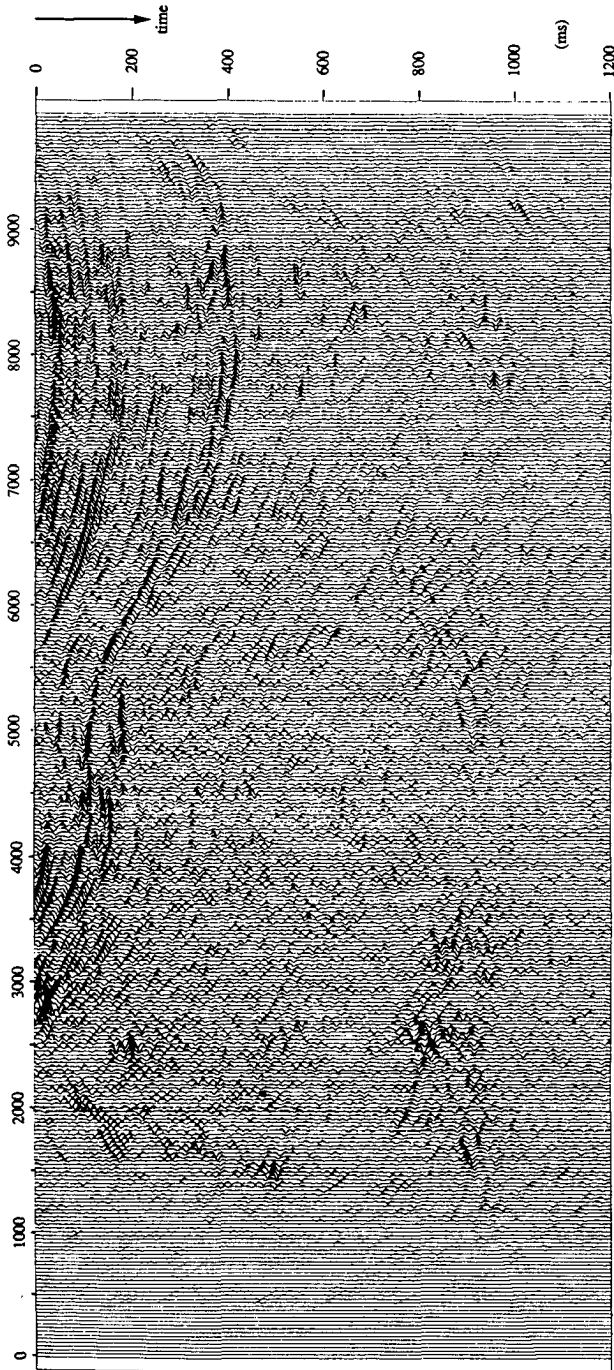
**Figure 5.22:** Zero offset data after redatuming to the intermediate datum at z = 1500 m.
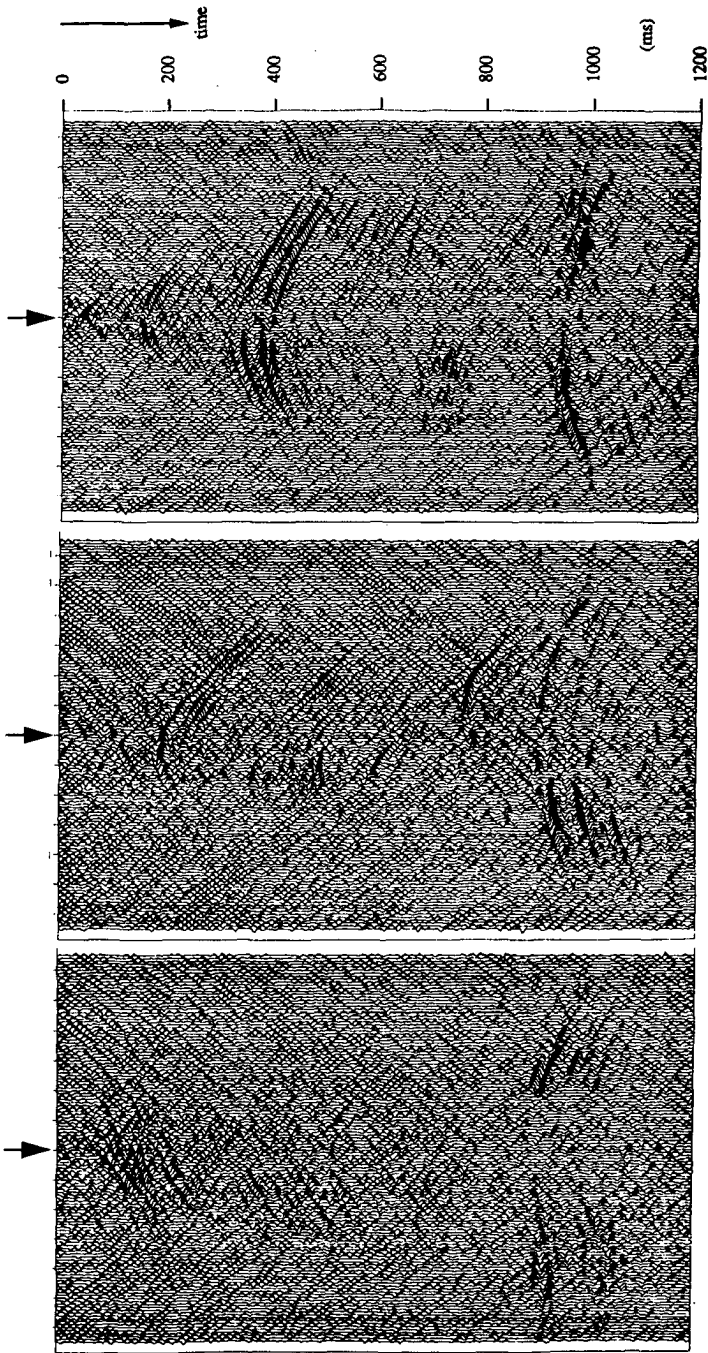
Figure 5.23: Three shot records after redatuming. Secondary sources at 4500, 6000 m and 7500 m.
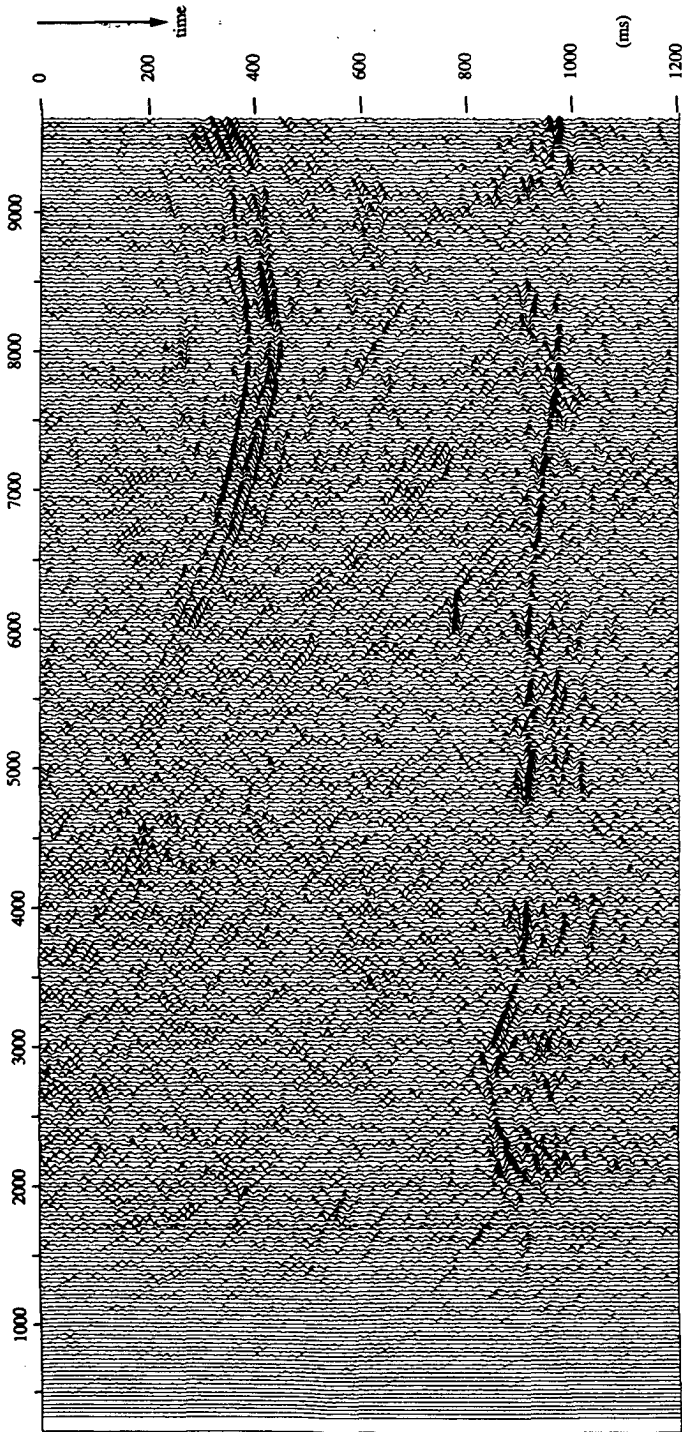
**Figure 5.24a:** Common offset gather at z = 1500 m for an offset of 600 m.
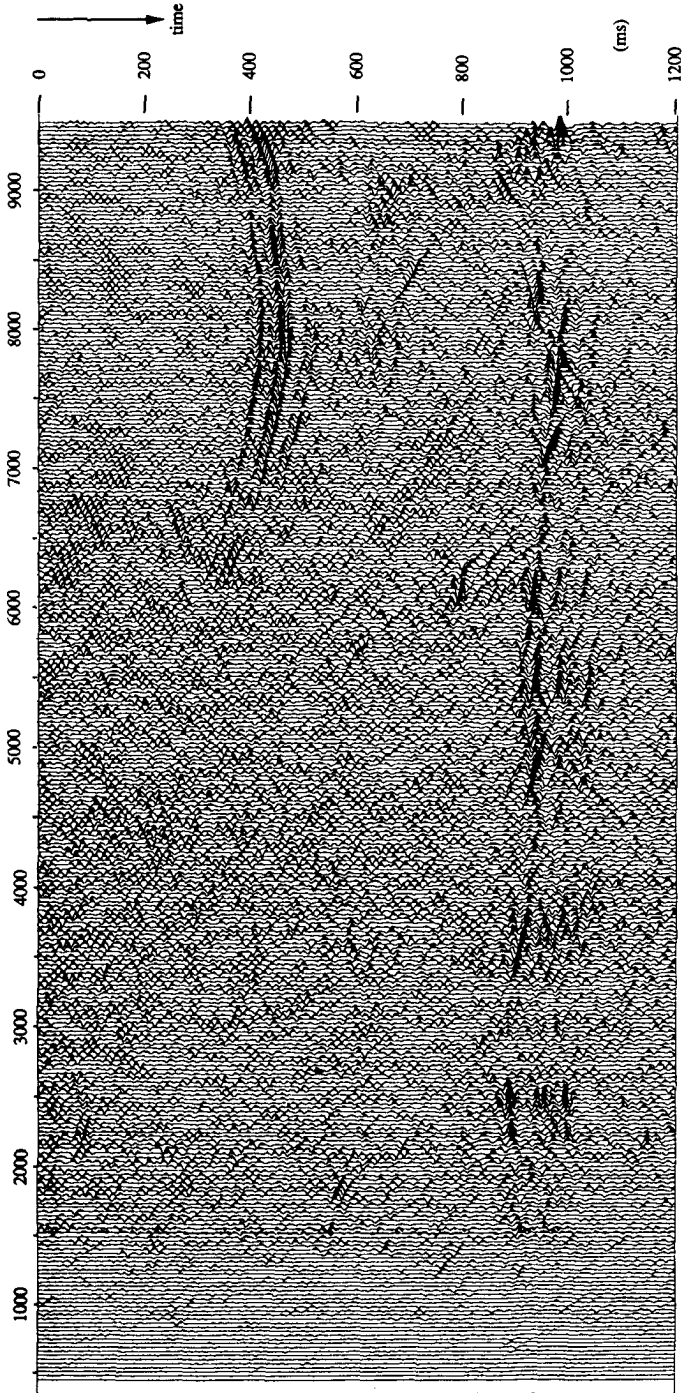
Figure 5.24b: Common offset gather at z = 1500 m for an offset of 900 m.
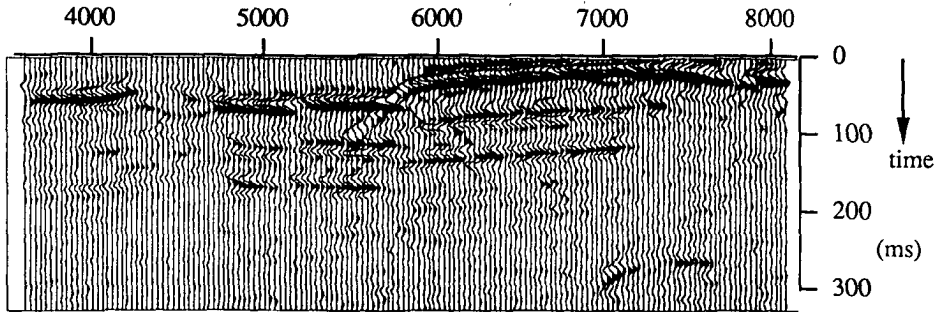
Figure 5.25a: Zero offset data after redatuming to z = 3250 m.

zero offset migration is useful to obtain a detailed reflectivity image of the reflectors in the first 1000 m below the new datum.

A second option is to perform conventional processing after the redatuming. On the data at the upper boundary of the target zone standard velocity analysis and stacking can be performed, followed by a poststack migration within the target zone. Such an approach is only valid when the target zone has a simple velocity structure. Note that the results of such a scheme could be far better than can be obtained by a conventional processing scheme with a CMP stacking at the surface.

For a complicated target zone the CMP stacking at the target's upper boundary may not be valid. In that case a full prestack migration after redatuming within the target zone is required. The results of prestack migration within the target zone will be exactly equal to the results of a prestack migration of the surface data. However, instead of recursively extrapolating the surface data to *all* depth levels, in the proposed scheme the data is extrapolated in one step to the upper boundary of the target zone and further recursively extrapolated to the depth levels in the target zone. Such a scheme will be much more efficient than full prestack migration that starts at the surface.

In figure 5.25a the result of redatuming the data to 3250 m is shown from 3450 m to 8000 m. Comparing these data with the result of the conventional CMP stacking at the surface (figure 5.21) shows the enormous increase in detailed information of this reflector. For the same part of the subsurface (3250 m < z < 4000 m) also the result of prestack depth migration is shown in figure 5.25b. The depth migration scheme was based on recursive finite difference extrapolation (see Van der Schoot et al., 1989). Comparison shows the very good correspondence of the detailed information of the reflector in the target zone. Because the new datum is very close to the reflectors, the propagation through
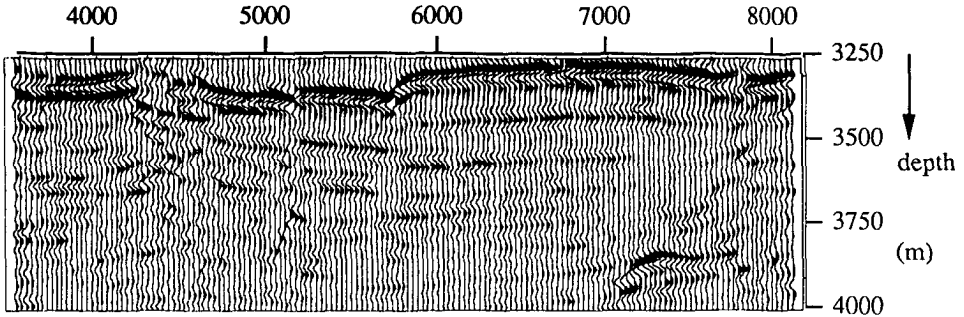
Figure 5.25b: Result of prestack migration for the same part of the subsurface as figure 5.25a.

the target zone do not effect the data seriously. In this case the redatuming results are comparable to the results from prestack migration. This confirms that redatuming can be used as a efficient processing step prior to prestack migration, if the effect of prestack migration must be examined. Finally for completeness the prestack migrated depth section of the complete subsurface is shown in figure 5.26.
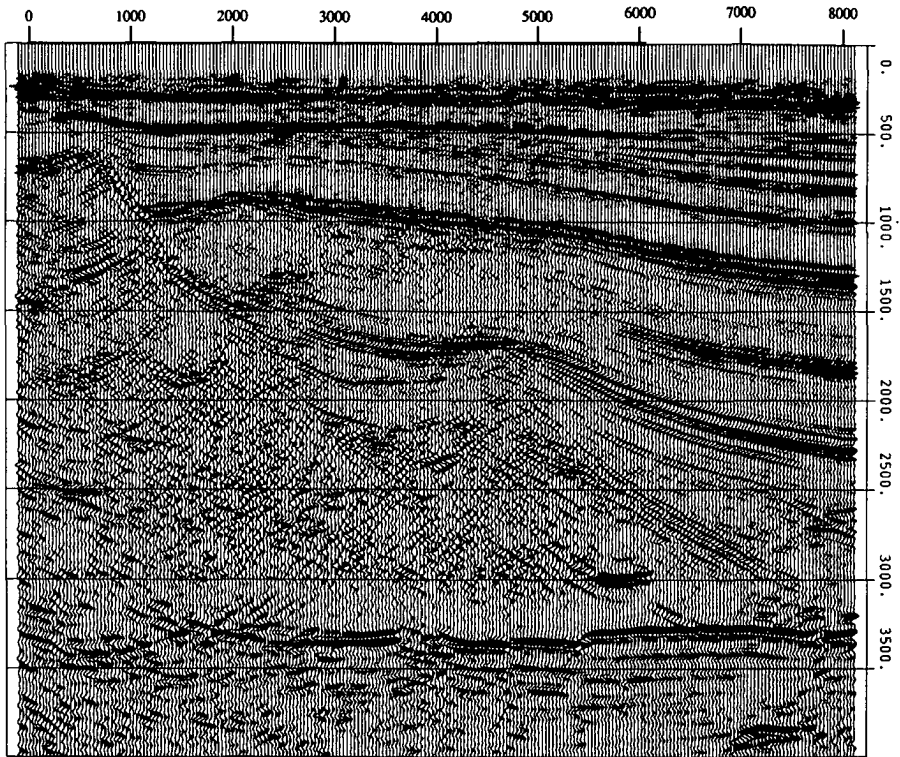
Figure 5.26: Result of prestack depth migration for the complete subsurface.

5.5 REDATUMING OF 3-D MODELED SHOT RECORDS

In this section two examples are presented of redatuming of modeled 3-D shot records is presented. The 3-D data, that are used in this section, are modeled with the scheme, that is explained in appendix B. With this scheme shot records were generated for the 3-D subsurface model of figure 5.27. In figure 5.27a a perspective view is given of the layers in the 3-D model and in the figure 5.27b and 5.27c two cross section through the model are shown. At a depth of 1000 m five point diffractors are placed, as indicated in figure 5.27.
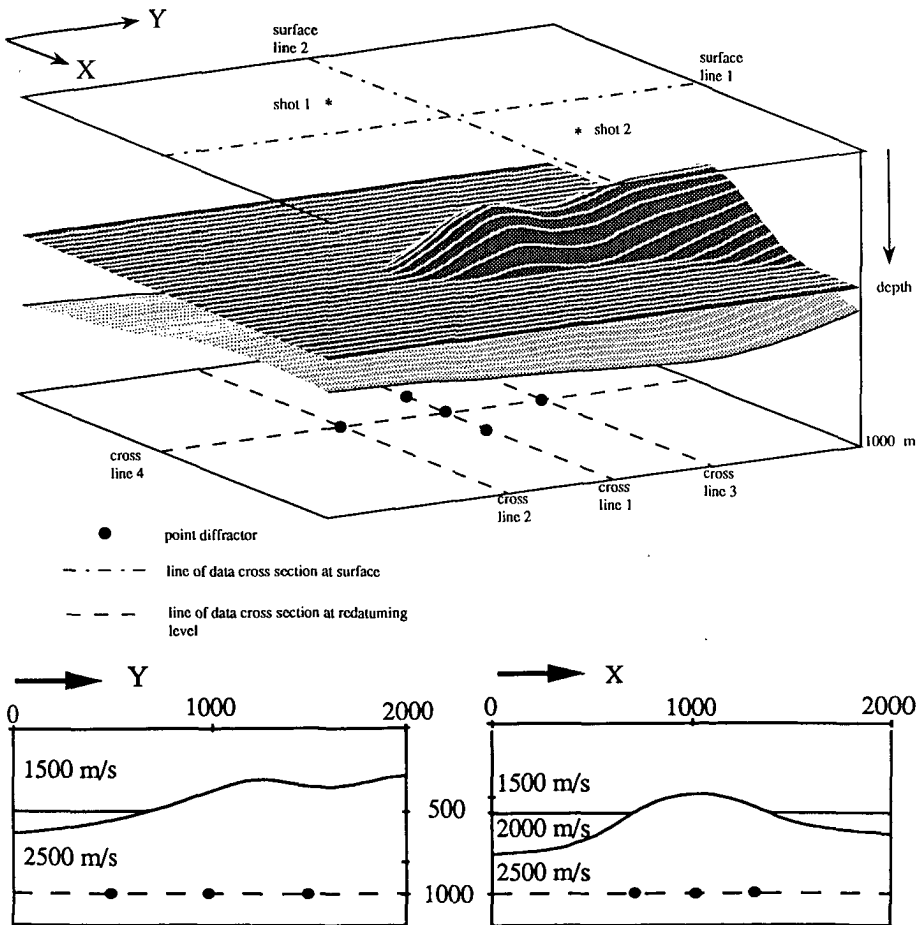
Figure 5.27: 3–D subsurface model with five point diffractors.

a. perspective view.

b. *cross section in Y direction.*

c. cross section in X direction.
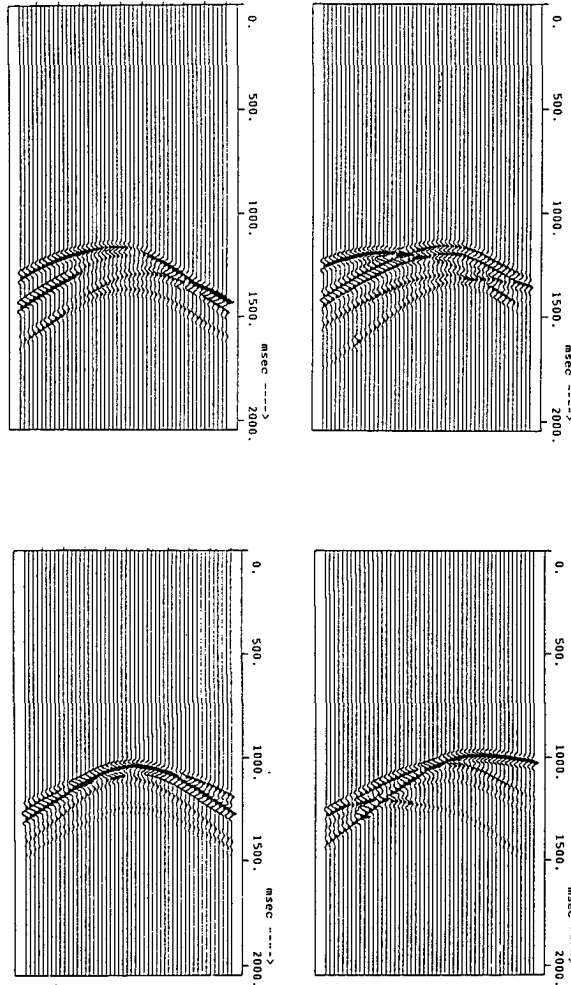
Figure 5.28: Cross section in X and Y for two shot records at the surface.

For this example the receivers were placed on a fixed acquisition grid at the surface. The detector spacing was 40 m in both the X and Y direction. The shot were positioned on a rectangular grid at the surface with a shot spacing of 40 m in the Y and 160 m in the Y directions. Using the 3-D prestack modeling scheme, that is described in appendix B, 600 shot records of 2500 traces each are modeled. The detectors for all shots were on a fixed grid of 50 × 50 detectors and the shots were on a grid of 24 × 25 sources. In figure 5.28 for two shots at the surface two cross sections through the data are shown. Using 3-D shot
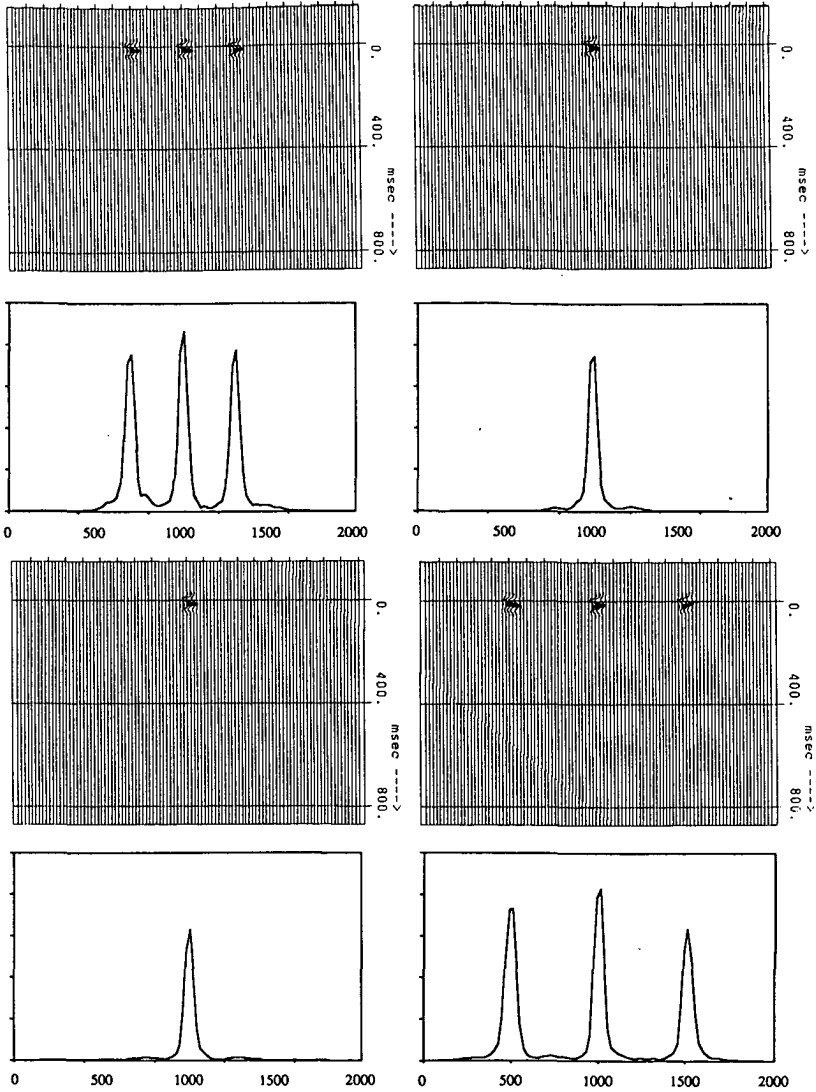
Figure 5.29: Result of 3-D shot record redatuming to z = 1000 m for the 4 cross sections as indicated in figure 5.27.
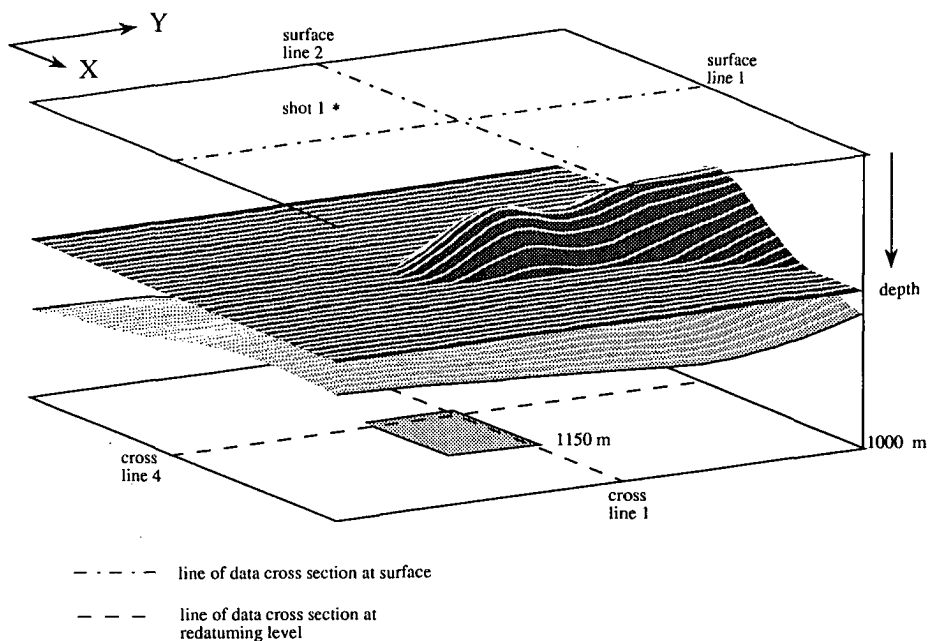
Figure 5.30: Respective view of 3-D subsurface model with rectangular reflector at 1150 m.

record redatuming these data are redatumed to 1000 m, the level of the point diffractors. In figure 5.29 the results of this redatuming are shown for four lines at the target level, as indicated in figure 5.27. Also the maximum amplitudes of each trace in the redatuming result are shown in figure 5.29. It can be seen that the 5 point diffractors are separated by the redatuming in a 3-D sense, which means that the propagation properties of the 3-D inhomogeneous overburden are eliminated properly. The diffractors are positioned at their correct spatial and temporal ($t = 0$ s) positions.

A second example of 3-D shot record redatuming concerns the redatuming of shot records with reflections of a plane reflector of limited length (figure 5.30). The reflector is rectangular and the position of the reflector is (750 m < X < 1250 m) and (850 m < Y < 1150 m).
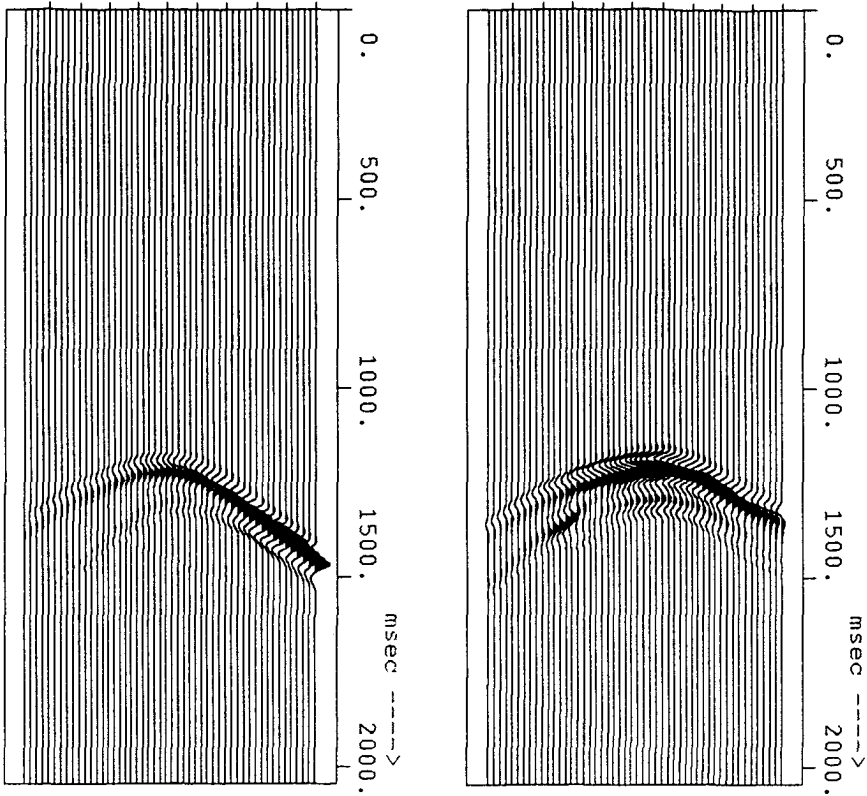
Figure 5.31: Cross sections in X and Y through shot record at (300 m, 700 m).

In figure 5.31 two cross sections through a shot record with source location (x,y) = (300 m, 700 m) is shown. The result after redatuming of this shot record is shown in figure 5.32 for the lines y = 1000 m and x = 1000 m at a depth of 1000 m. Clearly in this single shot redatuming result some truncation artifacts are visible, but the reflector can already be recognized. In figure 5.33 for the same lines at the target level the multi-experiment redatuming result is shown. The reflector is positioned correctly and due to the stacking over different experiments the amplitudes of the artifacts are now lower than the plotting resolution.

-100

0

100   time

200

(ms)

300

-100

0

100   time

200

(ms)

300
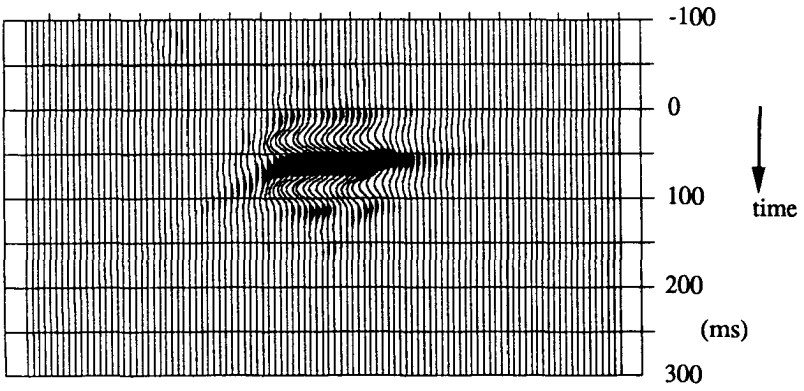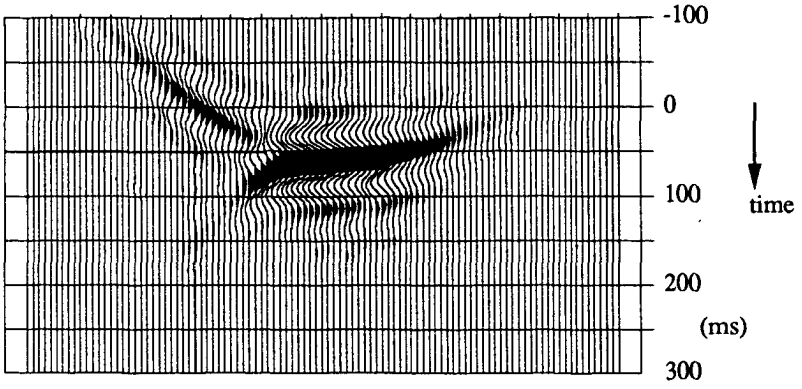
Figure 5.32: Single fold redatuming result for the shot record of figure 5.31.
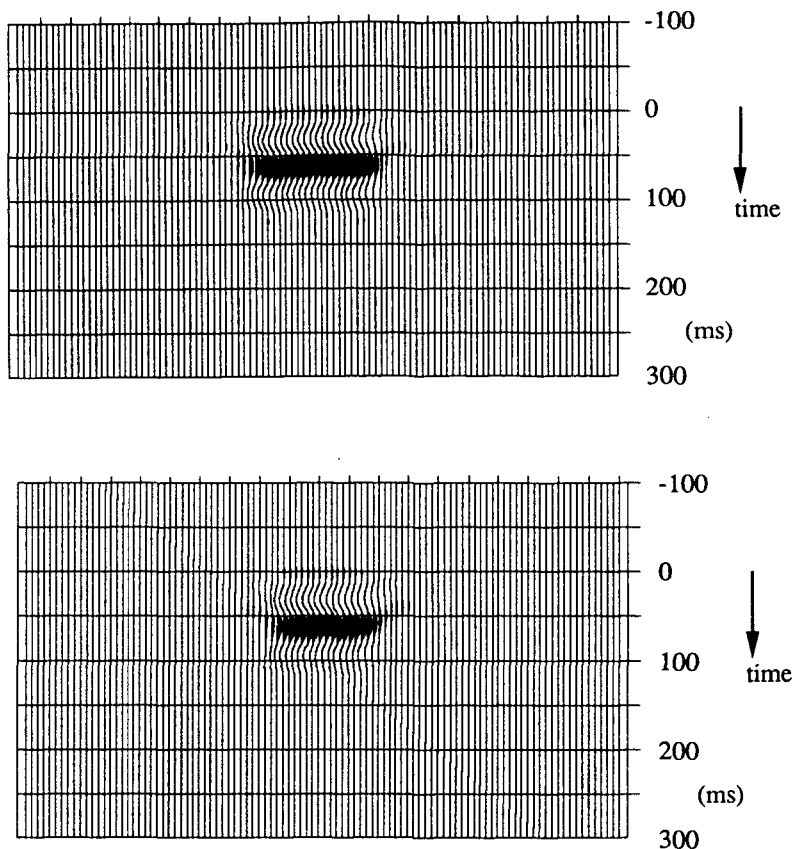
Figure 5.33: Multi-fold redatuming result to z = 1000 m.

The foregoing examples show that it is possible to perform shot record redatuming of 3-D prestack data in a very efficient way. The 3-D extrapolation operators properly eliminate the propagation effects through a 3-D inhomogeneous overburden and high quality zero offset data at the upper boundary of the target zone is generated. The quality of these data may be much better than can be reached by a conventional CMP stacking at the surface. By using a target-oriented migration scheme it is possible to perform prestack migration on modern computer systems within the economic limitations of a commercial processing center.

APPENDIX A

2–D GAUSSIAN BEAM MODELING

In this thesis one of the methods to calculate wave field extrapolation operators is Gaussian beam tracing. In this appendix the Gaussian beam method will be described as a modeling algorithm and the expressions used in this thesis will be derived. In this derivation I will mainly follow Cerveny et al. (1982).

In the vicinity of rays a high-frequency solution of the wave equation can be found. After a coordinate transformation to a *ray centered coordinate system* the expressions for Gaussian beams can be derived. The ray centered coordinate system is defined for an arbitrary ray Ω (figure A.1) with the two linearly independent coordinates s and n,

where   s is the arclength along the ray from a reference point s_0

and   n is the distance perpendicular to the ray in s.

The coordinate system is formed by two orthogonal unit vectors t and n, with t tangent to the ray in point s and n normal to the ray in s. The transformation from carthesian coordinates to the ray centered coordinates can be described by (see figure A.2),

$$\frac{\partial s}{\partial z} = \frac{1}{h\,(s,n)} \cos \alpha \,(s) \tag{A.1a}$$
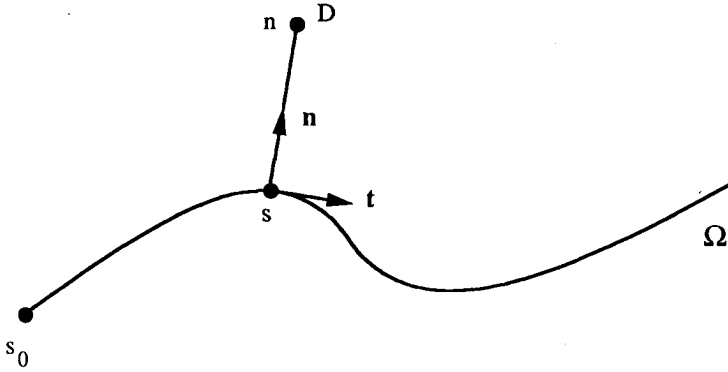
Figure A.1:   The ray centered coordinate system along ray Ω is formed by the unit vectors **n** and **t**. The coordinates are the distance s from a reference point s_0 along the ray and the distance n perpendicular to the ray.

$$\Delta s_x = \frac{\partial s}{\partial x} \Delta x = \frac{1}{h} \cos\alpha \, \Delta x$$

$$\Delta n_x = \frac{\partial n}{\partial x} \Delta x = \sin\alpha \, \Delta x$$
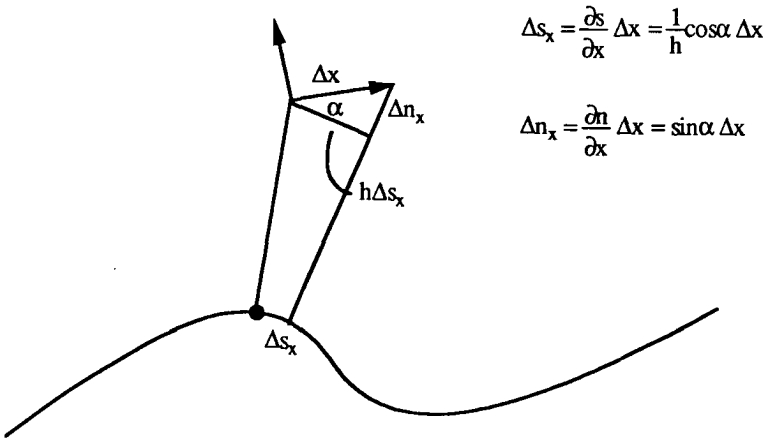
Figure A.2:   Geometry to derive the coordinate transformation from carthesian to ray centered coordinates.

$$\frac{\partial n}{\partial x} = -\sin\alpha \, (s) \tag{A.1b}$$

$$\frac{\partial s}{\partial y} = \frac{1}{h \, (s,n)} \sin\alpha \, (s) \tag{A.1c}$$

$$\frac{\partial n}{\partial y} = \cos \alpha \, (s)$$ (A.1d)

with

$$h \, (s,n) = 1 + \frac{1}{c \, (s,0)} \; \frac{\partial c \, (s,0)}{\partial n} \, n \quad ,$$ (A.2)

where $c(s_0)$ is the propagation velocity at the ray

and $\alpha(s)$ is the local angle of the ray with the positive x-axis.

The scaling factor h accounts for the irregularity of the coordinate system due to ray bending.

Gaussian beams give a high-frequency approximation of the solution of the wave equation in the ray-centered coordinate system. Therefore consider the 2-D acoustic wave equation in cartesian coordinates,

$$\frac{\partial^2 p(x,z,t)}{\partial x^2} + \frac{\partial^2 p(x,z,t)}{\partial z^2} - \frac{1}{c^2(x,z)} \frac{\partial^2 p(x,z,t)}{\partial t^2} = 0 \quad .$$ (A.3)

After a transformation to the ray centered coordinate system, using relation (A.1), the wave equation can also be written as,

$$\frac{1}{h} \frac{\partial^2 p}{\partial s^2} + h \frac{\partial^2 p}{\partial n^2} - \frac{h}{c^2} \frac{\partial^2 p}{\partial t^2} + \frac{\partial p}{\partial s} \frac{\partial}{\partial s} \left[\frac{1}{h} \right] + \frac{\partial p}{\partial n} \frac{\partial h}{\partial n} = 0 \quad ,$$ (A.4)

with $p = p(s,n,t)$ the acoustic pressure in the new coordinate system.

To find the parabolic wave equation I introduce a new coordinate υ, defined by:

$$\upsilon = n \, \omega^{1/2} \quad .$$ (A.5)

First the wave field is split into harmonic solutions of the form:

$$p(s,n,t) = \exp \left[i\omega \left[t - \int_{s_0}^{s} \frac{ds}{v(s)} \right] \right] P(s,n,\omega) \quad ,$$ (A.6)

where $P(s,n,\omega)$ denotes one frequency component of the Fourier transform of $p(s,n,t)$,

               $\omega = 2\pi f$ is the circle frequency

and $v(s) = c(s,0)$ is the propagation velocity along the ray.

Using equations (A.5) and (A.6) the wave equation for the ray-centered coordinate system (equation A.4) can now be written as,

$$\omega^2 h \left[\frac{1}{c^2} - \frac{1}{h^2 v^2} \right] P + \omega \left[\frac{1}{hv^2} \frac{\partial v}{\partial s} P - \frac{i}{v} \frac{\partial}{\partial s} \left[\frac{1}{h} \right] P - \frac{2i}{hv} \frac{\partial P}{\partial s} + h \frac{\partial P}{\partial \upsilon^2} \right]$$

$$+ \omega^{1/2} \frac{\partial P}{\partial \upsilon} \frac{\partial h}{\partial n} + \frac{1}{h} \frac{\partial P}{\partial s^2} + \frac{\partial P}{\partial s} \frac{\partial}{\partial s} \left[\frac{1}{h} \right] = 0 \quad , \tag{A.7}$$

with $c = c(s,n)$ the propagation velocity in the medium
and $v = v(s)$ the propagation velocity along the ray.

Note that no approximations have been made yet in deriving wave equation (A.7). To solve this equation asymptotically for $\omega \rightarrow \infty$, the terms with ω^0 and $\omega^{1/2}$ are neglected. Thus the parabolic wave equation near the ray becomes,

$$- \frac{2i}{v} \frac{\partial P}{\partial s} + \frac{\partial^2 P}{\partial \upsilon^2} - \left[\frac{\upsilon^2}{v^3} \frac{\partial^2 v}{\partial n^2} - \frac{i}{v^2} \frac{\partial v}{\partial s} \right] P = 0 \quad . \tag{A.8}$$

This equation can be further simplified by substitution of

$$P(s,\upsilon,\omega) = \sqrt{v(s)} \ W(s,\upsilon,\omega) \quad . \tag{A.9}$$

The parabolic wave equation then becomes,

$$- \frac{2i}{v} \frac{\partial W}{\partial s} + \frac{\partial^2 W}{\partial \upsilon^2} - \frac{\upsilon^2}{v_3} \frac{\partial^2 v}{\partial n^2} W = 0 \quad . \tag{A.10}$$

Let us try solutions of this equation of the form,

$$W(s,\upsilon) = A(s) \exp \left[\frac{-i}{2} \upsilon^2 M(s) \right] \quad , \tag{A.11}$$

with $A(s)$ a complex valued amplitude function
and $M(s)$ a complex valued function representing the second order travel time field.

Combining (A.10) and (A.11) gives

$$-i \left[\frac{2}{v} \frac{\partial A}{\partial x} + A M \right] - A \upsilon^2 \left[\frac{1}{v} \frac{\partial M}{\partial s} + M^2 + \frac{1}{v^2} \frac{\partial^2 v}{\partial n^2} \right] = 0 \quad . \tag{A.12}$$

This equation can be split into two separate equations for $M(s)$ and for $A(s)$,

$$\frac{\partial M}{\partial s} + v\, M^2 + \frac{1}{v^2} \frac{\partial^2 v}{\partial n^2} = 0 \qquad\qquad\text{(A.13a)}$$

and

$$\frac{\partial A}{\partial s} + \frac{1}{2}\, v\, A\, M = 0 \quad . \qquad\qquad\text{(A.13b)}$$

First equation (A.13a) will be investigated. To solve this equation two complex valued functions are introduced q(s), which represents the geometrical spreading, and p'(s), which represents the slowness vector normal to the ray. These two functions are defined by,

$$M(s) = \frac{1}{v\, q} \frac{\partial q}{\partial s} \qquad\qquad\text{(A.14a)}$$

and

$$\frac{\partial q}{\partial s} = v\, p' \quad . \qquad\qquad\text{(A.14b)}$$

Combining equations (A.13a), (A.14a) and (A.14b) we finally arrive at two first order differential equations, which are referred to as the *dynamical ray tracing system*,

$$\frac{\partial q}{\partial s} = v\, p' \qquad\qquad\text{(A.15a)}$$

and

$$\frac{\partial p'}{\partial s} = -\frac{1}{v^2} \frac{\partial^2 v}{\partial n^2}\, q \quad . \qquad\qquad\text{(A.15b)}$$

The solution of equation (A.13b), defining the amplitude term A(s) of the total solution can be found, using equation (A.14a) and is given by,

$$A(s) = \frac{\Psi}{\sqrt{q(s)}} \quad , \qquad\qquad\text{(A.16)}$$

where Ψ is a complex constant for a ray.
Note that Ψ can be different for different rays.

Combination of equations (A.6) through (A.16) finally gives the solution of the parabolic wave equation in the vicinity of the ray,

$$p(s,n,t) = \Psi \sqrt{\frac{v(s)}{q(s)}} \exp\left[i\omega\left[t - \int_{s_0}^{s}\frac{ds}{v(s)}\right] - \frac{i\omega}{2}\frac{p'}{q}n^2\right] \quad . \tag{A.17}$$

The procedure of Gaussian beam modeling to obtain this result consists of three main steps.

1) Calculate the ray with ray tracing
2) Solve the dynamic ray tracing system (A.15) for that ray
3) Compute the wave field according to (A.17)

Cerveny et al. (1982) show, that a wave field can be decomposed into Gaussian beams and that the total wave field at the detector position, due to a line source (in a 2-D medium) can be obtained by,

$$P(D,\omega) = \int_{0}^{2\pi} \Phi(\varphi)\, P_{\varphi}(s,n,\omega)\, d\varphi \quad , \tag{A.18}$$

with $P(D,\omega)$ the monochromatic wave field at point D,

          φ the take-off angle of the ray at the source,

          $\Phi(\varphi)$ a source dependent weighting function

and $P_{\varphi}(s,n,\omega)$ the monochromatic solution of the parabolic wave equation in D for
          a ray with take-off angle φ (described by equation A.17).

In order to have a physical interpretation of the expression of the monochromatic Gaussian beam solution (equation A.17), it can also be written as,

$$P(s,n,\omega) = \Psi \sqrt{\frac{v(s)}{q(s)}} \exp\left[-i\omega\int_{s_0}^{s}\frac{ds}{v(s)} - \frac{i\omega}{2v(s)}K(s)n^2 - \frac{n^2}{L^2(s)}\right] \quad , \tag{A.19}$$

with

$$K(s) = v(s)\, \text{Re}\left[\frac{p'(s)}{q(s)}\right] \tag{A.20a}$$

and

$$\frac{1}{L^2(s)} = -\frac{\omega}{2}\, \text{Im}\left[\frac{p'(s)}{q(s)}\right] \quad . \tag{A.20b}$$

K(s) may be interpreted as the curvature of the wave front of the beam and L(s) describes a frequency-dependent half width of the beam. From the last expression for the monochromatic solution, the expressions for the complex valued 'travel time' and 'amplitude' of the contribution of beam b in a detector point can be seen.

$$T_b(s,n) = \int_{s_0}^{s} \frac{ds}{v(s)} + \frac{1}{2v(s)} K(s)\, n^2 \qquad\qquad (A.21a)$$

and

$$A_b(s,n) = \Psi \sqrt{\frac{v(s)}{q(s)}} \exp\left[-\frac{n^2}{L^2(s)} \right] . \qquad\qquad (A.21b)$$

From expressions (A.21b) it is clear, that the amplitude has a Gaussian shape as function of the distance n to the ray. Expressions (A.21a) and (A.21b) are used to calculate non-recursive extrapolation operators, as explained in chapter 3 of this thesis.
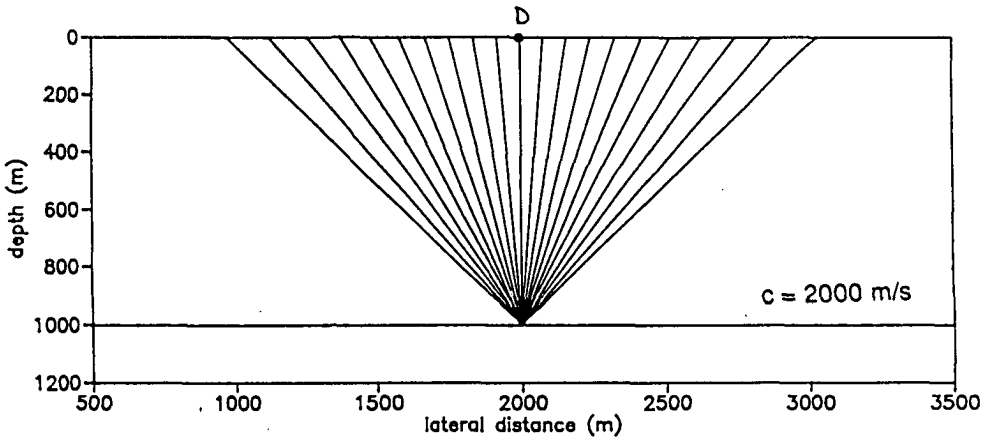
Figure A.3: Homogeneous medium with a source at z = 1000 m and x = 2000 m and the rays used for evaluation of the response at point D at the surface.

I will illustrate Gaussian beam modeling with a simple example from Budejicky (1988). Consider the geometry of figure A.3 with a homogeneous medium and a source at z=1000 m. The response of this source wave field at point D at the surface is considered. In figure A.3 also the rays are depicted, for which the Gaussian beam response in D is calculated. In
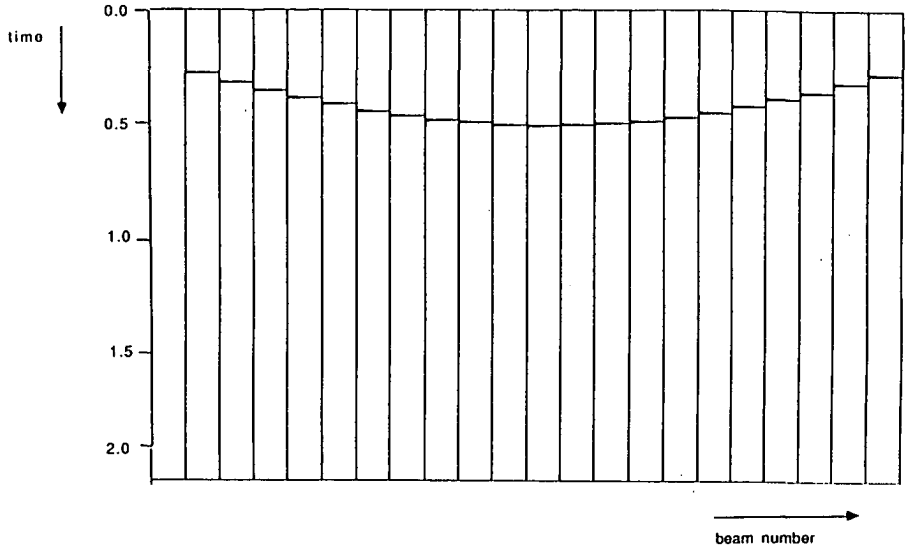
Figure A.4: Contribution per beam of the travel time expression (expression A.22a) in point D.
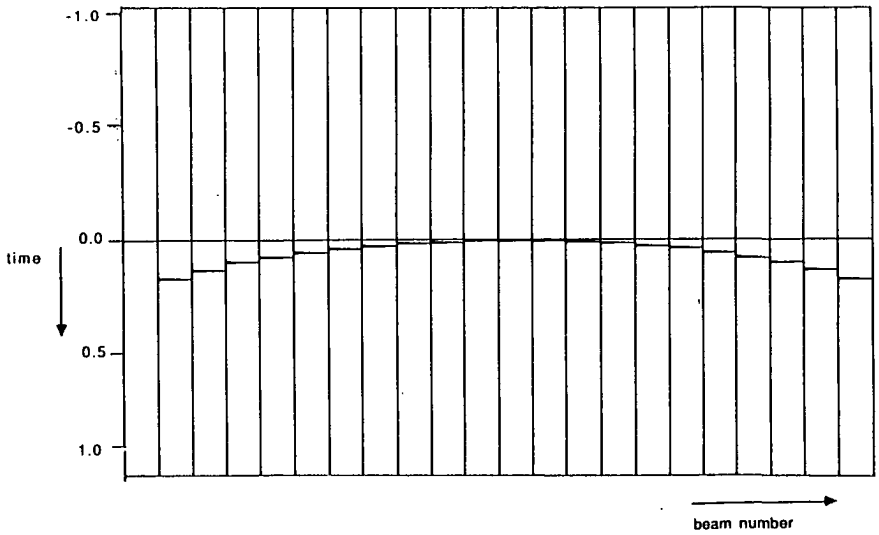

Figure A.5: Correction per beam for the wave front curvature (expression A.22b).

figure A.4 the travel times along the rays for each beam is shown. These travel times are given in equation (A.19) by the exponential term,

$$\exp\left[-i\omega \int_{s_0}^{s} \frac{ds}{v(s)}\right] \quad . \tag{A.22a}$$

Note that the travel times decrease with an increasing distance from the detector position to the ray. In figure A.5 the travel-time 'corrections', caused by the curvature of the wave front are depicted for each beam. This figure corresponds to the term in equation (A.19),

$$\exp\left[-\frac{i\omega}{2v(s)} K(s) n^2\right] \quad . \tag{A.22b}$$
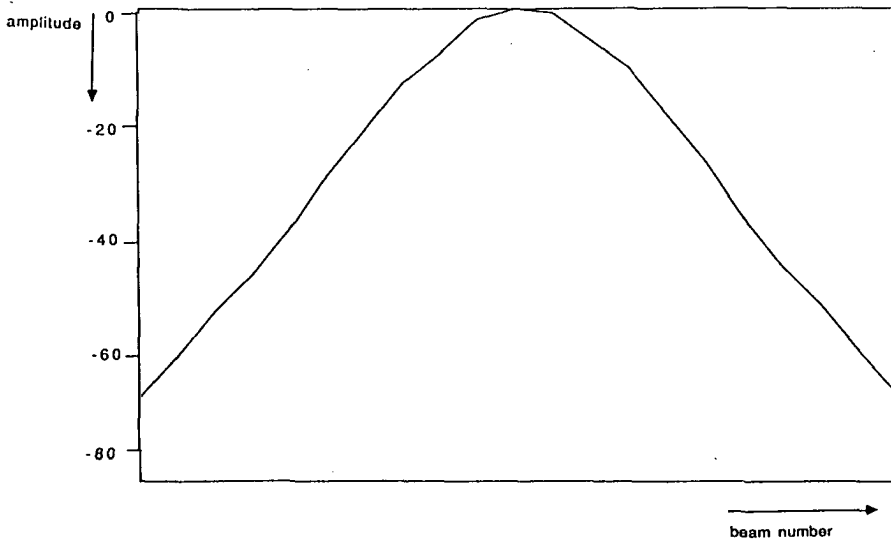
Figure A.6: Amplitude contribution per beam at point D (expression A.22c).

For this homogeneous case this term increases with increasing detector-ray distance. In figure A.6 the amplitude contribution per beam is shown. This term corresponds to,

$$\Psi \sqrt{\frac{v(s)}{q(s)}} \exp\left[-\frac{n^2}{K^2(s)}\right] \quad . \tag{A.22c}$$
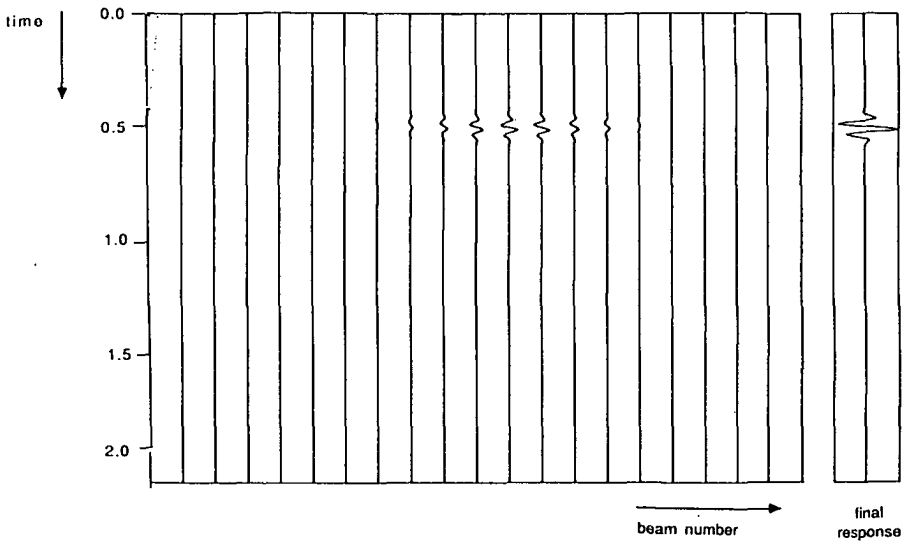
Figure A.7:   Combined contributions per beam convolved with a wavelet. The trace at the right
contains the summation over the contributions of all beams.

Combining the terms (A.22a), (A.22b) and (A.22c) gives per beam the contributions to the
response in point D, as shown in figure A.7. These contributions are summed to find the
final response in point D, which is depicted in the right hand side of figure A.7.

APPENDIX B

AN EFFICIENT PRESTACK STRUCTURAL MODELING SCHEME FOR REFLECTOR AND DIFFRACTOR ENERGY

One of the problems of developing 3-D prestack processing software is to simulate realistic measurements to test the quality of the scheme under investigation. One possibility for testing the algorithm is to use field data. Beside the problems of the size of the data set, which are difficult to overcome in a research environment, the input model for the data is not known. This makes field data unscientific for initial testing of the quality of a processing scheme. A second option is to use data measured in a watertank. These data can give problems of too few receiver station, spatial undersampling and limited apertures, which reduces the quality of the data. Therefore new algorithms are often first tested with numerically modeled data.

There is a number of requirements for data to test 3-D wave field extrapolation algorithms. The data must contain all relevant propagation effects through 3-D media, like e.g. diffraction energy. When diffractions are not present in the modeled data set artifacts can occur in the final processing result, which are caused by the quality of the input data and not by the quality of the processing scheme. To test the extrapolation techniques, described in this thesis, also arbitrary velocity variations must be handled properly. Data, that are used for testing of our shot record redatuming scheme, should also contain a large number of 3-D shot records, generated for a subsurface model with velocity variations in all spatial directions.
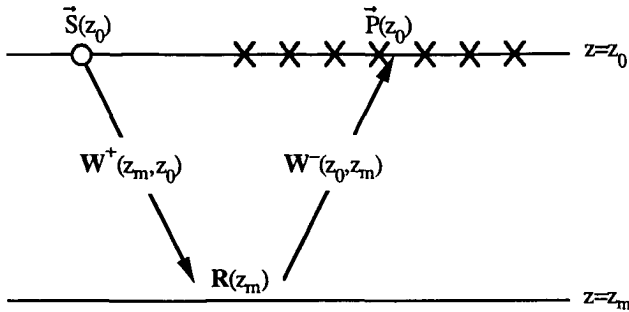
Figure B.1:   Schematic representation of a physical experiment with downward propagation of the source wave field, reflection at a layer interface and upward propagation of the reflected wave field.
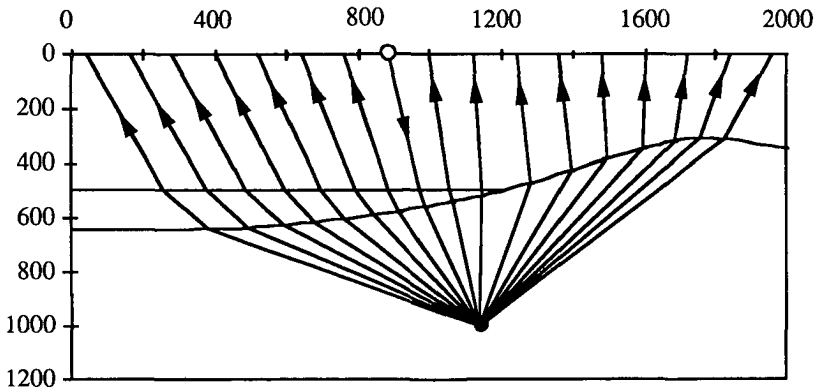
Figure B.2: Principle of modeling a point diffractor at the target zone in a shot record.

For 2-D, high quality test data can be generated using finite difference modeling, but for multi-experiment 3-D data these schemes are too much time consuming and their memory requirements are too large. So these schemes are of no practical use in 3-D. Calculation of reflections with standard ray tracing would also be very time consuming and this method generally does not generate prestack diffraction energy. In this appendix I will introduce a modeling scheme, based on standard ray tracing, that is very efficient in modeling large numbers of 3-D shot records and also generates diffraction energy. The scheme is based on the same extrapolation operators that were described in chapter 3 of this thesis. In this

scheme reflectors are modeled as a superposition of the response of a number of point diffractors.

Theory

A monochromatic seismic experiment can be described for shot j in the matrix notation by (see also section 2.4),

$$\vec{P}_j^-(z_0) = \sum_{m=1}^{M} W^-(z_0,z_m) \, R(z_m) \, W^+(z_m,z_0) \, \vec{S}_j^+(z_0) \quad , \tag{B.1}$$

with $\vec{S}_j^+(z_0)$ the downgoing source wave field at the surface,

$W^+(z_m,z_0)$ the forward extrapolation operator from z_0 to z_m

$W^-(z_0,z_m)$ the forward extrapolation operator from z_m to z_0

and $\vec{P}_j^-(z_0)$ the upgoing registered wave field at the surface.

This method of describing a physical experiment is illustrated for one depth level z_m in figure B.1 and the method is fully applicable to 3-D wave propagation. For a multi-shot seismic experiment equation (B.1) can be extended, where the vectors $S_j(z_0)$ and $P_j(z_0)$ form the j-th columns of the data matrices $S^+(z_0)$ and $P^-(z_0)$ respectively,

$$P^-(z_0) = \sum_{m=1}^{M} W^-(z_0,z_m) \, R(z_m) \, W^+(z_m,z_0) \, S^+(z_0) \tag{B.2}$$

In chapter 3 of this thesis much attention is paid to the calculation of the 3-D extrapolation operator matrices W for forward wave field extrapolation, using a standard ray tracing scheme. This method can also be used to develop an efficient prestack modeling scheme, which also can model diffraction energy.

Practice

For simplicity I will now regard only depth level z_m. Furthermore it is assumed that $R(z_m)$ just contains diagonal elements (locally reacting media) and that $S(z_0) = S(\omega)$ I with I the unity matrix. First consider the modeling of shot records for one point diffractor in the subsurface. This means that all elements of $R(z_m)$ are zero except for one diagonal element, corresponding to the position of the point diffractor. This also means that just one row of the extrapolation operator for the downgoing field $W^+(z_m,z_0)$ and just one column of the upward extrapolation operator $W^-(z_0,z_m)$ have to be calculated. In figure B.2 this approach is illustrated. Starting at the location of the point diffractor, rays are calculated, through the inhomogeneous overburden, to all detector and source positions at the surface. From these rays the appropriate row of $W^+(z_m,z_0)$ is calculated. For one shot this is indicated by the
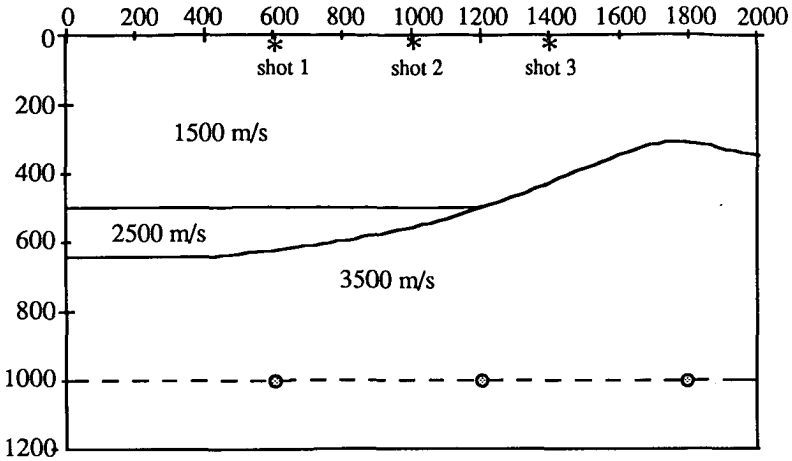
Figure B.3: 2-D subsurface model with three point diffractors at the target zone.

Figure B.4: Three shot records modeled for the subsurface model of figure B.3.

arrow pointing downward in figure B.2. From the same rays also the column of $\mathbf{W}^-(z_0, z_m)$, the arrows pointing downward in figure B.2, can be calculated. In practical terms this method generates a single shot record with the ray from the source location to the diffractor for downward propagation and all rays from the diffractor to the detectors at the surface for the upward propagation. The response of more point diffractors or a reflector can be modeled by superposition of single point diffractor responses.
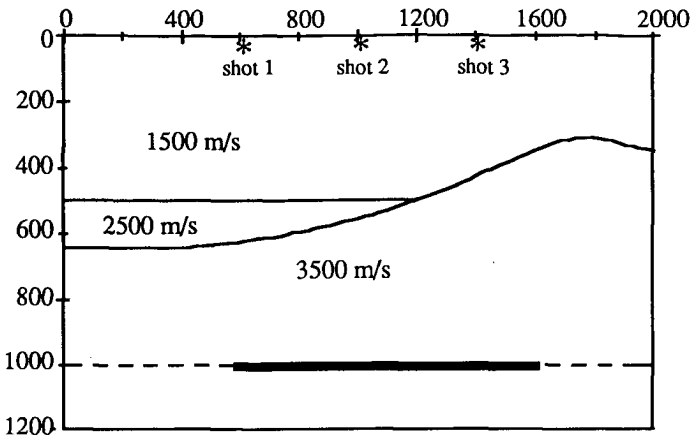
Figure B.5: 2-D subsurface model with a reflector of limited length at the target zone.
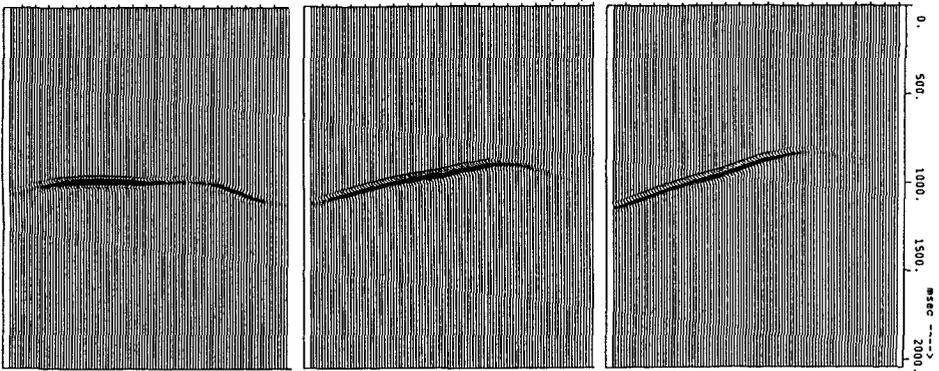
Figure B.6: Three shot records modeled for the subsurface model of figure B.5, where the reflector is modeled as a number of point diffractor.

Next I will give three examples of this scheme. First, the modeling of a few point diffractors in the subsurface model of figure B.3 is shown. In figure B.4 three shot records are shown modeled with this method. Clearly in each shot record the responses of the 3 separate point diffractors can be recognized as well as the lateral velocity variation in this subsurface model. In the second example the shot records were generated for a reflector of
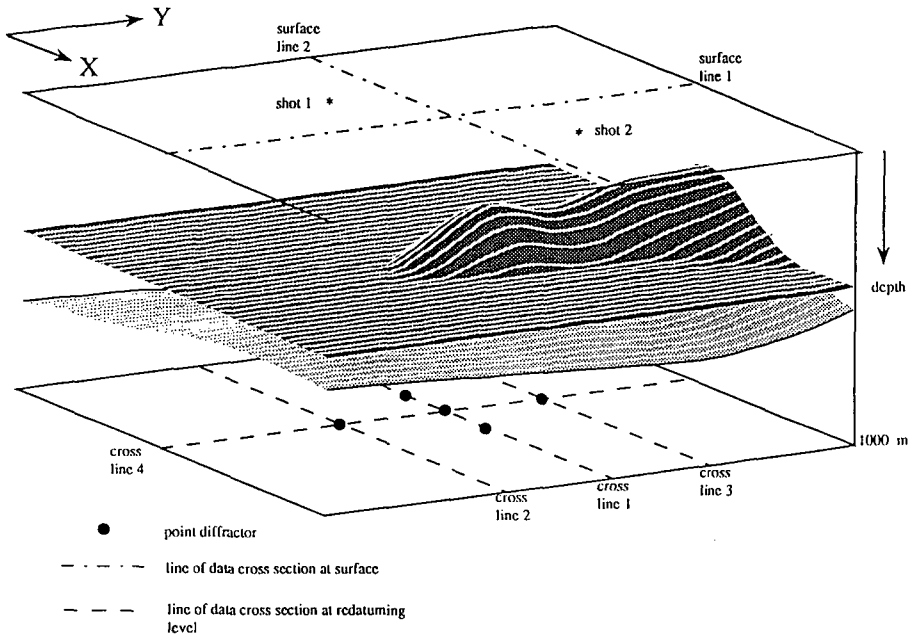
Figure B.7a: 3-D subsurface model (perspective view).
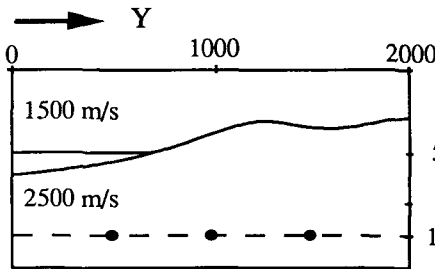
Figure B.7b: Cross section in the Y direction through the 3-D subsurface model of figure B.7a.
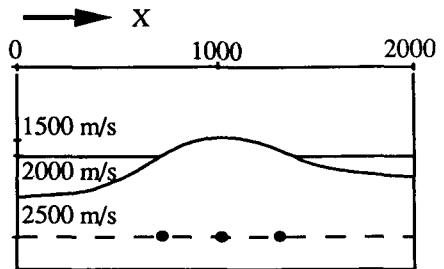
Figure B.7c: Cross section in the X direction through the 3-D subsurface model of figure B.7a.

limited length. The reflector extends from X = 600 m to x = 1600 m as indicated in figure B.5. In figure B.6 three shot records, modeled by superposition of point diffractors, are shown. It is clear that with this method also diffraction energy of the edges of the reflector was modeled. For the last example consider the 3-D subsurface model, shown in figure B.7. In figure B.7a a perspective view is given of this subsurface model. The model
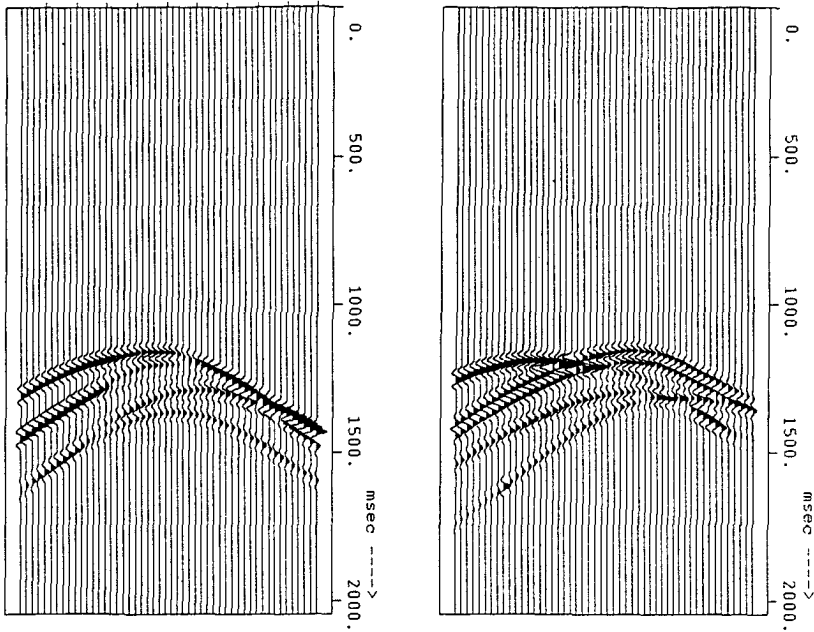
Figure B.8: Two lines of a shot record with source location (x,y) = (600 m, 600 m).

contains three layers with propagation velocities of 1500 m/s, 2000 m/s and 2500 m/s respectively. In both the lateral directions velocity variations are present. In figure B.7b and B.7c two cross sections through this model are shown in the X and Y direction. At a depth of 1000 m 5 point diffractors were positioned as indicated in figure B.7. For two shots at the surface the 3-D data were modeled. From these 3-D data in figure B.8 and B.9 two cross sections are shown. In the cross sections the 5 point diffractor are clearly visible.
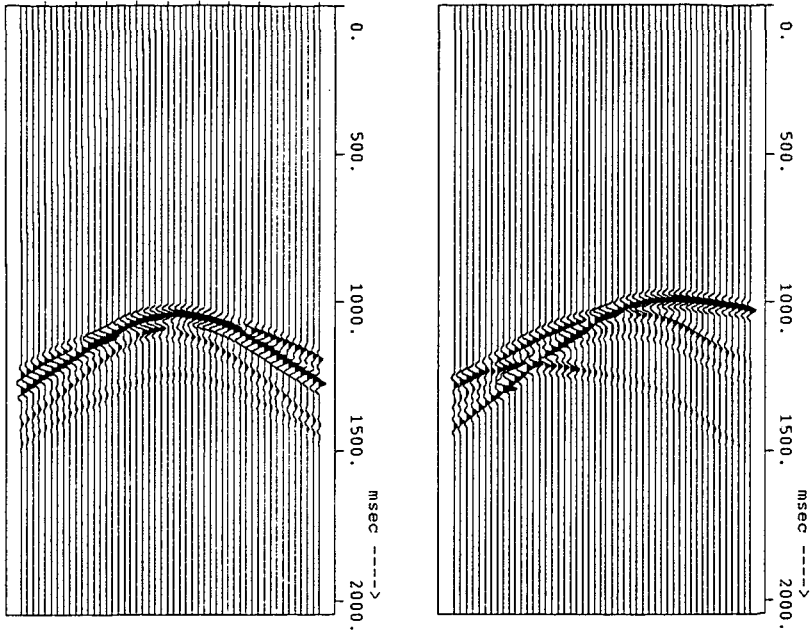
Figure B.9: Two lines of a shot record with source location (x,y) = (1400 m, 1400 m).

This method modeled 3-D wave propagation through an inhomogeneous overburden. This method of modeling data suffers from the same disadvantages as the 3-D extrapolation operators, based on ray tracing. In the ray tracing shadow zones can occur, rays can not always be found and also the amplitudes are not perfect. However, the method is more stable and the amplitudes of this method are better than a direct modeling of the reflection with a ray tracing scheme. In this way in an efficient way 3-D prestack data can be generated to test 3-D processing algorithms.

REFERENCES

Berkhout, A.J., 1985,
>   Seismic Migration, Volume A: Theoretical Aspects (3rd edition),
>   Elsevier Science Publ. Comp.

Berkhout, A.J., 1984,
>   Seismic Migration, Volume B: Practical Aspects,
>   Elsevier Science Publ. Comp.

Berkhout, A.J. and Wapenaar, C.P.A., 1989,
>   One-way versions of the Kirchhoff integral,
>   Accepted for publication in Geophysics (April issue)

Berryhill, J.R., 1986,
>   Submarine canyons velocity replacement by wave equation datuming before stack,
>   Geophysics, **51**, 1572-1579

Beydoun, W.B. and Keho, T.H., 1987,
>   The paraxial ray method,
>   Geophysics, **52**, 1639-1653

Blacquière, G., Debeye, H.W.J., Wapenaar, C.P.A. and Berkhout, A.J., 1989,
>   Three dimensional table driven migration
>   Accepted for publication in Geophysical Prospecting

Bleistein, N., 1984,
>   Mathematical methods for wave phenomena,
>   Academic Press Inc.

Budejicky, V., 1988,
>   Inverse wavefield extrapolation with Gaussian beam modeled Green's functions,
>   Master's thesis, Delft University of Technology

Cerveny, V., Popov, M.M., and Psencik, I., 1982,
    Computation of wave fields in inhomogeneous media - Gaussian beam approach,
    Geoph. J. R. Astr. Soc., **70**, 109-128

Cox, H.L.H., Ooms, F.P.J., Wapenaar, C.P.A. and Berkhout, A.J., 1988,
    Verification of macro subsurface models using a shot record approach,
    58th SEG meeting, Anaheim, Expanded Abstracts, 904-908

Delphi, 1988
    Delft philosophy on inversion,
    Consortium proposal, Delft University of Technology

Dix, C.H., 1955,
    Seismic velocities from surface measurements,
    Geophysics, **20**, 68-86

Hatton, L., Worthington, M.H. and Malin, J., 1986,
    Seismic data processing,
    Blackwell Scientific Publ.

Hubral, P., 1976,
    Interval velocities from surface measurements in the three-dimensional plane layer
    case,
    Geophysics, **41**, 233-242

Jeannot, J.P., Faye, J.P. and Denelle, E., 1986,
    Prestack migration velocities from depth focussing analysis,
    56th SEG meeting, Houston, Expanded Abstracts, 438-440

Keho, T.H. and Beydoun, W.B.,1988,
    Paraxial ray Kirchhoff migration,
    Accepted for publication in Geophysics

Kinneging, N.A., Budejicky, V., Wapenaar, C.P.A. and Berkhout, A.J., 1989,
    Efficient 2-D and 3-D shot record redatuming,
    Accepted for publication in Geophysical Prospecting

Peels, G.L., 1988,
    True amplitude wave field extrapolation with applications in seismic shot record
    redatuming,
    Ph.D. Thesis, Delft University of Technology

Postma, R.W. and Jeannot, J.P., 1988,
    Prestack depth imaging beneath complex overburden,
    58th SEG meeting, Anaheim, Expanded Abstracts, 596-598

Schultz, P.S. and Sherwood, J.W.C., 1980,
    Depth migration before stack,
    Geophysics, **45**, 361-375

Sierra, 1987,
    Quick ray tracing, User manual,
    Sierra Geophysics Inc.

Triton, 1985,
    Target oriented 3-D migration,
    Consortium proposal, Delft University of Technology

Van der Made, P.M., 1988,
    Determination of macro subsurface models by generalized inversion,
    Ph.D. Thesis, Delft University of Technology

Van der Schoot, A., Romijn, R., Larson, D.E. and Berkhout, A.J., 1989,
    Prestack migration by shot record inversion and common-depth-point stacking: a
    case study,
    Accepted for publication in First Break

Verschuur, D.J., Herrmann, P., Kinneging, N.A., Wapenaar, C.P.A. and Berkhout,
    A.J., 1988,
    Elimination of surface-related multiply reflected and converted waves,
    58th SEG meeting, Anaheim, Expanded Abstracts, 1017-1020.

Wapenaar, C.P.A., Peels, G.L., Budejicky, V. and Berkhout, A.J., 1989,
    Inverse extrapolation of primary seismic waves,
    Accepted for publication in Geophysics

Yilmaz, O. and Lucas, D., 1986,
        Prestack layer replacement,
        Geophysics, **51**, 1355-1369

Yilmaz, O., 1987
        Seismic data processing,
        Society of Exploration Geophysicists

SUMMARY

The major problem in three-dimensional seismic processing is the large amount of data and the enormous computation times, that are needed for a proper processing. Therefore a target oriented approach is needed to make 3-D prestack migration possible within the economic limitations of a seismic processing center. In this approach the output of the scheme is limited to a detailed reflectivity image of a part of the subsurface, that is of special interest to the geologists, the target zone. Such a target oriented scheme will in general consist of five major steps:

1) Surface related preprocessing, where for all surface related effects is inverted, like surface related multiples.

2) Estimation of the macro subsurface model, which describes the global propagation properties of the subsurface.

3) Redatuming of the shot records from the surface to the upper boundary of the target zone. In this step from data measured at the surface, data are calculated as if they were measured at the upper boundary of the target zone.

4) Verification of the macro subsurface model. In case the macro model is slightly in error, the redatumed data can be corrected with a residual NMO correction. For large errors this model must be updated and the redatuming must be repeated using the new macro model.

5) Finally the data at the upper boundary of the target zone is migrated, giving a detailed reflectivity image of the target zone.

In this thesis the third step of this target oriented processing scheme, the redatuming, is treated. In the redatuming the propagation properties of the inhomogeneous overburden are eliminated by wave field extrapolation from the surface to the target's upper boundary. In order to perform a proper redatuming much attention must be paid to the calculation of the wave field extrapolation operators. Because in redatuming the wave field is not needed at intermediate level non-recursive wave field extrapolation is best suited, where the wave field at the upper boundary of the target zone is calculated in one step from the wave field at the surface. For application to 3-D shot records these operators must be calculated very efficiently.

The main part of wave field extrapolation, both forward and inverse, is the modeling of the Green's functions. These Green's functions can in principle be modeled with any modeling algorithm. In this thesis two modeling algorithms are discussed in more detail, the ray tracing method and the Gaussian beam modeling algorithm. These algorithm enable calculation of extrapolation operators for any irregular acquisition geometry. For operators based on ray tracing the rays are interpolated to the irregular acquisition geometry using a local plane wave approximation in the vicinity of the rays. In the Gaussian beam method the interpolation of the operators is described by the theory itself.

Results of inverse wave field extrapolation with these methods show, that the amplitude behavior of the Gaussian beam operators is better than the amplitude behavior of the ray tracing operators. One of the major causes of the worse amplitudes of the ray tracing method is the existence of shadow zones, for which no rays can be calculated. In Gaussian beam modeling no shadow zones exist, which makes the amplitude behavior much better. With these operators the effects of wave propagation are correctly eliminated. Because of the efficiency of the operators they are well suited for 3-D application.

Redatuming per shot record has several advantages over conventional redatuming by downward extrapolation of receivers and sources. In the conventional schemes a reordering of the data is needed. Therefore the enormous amount of data makes 3-D application very inefficient. In shot record redatuming no reordering of the data is needed, which makes 3-D application possible. After redatuming also single fold redatuming results can be examined as well as genuine common depth point gathers. Also the illumination of the surface by the different shots can be studied in more detail.

Shot record redatuming is not only the first step in the target oriented processing scheme. The redatuming itself can also be an important tool in seismic processing. Redatuming to a target level close to the target reflectors gives in a very efficient way information, which is comparable to the results for those reflectors from prestack migration.

With a target oriented scheme 3-D data processing, of which the shot record redatuming is a very important step, is feasible on modern computer systems.

SAMENVATTING

Het grootste probleem bij drie dimensionale seismische dataverwerking is de grote hoeveelheid data en de enorme rekentijden die er voor nodig zijn. Daarom is een doelgerichte aanpak noodzakelijk om deze 3–D dataverwerking mogelijk te maken op een economisch verantwoorde wijze. Bij zo'n doelgerichte aanpak wordt het resultaat beperkt tot een gedetailleerd beeld van de reflectiviteit van een zeker interessegebied in plaats van een beeld van de gehele ondergrond. Door deze beperking wordt de rendement van het schema aanzienlijk verbeterd maar blijft de kwaliteit van de dataverwerking voor het interessegebied gelijk. Zo'n aanpak bestaat uit vijf stappen:

1) Een voorbewerking om voor alle aan het oppervlak gerelateerde effecten te inverteren.

2) Schatting van het macro model, dat de globale voortplantingseigenschappen van de ondergrond beschrijft.

3) Redatuming van de seismische metingen van het oppervlak naar de *bovengrens* van het interessegebied. Hierbij wordt uit oppervlaktemetingen data berekend alsof deze waren gemeten aan de bovengrens van het interessegebied.

4) Controle van het macro model. Indien het macro model een kleine afwijking vertoont, kunnen de data gecorrigeerd worden met een residuele NMO correctie. Bij grote afwijkingen moet het macro mode verbeterd worden en moet de redatuming herhaald worden met het nieuwe model.

5) Ten slotte worden de data aan de bovengrens van het interessegebied gemigreerd, wat een gedetailleerd beeld van de structuren in het interessegebied levert.

In dit proefschrift wordt de derde stap van dit doelgerichte schema, de redatuming, beschreven. Hier worden de effecten van de golfvoortplanting door de inhomogene ondergrond geëlimineerd. Veel aandacht moet daarom besteed worden aan de berekening van de operatoren voor golfveld extrapolatie, die de golfvoortplanting beschrijven. Omdat bij redatuming het golfveld niet op tussenliggende niveau's berekend hoeft te worden, is een niet-recursieve extrapolatie methode het meest geschikt. Hierbij wordt het golfveld aan de bovengrens van het interessegebied in één stap berekend uit het golfveld aan het

oppervlak. Voor toepassing op 3–D data is het nodig dat de operatoren zeer efficient worden berekend en toegepast.

Het belangrijkste onderdeel van golfveld extrapolatie is de berekening van de Greense functies. In principe kunnen deze Greense functies berekend worden met elk soort moleringsschema. In dit proefschrift worden twee methodes uitvoerig behandeld, namelijk de raytracing methode en het modeleren met behulp van Gausse bundels. Met deze methodes is het mogelijk extrapolatie operatoren te berekenen voor onregelmatige acquisitie geometrieën. Bij de raytracing methode wordt de golfvoortplanting benaderd met een stralenmodel, waarna met een vlakke golf benadering de stralen worden geïnterpoleerd naar het onregelmatige acquisitie rooster, terwijl de theorie van de Gausse bundels zelf al een interpolatie van golfvelden beschrijft.

Toepassing van deze methodes in een inverse golfveld extrapolatie toont aan dat het amplitude gedrag van de Gausse bundel operatoren beter is dan dat van de raytracing operatoren. Dit komt onder andere door schaduw gebieden, een van de voornaamste problemen van de raytracing methode. In schaduw gebieden kunnen met raytracing geen stralen berekend worden. Bij Gausse bundels komen schaduw gebieden niet voor, waardoor het amplitude gedrag veel beter is. Het blijkt dat met deze operatoren de effecten van golfvoortplanting goed kunnen worden geëlimineerd. Bovendien zijn de operatoren zeer efficient, waardoor ze geschikt zijn voor toepassing op 3–D seismische data.

Redatuming per seismisch experiment heeft diverse voordelen ten opzichte van de conventionele redatuming methodes. In conventionele methodes moeten de metingen gereorganiseerd worden. Gezien de enorme hoeveelheid data is 3–D toepassing van deze schema's zeer inefficient. Bij toepassing per seismisch experiment is geen reorganisatie nodig, waardoor ook 3–D toepassing mogelijk is. Bovendien kan het resultaat van de redatuming van één seismisch experiment afzonderlijk bestudeerd worden en ook de belichting van het interessegebied door de diverse bronnen aan het opervlak kan goed onderscheiden worden.

Verder is redatuming niet alleen een van de stappen in het algemene doelgerrichte schema, maar de redatuming op zich is ook een belangrijk hulpmiddel in de seismische dataverwerking. Bij redatuming naar een niveau dicht boven de interessante reflectoren is het resultaat vergelijkbaar met het resultaat van prestack migratie voor die reflectoren, maar bij redatuming is dit resultaat op een veel efficientere manier verkregen.

Met een doelgericht schema, waarvan redatuming een essentieel onderdeel is, wordt 3–D dataverwerking mogelijk op de huidige computer systemen.

CURRICULUM VITAE

11 februari 1961   geboren te Haarlem

1973-1979   Gymnasium β aan de R.K. Scholengemeenschap "Sancta Maria" te Haarlem

1979-1985   studie Technische Natuurkunde aan de Technische Hogeschool te Delft met als afstudeeronderzoek:
"Modeling and migration using the two-way full elastic wave equation"

1981-1985   secretaris afdeling waterpolo
Zandvoortse Zwem- en Poloclub "de Zeeschuimers"

1982-heden   scheidsrechter waterpolo

1985-1989   promotieonderzoek bij het TRITON project aan de Technische Universiteit te Delft met als onderwerp:
"Three dimensional redatuming of seismic shot records"

1987-heden   verenigingssecretaris Haarlemse zwemvereniging "de Watertrappers"

Stellingen

behorende bij het proefschrift
"Three-dimensional redatuming of seismic shot records"

1. Snelheidsanalyse dient bij voorkeur met behulp van multi-offset niet-recursieve golfveldextrapolatie te worden uitgevoerd.

2. De conversie van tijd naar diepte vereist een grotere integratie van seismische processing en interpretatie dan nu gebeurt.

3. Een beschrijving van het macro model aan de hand van overwegingen over de frequentie-inhoud is onjuist.

4. Inverteren is modelleren.

5. Politiek en seismiek hebben gemeen dat het belangrijk is de trend van het detail te onderscheiden.

6. De grafische representatie van meetresultaten dient als integraal onderdeel van de totale dataverwerking te worden gezien.

7. Universitaire medewerkers hebben de neiging hun eigen economische waarde te laag in te schatten.

8. De begrippen afspreken en afzeggen liggen soms even dicht bij elkaar als spreken en zeggen.

9. Voorspellingen doen over stellingen bij proefschriften is zeer gevaarlijk.
   (Stelling 12 bij het proefschrift "True amplitude wave field extrapolation with applications in seismic shot record redatuming", 1988, G.L. Peels)

10. Een stelling dient provocerend te zijn.

Delft, 20 juni 1989
Niels Kinneging